

Higher Order Corrections to Supersymmetric Production and Decay Processes

Zur Erlangung des akademischen Grades eines
DOKTORS DER NATURWISSENSCHAFTEN
von der Fakultät für Physik des
Karlsruher Instituts für Technologie (KIT)

genehmigte

DISSERTATION

von

Dipl.-Phys. Eva Popena
aus Świętochłowice

Tag der mündlichen Prüfung: 26. Oktober 2012

Referentin: Prof. Dr. Margarete Mühlleitner
Korreferent: Prof. Dr. Matthias Steinhauser

Abstract

In the first part of this thesis the decay of the light stop into a charm quark and the lightest neutralino, $\tilde{t}_1 \rightarrow c\tilde{\chi}_1^0$, is calculated at one-loop level in the Minimal Supersymmetric extension of the Standard Model (MSSM) in the framework of Minimal Flavor Violation (MFV). In a previous calculation only leading logarithms of the scale of MFV have been taken into account. The neglected terms lead to deviations in the decay width of about 10%. Moreover, if MFV is assumed at a high scale the large logarithms of this scale need to be resummed to all orders. These resummation effects can decrease the stop decay width by a factor 20 and reduce the branching ratio, which is widely assumed to be near 1, to 0.5.

The second part of this thesis covers the calculation of next-to-leading order (NLO) corrections in the strong coupling constant α_s to the pair production of squarks of the first two generations in the MSSM. In contrast to previous works no assumptions regarding the squark masses have been made and the different subchannels have been treated independently. The results have been implemented in a Monte-Carlo program which allows to calculate the QCD corrections for arbitrary distributions. It is investigated whether the assumption made so far that K -factors are flat in distributions is correct. Since it turns out that the differential K -factor can vary in a range of 35% the full NLO corrections should be taken into account in phenomenological studies.

Zusammenfassung

Im ersten Teil der Arbeit wird der Zerfall des leichten Stops in ein Charm-Quark und das leichteste Neutralino, $\tilde{t}_1 \rightarrow c\tilde{\chi}_1^0$, auf Ein-Schleifen-Niveau in der Minimalen Supersymmetrischen Erweiterung des Standardmodells (MSSM) unter der Annahme von Minimaler Flavorverletzung (MFV) berechnet. Zum ersten Mal werden nicht nur führende Logarithmen der MFV-Skala berücksichtigt. Die bisher vernachlässigten Terme wirken sich in der Größenordnung von 10% auf die Zerfallsbreite aus. Wird MFV an einer hohen Skala angenommen, so müssen die großen Logarithmen dieser Skala resummiert werden. Diese Resummationseffekte können die Zerfallsbreite um einen Faktor 20 reduzieren und dazu führen, dass sich das Verzweigungsverhältnis, das bisher immer als nahezu 1 angenommen wurde, auf 0.5 verringert.

Im zweiten Teil werden Korrekturen nächst-führender Ordnung in der starken Kopplungskonstante α_s der QCD zur Paarproduktion von Squarks der ersten beiden Generationen im MSSM berechnet. Im Gegensatz zu älteren Arbeiten werden die einzelnen Squark-Massen nicht als entartet angenommen und die verschiedenen Subkanäle einzeln betrachtet. Die Ergebnisse sind in einem Monte-Carlo-Programm implementiert, so dass QCD Korrekturen für beliebige Verteilungen berechnet werden können. In einer ersten Anwendung wird überprüft, ob die verbreitete Annahme, dass der K -Faktor in den Verteilungen flach ist, gerechtfertigt ist. Es stellt sich heraus, dass der differentielle K -Faktor in einem Bereich von 35% variieren kann und deshalb die vollständigen Verteilungen für phänomenologische Studien berücksichtigt werden sollten.

Contents

1	Introduction	1
2	Supersymmetry	5
2.1	Introduction	5
2.2	The Minimal Supersymmetric Extension of the SM	7
2.3	Experimental Searches	12
2.3.1	Searches for the First Two Generations of Squarks	13
2.3.2	Searches for the Top Squark	14
3	Calculational Concepts	17
3.1	Hadronic Collisions	17
3.2	Renormalization	18
3.3	The Catani-Seymour Subtraction Formalism	20
4	Light Stop Decay in the MSSM with Minimal Flavor Violation	23
4.1	Introduction	23
4.2	Flavor Mixing in the SM and MSSM	25
4.3	Light Stop Decay $\tilde{t}_1 \rightarrow c + \tilde{\chi}_1^0$ at One-Loop Level	29
4.3.1	Counterterms and Renormalization	31
4.3.2	Analytical Results	34
4.4	Numerical Analysis	36
4.5	Conclusion and Outlook	44
5	Squark Pair Production at NLO	45
5.1	Introduction	45
5.2	Squark Pair Production at LO	47
5.3	The Virtual Corrections	49
5.4	The Real Emission and Subtraction Dipoles	54
5.5	The Integrated Dipoles	60
5.5.1	I terms	60
5.5.2	PK terms	62
5.6	Numerical Evaluation	65
5.6.1	Tests and Comparisons	67
5.6.2	Phenomenological Results	74
5.7	Conclusion and Outlook	80

A Color Algebra Relations	83
B FCNC Vertex Counterterm	85
C Catani Seymour Expressions	89
C.1 Singular Functions for Integrated Dipoles	89
C.2 Finite Collinear Terms	91
C.3 Solutions to Integrals with +-Distributions	95
Bibliography	97
Danksagung	109

Chapter 1

Introduction

*Człowiek nigdy nie ogląda się na to, co zrobione;
Ale na to patrzy, co ma przed sobą do zrobienia.*

*One never notices what has already been done;
One only sees what still remains to be done.*

- Marie Skłodowska-Curie
Letter to her brother, 18 Mar 1894

The world and universe we live in is full of fascinating natural phenomena. It is even more fascinating that in the course of the past centuries it was possible to understand a multitude of these phenomena on the smallest scales. By uniting all known elementary particles and the fundamental forces between them, apart from the gravitational force, in a consistent theoretical framework, the Standard Model (SM) of particle physics is a remarkable achievement in modern physics. The SM comprises Quantum Chromodynamics (QCD), the theory of strong interactions, and the unified theory of electromagnetism and the weak interactions in a renormalizable quantum field theory, which accounts for a wide variety of experimental data over an energy range of more than twelve orders of magnitude. However, in contrast to this incredible accuracy in the confirmation of SM predictions there are experimental as well as the theoretical arguments suggesting that it cannot be the ultimate theory: Not only is the gravitational force not incorporated in the theory but the experimental evidence for Dark Matter and Dark Energy clearly reveals the limitations of the SM, since it does not offer a satisfactory explanation for these observations - just to mention two of the existing problems.

Among the many propositions for physics beyond the Standard Model (BSM), so-called supersymmetric (SUSY) theories provide a very elegant way to solve part of the problems of the SM. In their simplest realization, the Minimal Supersymmetric extension of the SM (MSSM) [1–7], each SM particle is paired with a SUSY partner with identical quantum numbers except for a difference of half a unit in spin.

Since none of the SUSY particles have been observed so far they are assumed to be heavier than their SM partners which means that SUSY is not an exact symmetry. Theoretical considerations imply that these new particles should have masses no larger than a few TeV otherwise SUSY would not provide a solution to the so-called fine-tuning problem of the SM ([8] and references therein). Roughly speaking, the fine-tuning problem refers to the circumstance that the parameters of the SM must be adjusted very precisely in order to agree with experimental observations. Due to the conservation of a symmetry called R-parity SUSY particles can only be produced pairwise and the lightest supersymmetric particle (LSP) is stable. In many MSSM scenarios the LSP is neutral and can be identified as a suitable Dark Matter candidate. This leads to typical experimental signatures consisting of multiple jets or leptons originating from the final state particles of SUSY decay cascades and missing transverse energy as a consequence of the LSP being weakly interacting and neutral and therefore escaping the detector.

A lot of effort has been put in phenomenological investigations of SUSY in the past 30 years, which has influenced the detector design of the Large Hadron Collider (LHC) located at CERN near Geneva. This proton-proton accelerator currently operates at a center-of-mass energy of 8 TeV and is a perfect experimental tool to test predictions of theories beyond the SM. With the discovery of a new boson [9, 10], potentially a Higgs boson originating from the mechanism of electroweak symmetry breaking [11–15], the LHC has already attained one of its major goals. The recorded data has also been used to search for SUSY particles. No excesses over the SM expectations have been reported so far in these searches and these results have been translated into exclusion limits on the masses of the potential SUSY particles [16, 17].

For the interpretation of the experimental data precise theoretical predictions are needed. This thesis contributes to this effort by calculating higher order corrections in perturbation theory to supersymmetric production and decay processes.

In the first part of this thesis the flavor changing neutral current (FCNC) decay of one of the SUSY partners of the top quark, the light stop \tilde{t}_1 , to a charm quark c and the lightest neutralino $\tilde{\chi}_1^0$, which is the LSP in most MSSM scenarios, is calculated at one-loop level. In the MSSM the scalar partners of the right-handed and left-handed quarks, called squarks and denoted by \tilde{q}_L and \tilde{q}_R , mix to form two mass eigenstates, \tilde{q}_1 and \tilde{q}_2 , with \tilde{q}_1 defined to be the lighter one. In the case of the SUSY partners to the top quark large mixing effects can lead to one stop mass eigenstate, \tilde{t}_1 , being significantly lighter than all other squarks and also lighter than the top quark. If additionally the mass difference of the lighter stop \tilde{t}_1 to the lightest neutralino $\tilde{\chi}_1^0$ is small, the decay considered here $\tilde{t}_1 \rightarrow c + \tilde{\chi}_1^0$ can be the dominant decay channel. So far, only an approximate formula for the decay width at one-loop level has been available [18]. Apart from calculating the exact one-loop decay, the impact of resummation effects which take into account certain terms to all orders of perturbation theory is analyzed.

In the second part of this thesis the pair production of squarks of the first two generations is calculated at next-to-leading order (NLO) in SUSY QCD perturba-

tion theory. Squark pair production is the dominant production channel for colored SUSY particles in the rather high mass regions [19], which are still allowed by the LHC exclusion limits for squarks and gluinos. In contrast to the existing calculation in [20] the squark masses are not assumed to be degenerate and all contributing subchannels, characterized by different flavor and chirality combinations, are treated independently. In order to provide not only inclusive cross sections but also distributions for arbitrary observables the calculation has been implemented in a fully flexible parton-level Monte-Carlo program. With this set-up it is possible to study the effects of the NLO corrections in the various subchannels as well as their impact on the shapes of distributions. Since the NLO corrections are known to be large on the one hand and the shapes of distributions are widely used for phenomenology on the other hand the recalculation of this process and its implementation in a Monte-Carlo framework provides a useful tool for a variety of phenomenological studies.

This thesis is organized as follows: The following chapter introduces the relevant theoretical aspects of SUSY and summarizes the status of the experimental searches for squarks of the first two generations and for the top squarks. Since the third generation squarks are subject to large mixing effects the strategies of the searches for the first two generations cannot be straightforwardly adopted. In Chapter 3 concepts in theoretical particle physics necessary for the calculations in this thesis are presented. Chapter 4 contains the detailed discussion of the first part of the thesis, the calculation and the results of the numerical evaluation of the FCNC decay $\tilde{t}_1 \rightarrow c + \tilde{\chi}_1^0$ at one-loop level. The second part of this thesis, the calculation of the NLO SUSY QCD corrections to squark pair production, is described in Chapter 5. Both calculations as well as their results and implications are summarized at the end of Chapter 4 and Chapter 5, respectively.

Chapter 2

Supersymmetry

2.1 Introduction

Before first supersymmetric theories were developed, the list of potential space-time symmetry transformations was considered complete since the formulation of Einsteins theory of relativity, which was accomplished in 1905. In 1967 the Coleman-Mandula theorem [21] seemed to confirm this point of view. This theorem states that the space-time symmetries of the Poincaré algebra and internal symmetries cannot be combined in any but a trivial way and implies that apart from the known generators - the generator of space-time translations P_μ and the generator of homogeneous Lorentz transformations $M_{\mu\nu}$ - no other generators with non-trivial Lorentz transformation properties exist. However, the argumentation of the theorem does not exclude generators which transform as spinors under Lorentz transformations. For generators Q_a , with a being the spinor index, the Coleman-Mandula theorem cannot be applied and non-trivial combinations of space-time and other continuous symmetries can be constructed. In 1971 Golfand and Likhtman have shown [22] that it is possible to combine such a generator, which will be the generator of the new SUSY transformations, together with the known generators P_μ and $M_{\mu\nu}$ consistently in an algebra. The most general form of such a SUSY algebra in a consistent interacting quantum field theory was constituted 1975 by the Haag-Lopuszański-Sohnius theorem [23]. The non-trivial commutation relations between the operators Q_a , P_μ and $M_{\mu\nu}$ of such an algebra will be specified in Section 2.2.

Although originally not developed nor designed for, SUSY theories can solve some of the problems of the SM in an elegant way. The SM is a consistent, renormalizable quantum field theory, based on the gauge group $SU(3)_C \times SU(2)_L \times U(1)_Y$, that accounts for a plethora of experimental data over an energy range of over twelve orders of magnitude. Nevertheless the SM is incomplete. There are experimental as well as theoretical arguments which suggest that the SM cannot be the ultimate theory [24]. On the experimental side studies of the fluctuations in the spectrum of the relic microwave background from the Big Bang have established the existence of Cold Dark Matter in the Universe, for which there is no candidate in the SM. Observations of type Ia supernovae at large red shifts as well as the cosmic microwave

background radiation both suggest that the bulk of energy in the Universe must reside in the so-called Dark Energy, a novel form of energy which cannot be explained so far. Although gravitational effects are tiny and can be safely neglected at the level of elementary particle interactions, it is unsatisfactory from the theoretical point of view that gravity is not incorporated in the SM. Furthermore, a unification of the strong and electroweak interactions has not been achieved yet. Extrapolating the corresponding couplings to a high energy scale by using the renormalization group equations of the SM suggests that the couplings should unify but this unification is not realized completely within the SM. Another problem is related to the electroweak sector of the SM. Although the spontaneous breaking of the electroweak symmetry can be incorporated by introducing new scalar fields, this has to be done “by hand” via an arbitrary scalar potential. That means that there is no understanding of why the squared mass parameter for the Higgs field is negative.

Most of these arguments point to new physics but do not point decisively to the scale for this new physics. The so-called fine-tuning problem, which has already been mentioned in the introduction, not only suggests that there should be new physics, but also that the scale of the new physics has to be close to the electroweak scale. This fine-tuning problem is not a difficulty of the SM itself but rather an unnatural sensitivity of the Higgs potential to new physics in almost any potential extension of the SM. The electrically neutral part of the SM Higgs field is a complex scalar H with a classical potential

$$V = m_H^2 |H|^2 + \lambda |H|^4 . \quad (2.1)$$

The SM requires a non-vanishing vacuum expectation value for H at the minimum of the potential. This will occur if $\lambda > 0$ and $m_H^2 < 0$. It is known experimentally that the mass parameter m_H^2 is very roughly of order $-(100 \text{ GeV})^2$. The problem resides in m_H^2 receiving large virtual corrections from every particle that couples to the Higgs field. For example, the correction to m_H^2 from a loop based on the 4-boson self interaction yields

$$\Delta m_H^2 = \frac{\lambda}{16\pi^2} \Lambda^2 + \dots . \quad (2.2)$$

Here Λ is an ultraviolet momentum cutoff used to regularize the loop integral. It should be interpreted as at least the energy scale at which new physics enters to alter the high-energy behavior of the theory. Terms which grow at most logarithmically with Λ are neglected in this discussion. Assuming that the SM is valid up to the scale where electroweak and strong forces unify, then Λ is of the order $\sim 10^{16} \text{ GeV}$. The problem is then that the correction to m_H^2 is some 30 orders of magnitude larger than the required value of $m_H^2 \sim -(100 \text{ GeV})^2$ and an enormous amount of fine-tuning is necessary. Since quarks, leptons and the electroweak gauge bosons of the SM all obtain masses from the vacuum expectation value of the Higgs field, the entire mass spectrum of the SM is indirectly sensitive to the cutoff Λ . Not accepting this high sensitivity to new physics entering at $\Lambda \gg 1 \text{ TeV}$, a potential solution would be to assume the existence of new degrees of freedom already at the TeV scale. These new degrees of freedom must then serve to cancel the quadratic divergence. In this

context it is useful to examine the correction to m_H^2 from a loop containing a Dirac fermion f . If the Higgs field couples to f with a term in the Lagrangian $\lambda_f H \bar{f} f$, the virtual correction yields

$$\Delta m_H^2 = -\frac{\lambda_f^2}{8\pi^2} \Lambda^2 + \dots, \quad (2.3)$$

where the minus sign is due to the closed fermion loop. Comparing this equation with Eq. (2.2) suggests that the opposite signs in the fermionic and bosonic corrections could lead to the cancellation of the quadratic divergencies. However, the particle content of the SM is not sufficient and a total cancellation can only be achieved by introducing new degrees of freedom. Moreover, it is desirable to have this cancellation occur to all orders, not just at the one-loop level. In general, one would not expect this cancellation to be complete unless a relation between the couplings of fermions and bosons exists, which guarantees that

$$\lambda_f^2 = \lambda. \quad (2.4)$$

Such relations occur only due to symmetries. A symmetry which relates properties of bosons and fermions is referred to as a supersymmetry. As it will become clear later on, SUSY requires that for every boson, a fermion partner should exist, and vice versa. Apart from providing a solution to the fine-tuning problem, there are several more motivations for examining SUSY. For example by using SUSY evolution equations the extrapolation of the electroweak and strong couplings to a high energy scale can lead to a common unification point, in contrast to the SM. Furthermore, in SUSY models with conservation of a symmetry called R-parity the LSP is stable. In many scenarios this LSP is a massive, neutral and weakly interacting particle representing a suitable Dark Matter candidate. The last point which should be mentioned here, is that most SUSY models provide a dynamical electroweak symmetry breaking mechanism. Renormalization effects drive the Higgs boson squared mass parameter to negative values, while those for other scalars are left positive, resulting in the observed electroweak symmetry breaking pattern. The wide array of issues addressed by SUSY theories can be seen as hint for SUSY being realized in nature.

2.2 The Minimal Supersymmetric Extension of the SM

The MSSM [1–7], the Minimal Supersymmetric extension of the Standard Model, is minimal in the sense that the particle spectrum of the SM is only extended by the necessarily required amount of SUSY particles. Comparing Eqs. (2.2) and (2.3) in detail visualizes that each fermion of the SM needs to be paired with two complex scalars with $\lambda_f^2 = \lambda$ in order to cancel the quadratic divergencies completely. Therefore, SUSY transformations generated by the operator Q have to turn a bosonic state into a fermionic state, and vice versa:

$$Q|\text{Boson}\rangle = |\text{Fermion}\rangle \quad Q|\text{Fermion}\rangle = |\text{Boson}\rangle. \quad (2.5)$$

Since spinors are complex the hermitian conjugate of Q , Q^\dagger , is also a symmetry generator. The possible forms for such symmetries in an interacting quantum field theory are restricted by the Haag-Lopuszański-Sohnius theorem mentioned in the introduction. For theories like the SM, which have fermions whose left- and right-handed pieces transform differently under the gauge group, this theorem implies that the generators Q and Q^\dagger must satisfy an algebra of anticommuting and commuting relations of the following form:

$$\{Q_a, Q_b^\dagger\} = 2 (\sigma^\mu)_{ab} P_\mu \quad (2.6)$$

$$\{Q_a, Q_b\} = \{Q_a^\dagger, Q_b^\dagger\} = 0 \quad (2.7)$$

$$[Q_a, P_\mu] = [Q_a^\dagger, P_\mu] = 0 \quad (2.8)$$

$$[Q_a, M_{\mu\nu}] = i (\sigma_{\mu\nu})_{ab} Q_b . \quad (2.9)$$

Here, the Q_a are two-component Weyl spinors, so that $a, b = 1, 2$. The expressions $\sigma^\mu = (\mathbf{1}, \sigma^i)$, $\bar{\sigma}^\mu = (\mathbf{1}, -\sigma^i)$ and $\sigma^{\mu\nu} = \frac{i}{4}(\sigma^\mu \bar{\sigma}^\nu - \sigma^\nu \bar{\sigma}^\mu)$ are based on the Pauli matrices σ^i ($i = 1, 2, 3$). The operator P_μ is the four-momentum generator of space-time translations and the operator $M_{\mu\nu}$ is the generator of homogeneous Lorentz transformations. Together with the Poincaré algebra the Eqs. (2.6)-(2.9) constitute the Super-Poincaré algebra.

The single-particle states of a SUSY theory fall into irreducible representations of the Super-Poincaré algebra, which are called supermultiplets. Each supermultiplet contains fermions and bosons, which are the superpartners of each other. Equation (2.6) implies that the squared mass operator P^2 commutes with Q and Q^\dagger and thus, that particles inhabiting the same supermultiplet must have equal eigenvalues of P^2 and therefore equal mass. The generators Q and Q^\dagger commute also with the generators of the gauge transformations. As a consequence, particles in one supermultiplet must have equal internal quantum numbers, i.e. electric charges, weak isospin and color charges. Furthermore, it can be derived from Eqs. (2.6)-(2.9) that each supermultiplet contains an equal number of fermionic and bosonic degrees of freedom.

The simplest possibility to construct a supermultiplet with an equal number of fermionic and bosonic degrees of freedom is to combine a Weyl fermion and two real scalars. The Weyl fermion has two spin helicity states, and therefore two fermionic degrees of freedom, whereas each real scalar has one bosonic degree of freedom. These two real scalar degrees of freedom can be assembled into one complex scalar field. This combination of a two-component Weyl fermion and a complex scalar field is called a chiral supermultiplet.

The next possibility for a supermultiplet contains a spin-1 vector boson. In order to guarantee the renormalizability of the theory, this must be a massless gauge boson, at least before the gauge symmetry is spontaneously broken. A massless spin-1 boson has two helicity states and therefore two bosonic degrees of freedom. Its superpartner is a massless spin-1/2 Weyl fermion with two fermionic degrees of freedom. Gauge bosons must transform as the adjoint representation of the gauge group and so must their fermionic partners, which are called gauginos. Since the adjoint representation of the gauge group is its own conjugate, the left- and right-handed

components of the gauginos must have same gauge transformation properties. Such a combination of a spin-1/2 gaugino and spin-1 gauge boson is called a gauge supermultiplet.

In the MSSM each particle is therefore part of a chiral or a gauge supermultiplet and is paired with a superpartner which differs in spin by half a unit. Only the chiral supermultiplet can contain fermions with left- and right-handed parts transforming differently under gauge group transformations. All known fermions, the quarks and leptons of the SM, have this property and have to be assembled in chiral supermultiplets. The left- and right-handed components of quarks and leptons are separate two-component Weyl fermions, so each of them must have its own complex scalar partner. The names for these spin-0 partners are constructed by prepending an “s”. So they are called “squarks” and “sleptons”. The symbols are the same as for quarks and leptons but a tilde ($\tilde{}$) denotes the superpartners. The superpartners of the left- and right-handed parts of the squarks are thus the left- and right-handed squarks, \tilde{q}_L and \tilde{q}_R . Since squarks are spin-0 particles, the indices L and R do not refer to their helicity but to the helicity of their superpartners.

The Higgs boson as a spin-0 particle must also reside in a chiral supermultiplet. However, one supermultiplet is not enough. With only one Higgs chiral supermultiplet the electroweak gauge symmetry would suffer from a gauge anomaly. This can be avoided by introducing two Higgs supermultiplets, one with weak hypercharge $Y = +1/2$ and another one with $Y = -1/2$. Furthermore, only a $Y = +1/2$ Higgs supermultiplet can give masses to up-type quarks and only a $Y = -1/2$ Higgs supermultiplet can give masses to down-type quarks. The $SU(2)_L$ doublet with $Y = +1/2$ is denoted $H_u = (H_u^+, H_u^0)$ and the one with $Y = -1/2$ with $H_d = (H_d^0, H_d^-)$. For spin-1/2 superpartners the ending “-ino” is added to the name of the corresponding SM particle. The fermionic partners of the scalar Higgs particles are called the higgsinos and are denoted by a tilde. All chiral supermultiplets of the MSSM are summarized in Table 2.1 and classified according to their transformation properties under the SM gauge group $SU(3)_c \times SU(2)_L \times U(1)_Y$.

Table 2.2 summarizes the gauge supermultiplet of the MSSM which contain the vector bosons of the SM. The $SU(3)_C$ color gauge interaction is mediated by the gluon g whose spin-1/2 superpartner is the gluino \tilde{g} . The gauge bosons W^+, W^0, W^- and B^0 of the electroweak gauge symmetry $SU(2)_L \times U(1)_Y$ are paired with the spin-1/2 partners called winos $\tilde{W}^+, \tilde{W}^0, \tilde{W}^-$ and bino \tilde{B}^0 .

Supersymmetry breaking and mass eigenstates

The chiral and gauge supermultiplets listed in Tables 2.1 and 2.2 illustrate the particle content of the MSSM. If SUSY was an unbroken symmetry, then all SUSY particles would have the same masses as their SM partners. Such particles could not have evaded experimental detection. The fact that none of the predicted SUSY particles have been observed so far suggests that they must be heavier than the known SM particles and that SUSY must be a broken symmetry. Thus a realistic phenomenological model must contain SUSY breaking. Fortunately, it can be shown that the breaking of SUSY does not destroy the cancellation of quadratic di-

Name	Spin 0	Spin 1/2	$SU(3)_C, SU(2)_L, U(1)_Y$
Squarks, Quarks	$(\tilde{u}_L \tilde{d}_L)$	$(u_L d_L)$	$(\mathbf{3}, \mathbf{2}, \frac{1}{6})$
	\tilde{u}_R^*	\overline{u}_R	$(\bar{\mathbf{3}}, \mathbf{1}, -\frac{2}{3})$
	\tilde{d}_R^*	\overline{d}_R	$(\bar{\mathbf{3}}, \mathbf{1}, \frac{1}{3})$
Sleptons, Leptons	$(\tilde{\nu} \tilde{e}_L)$	(νe_L)	$(\mathbf{1}, \mathbf{2}, -\frac{1}{2})$
	\tilde{e}_R^*	\overline{e}_R	$(\mathbf{1}, \mathbf{1}, 1)$
Higgs, Higgsinos	$(H_u^+ H_u^0)$	$(\tilde{H}_u^+ \tilde{H}_u^0)$	$(\mathbf{1}, \mathbf{2}, +\frac{1}{2})$
	$(H_d^0 H_d^-)$	$(\tilde{H}_d^0 \tilde{H}_d^-)$	$(\mathbf{1}, \mathbf{2}, -\frac{1}{2})$

Table 2.1: Chiral supermultiplets in the MSSM. There are three families for each of the quark and lepton supermultiplets, but only the first-family representatives are presented.

Name	Spin 1/2	Spin 1	$SU(3)_C, SU(2)_L, U(1)_Y$
Gluino, Gluon	\tilde{g}	g	$(\mathbf{8}, \mathbf{1}, 0)$
Winos, W-Bosons	$\tilde{W}^\pm \tilde{W}^0$	$W^\pm W^0$	$(\mathbf{1}, \mathbf{3}, 0)$
Bino, B-Bosons	\tilde{B}^0	B^0	$(\mathbf{1}, \mathbf{1}, 0)$

Table 2.2: Gauge supermultiplets in the MSSM.

vergences mentioned in the introduction of this chapter. If SUSY is explicitly broken due to scalar masses differing from their fermion counter parts, no new quadratic divergences occur [24]. From a theoretical point of view it is appealing to consider that, like electroweak gauge symmetry, SUSY is broken spontaneously. Many models of spontaneous SUSY breaking have been proposed [25–33]. However, the exact mechanism of spontaneous SUSY breaking is unknown, therefore it is useful to parametrize this ignorance by introducing so-called soft SUSY breaking terms in the effective MSSM Lagrangian [34]. The denotation “soft” refers to terms of positive mass dimension. Based on the fine-tuning problem, it has been illustrated in the introduction of this chapter that by introducing two complex scalar fields for every SM fermion quadratic divergencies can be canceled. In particular, this cancellation can only be done when the relation $\lambda_f^2 = \lambda$ between the coupling constants holds. SUSY breaking terms with positive mass dimension ensure that this relation is fulfilled and a broken SUSY still provides a solution to the fine-tuning problem. This means, that the effective MSSM Lagrangian can be written as

$$\mathcal{L} = \mathcal{L}_{\text{SUSY}} + \mathcal{L}_{\text{soft}} . \quad (2.10)$$

Name	Spin	Gauge Eigenstates	Mass Eigenstates
Squarks	0	$\tilde{u}_L \tilde{u}_R \tilde{d}_L \tilde{d}_R$ $\tilde{s}_L \tilde{s}_R \tilde{c}_L \tilde{c}_R$ $\tilde{t}_L \tilde{t}_R \tilde{b}_L \tilde{b}_R$	$\tilde{u}_L \tilde{u}_R \tilde{d}_L \tilde{d}_R$ $\tilde{s}_L \tilde{s}_R \tilde{c}_L \tilde{c}_R$ $\tilde{t}_1 \tilde{t}_2 \tilde{b}_1 \tilde{b}_2$
Higgs bosons	0	$H_u^0 H_d^0 H_u^+ H_d^-$	$h^0 H^0 A^0 H^\pm$
Neutralinos	1/2	$\tilde{B}^0 \tilde{W}^0 \tilde{H}_u^0 \tilde{H}_d^0$	$\tilde{\chi}_1^0 \tilde{\chi}_2^0 \tilde{\chi}_3^0 \tilde{\chi}_4^0$
Charginos	1/2	$\tilde{W}^+ \tilde{W}^- \tilde{H}_u^+ \tilde{H}_d^-$	$\tilde{\chi}_1^+ \tilde{\chi}_1^- \tilde{\chi}_2^+ \tilde{\chi}_2^-$
Gluino	1/2	\tilde{g}	\tilde{g}

Table 2.3: Gauge and mass eigenstates of SUSY particles relevant for this thesis.

All gauge and Yukawa interactions are contained in $\mathcal{L}_{\text{SUSY}}$ which is invariant under SUSY transformations, whereas $\mathcal{L}_{\text{soft}}$ breaks SUSY but includes only terms with positive mass dimension.

The superpartners listed in Tables 2.1 and 2.2 are not necessarily the mass eigenstates of the theory. Due to the effects of electroweak symmetry breaking the higgsinos and electroweak gauginos with same electric charges mix with each other, and so do the scalar Higgs particles. Furthermore, the squarks and sleptons, respectively, with same electric charge and color quantum number can mix with each other. Just the gluino, being the only color octet fermion, cannot mix with any other particle of the MSSM.

In the first part of this thesis the decay of a top squark into a charm quark and the so-called neutralino is calculated at one-loop level with charged particles in the loops. The second part contains the calculation of NLO corrections in SUSY QCD for squark pair production. Table 2.3 gives an overview of the gauge eigenstates and the corresponding mass eigenstates relevant for these calculations.

With arbitrary soft terms the mass eigenstates of the squarks should be obtained by diagonalizing two 6×6 matrices, one for the up-type squarks and one for the down-type squarks. However, most of the SUSY breaking models assume flavor-blind soft terms and predict that most of the mixing angles are small. In particular, mixing angles between squarks of different generations are suppressed. Furthermore Yukawa interactions of the first two generations can be neglected, since they are proportional to the fermion masses. With these assumptions left-right mixing is only taken into account in the third generation of the squarks. Therefore, the mass eigenstates of the first two generations of squarks are assumed to be identical with the gauge eigenstates, but the mass eigenstates of the third generation squarks differ from the gauge eigenstates and are therefore denoted \tilde{t}_1, \tilde{t}_2 and \tilde{b}_1, \tilde{b}_2 .

Within the SM with just one complex Higgs doublet a single neutral spin zero particle, the Higgs boson, is left in the spectrum as a relic of the spontaneous breakdown

of the electroweak symmetry. This is because the charged component of the doublet and one of the neutral components are the three would-be Goldstone bosons which become the longitudinal components of the W^\pm and Z^0 bosons after electroweak symmetry breaking. Since the symmetry breaking pattern of the MSSM is the same as the one of the SM, the same set of would-be Goldstone bosons is expected. However, since now two sets of complex doublets are available, two charged, H^+ and H^- , and three neutral spin zero bosons, h^0 , H^0 and A^0 , remain in the physical spectrum of the MSSM.

Mass eigenstates due to the mixing of the neutral higgsinos and gauginos are called neutralinos. The diagonalization of the corresponding 4×4 mass matrix for the four fields $(\tilde{B}^0, \tilde{W}^0, \tilde{H}_u^0, \tilde{H}_d^0)$ yields the four neutralino mass eigenstates denoted by $\tilde{\chi}_i^0$ ($i = 1, 2, 3, 4$). By convention, they are labeled in ascending order, so that $m_{\tilde{\chi}_1^0} < m_{\tilde{\chi}_2^0} < m_{\tilde{\chi}_3^0} < m_{\tilde{\chi}_4^0}$.

Finally, charginos are the mass eigenstates based on the mixing of the charged higgsinos and winos. In the basis of these four eigenstates $(\tilde{W}^+, \tilde{H}_u^+, \tilde{W}^-, \tilde{H}_d^-)$, the 4×4 mass matrix can be diagonalized by means of two unitary 2×2 matrices leading to two negatively charged mass eigenstates $\tilde{\chi}_{1,2}^-$ and two positively charged mass eigenstates $\tilde{\chi}_{1,2}^+$ with mass conventions $m_{\tilde{\chi}_1^\pm} < m_{\tilde{\chi}_2^\pm}$.

This concludes the general presentation of theoretical aspects of SUSY relevant for this thesis. Detailed expressions for the MSSM Lagrangian and the soft SUSY breaking terms can be found in [35]. Specific details needed for the discussion of the calculation of the stop decay and the squark pair production process will be given in the corresponding Chapters 4 and 5.

2.3 Experimental Searches

Experimental searches for SUSY particles have been performed in the past in a variety of different channels at various accelerators, such as the Large Electron Positron collider located at CERN near Geneva, and the Tevatron proton-antiproton collider at Fermilab, without finding any of these particles. The LHC, which is currently running at a center-of-mass energy of 8 TeV, allows for searches at higher energies and therefore in a wider range of the SUSY parameter space than has been possible so far.

In most of these searches SUSY models with conserved R-parity are assumed. This symmetry is introduced in order to prevent the occurrence of baryon and lepton number violating processes which are severely constrained experimentally, in particular by the non-observation of the proton decay. All SM particles have R-parity of 1, while SUSY partners have R-parity -1 . R-parity conservation thus implies that SUSY particles are produced in pairs and that the LSP is stable. In a large fraction of the SUSY parameter space, the LSP is the weakly interacting lightest neutralino, $\tilde{\chi}_1^0$. This gives rise to the typical SUSY signature of missing transverse momentum with a magnitude denoted by E_T^{miss} . Since no excess above the SM expectation is observed, limits on the SUSY particle masses are derived. As it is impossible to cover the entire SUSY parameter space the sensitivity of the searches is estimated

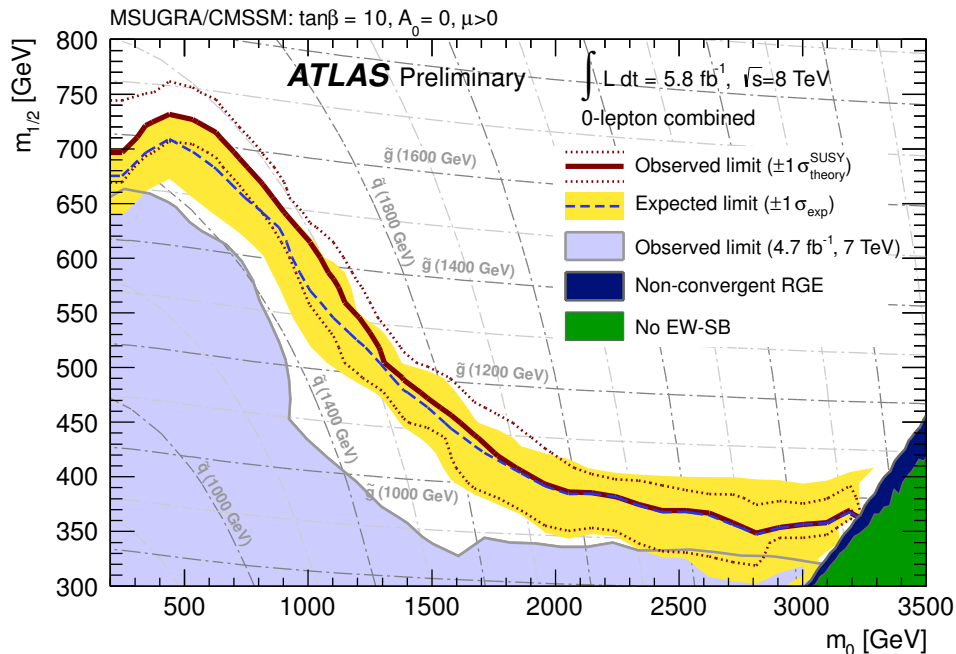


Figure 2.1: Exclusion limits from the ATLAS experiment derived from an analysis of final states with jets and missing transverse momentum for mSUGRA models with $\tan\beta = 10$, $A_0 = 0$ and $\mu_h > 0$ presented in the $m_0 - m_{1/2}$ plane [16].

in the framework of a specific SUSY theory or in simplified models. The model used throughout the thesis is the so-called “Minimal Supergravity” (mSUGRA) model [27–30]. It is defined in terms of a small number of parameters which can be interpreted as boundary conditions on all parameters at a high energy scale. These parameters are given by common soft SUSY breaking scalar and gaugino masses, m_0 and $m_{1/2}$, a common SUSY breaking trilinear coupling A_0 , the ratio of the two vacuum expectation values $\tan\beta$ of the two Higgs doublets and the sign of the Higgsino parameter μ_h .

In the following two sections the current status of searches for squarks of the first two generations and for the top squark, the SUSY particles most relevant for this thesis, is briefly summarized.

2.3.1 Searches for the First Two Generations of Squarks

Heavy colored particles like squarks and gluinos have the largest SUSY production cross sections at the LHC and are thus candidates for the most inclusive searches for SUSY. The production of gluinos and squarks of the first two generations proceeds via $pp \rightarrow \tilde{q}\tilde{q}, \tilde{q}\tilde{q}^*, \tilde{q}\tilde{g}, \tilde{g}\tilde{g}$. These squarks and gluinos decay in cascades to the lightest neutralino $\tilde{\chi}_1^0$. Therefore, event topologies with multiple jets are expected. When gluinos are produced in the decay chain, leptons can be present via the decays into virtual W and Z bosons. The most inclusive searches for SUSY are therefore based on the presence of multiple jets, one or more leptons, and missing transverse

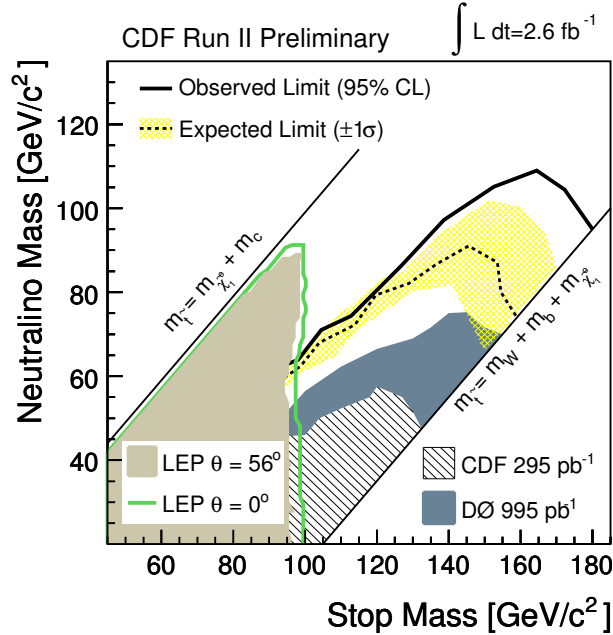


Figure 2.2: Exclusion limits from the CDF and D0 experiments derived from analyses of final states with two charm jets and missing transverse momentum presented in the $m_{\tilde{t}_1} - m_{\tilde{\chi}_1^0}$ plane [36, 37].

momentum. At the moment, the most stringent limits for squark and gluino masses come from an analysis of final states containing jets, missing transverse momentum and no leptons [16]. Limits derived in the mSUGRA model are presented in Fig. 2.1 in the $m_0 - m_{1/2}$ plane. The observed limits are indicated by the dark red curves, where the solid contour represents the nominal limit, and the dotted lines are obtained by including theoretical and PDF uncertainties and imply that squarks and gluinos of roughly equal mass are excluded for masses below 1500 GeV.

2.3.2 Searches for the Top Squark

The large mixing effects in the third generation of squarks, already mentioned in Section 2.2, necessitate dedicated search strategies. In this thesis the decay $\tilde{t}_1 \rightarrow c\tilde{\chi}_1^0$ is calculated, which is only dominant for very light stops \tilde{t}_1 and for small mass differences $m_{\tilde{t}_1} - m_{\tilde{\chi}_1^0}$. The cross section for producing a pair of third generation squarks is much smaller than that for producing first generation squarks, since no “flavor excitation” contributions exist for third generation squarks. Additionally, in \tilde{t}_1 pair production followed by the decay $\tilde{t}_1 \rightarrow c\tilde{\chi}_1^0$ the charm jets only become energetic enough to look for a di-jet plus E_T^{miss} signature for a sufficiently large mass splitting between the stop and the lightest neutralino. At the LHC no analysis investigating this decay channel has been published so far. LHC searches for light stops consider the mass hierarchy $m_{\tilde{t}_1} > m_{\tilde{\chi}_1^\pm} + m_b$ and a \tilde{t}_1 decaying exclusively via $b + \tilde{\chi}_1^\pm$ [17]. In these searches \tilde{t}_1 masses in the range 112 – 140 GeV for $\tilde{\chi}_1^0$ masses

up to 80 GeV are excluded. However, the Tevatron experiments, CDF and D0, were sensitive to mass splittings $m_{\tilde{t}_1} - m_{\tilde{\chi}_1^0}$ above 40 GeV in the channel with \tilde{t}_1 pair production with subsequent decay into $\tilde{t}_1 \rightarrow c + \tilde{\chi}_1^0$ [36, 37]. Figure 2.2 presents the results of the CDF and D0 experiments in terms of exclusion limits in the $m_{\tilde{t}_1} - m_{\tilde{\chi}_1^0}$ plane assuming $\text{BR}(\tilde{t}_1 \rightarrow c + \tilde{\chi}_1^0) = 1$. Stop masses up to 180 GeV for a neutralino mass of 90 GeV are excluded, however for $\tilde{\chi}_1^0$ masses above 90 GeV light stops \tilde{t}_1 at least in the mass range 100 – 130 GeV are still allowed.

Chapter 3

Calculational Concepts

3.1 Hadronic Collisions

At the LHC two beams of protons¹ travel in opposite directions inside the circular accelerator. By colliding the two beams head-on scattering processes and the particles created in the collisions can be investigated. The hadronic cross section for a process in which two protons with momenta P_1 and P_2 collide, leading to m particles in the final state with momenta k_1, \dots, k_m , is given in the so-called parton model [38] by

$$\begin{aligned} \sigma^{\text{had}}(P(P_1) P(P_2) \rightarrow k_1, \dots, k_m) = & \quad (3.1) \\ \sum_{a,b} \int_0^1 \int_0^1 dx_a dx_b f_a^P(x_a) f_b^P(x_b) \sigma(a(p_1 = x_a P_1) b(p_2 = x_b P_2) \rightarrow k_1, \dots, k_m) . \end{aligned}$$

Here f_a^P , the parton distribution function (PDF) of parton a , denotes the probability of finding a parton a with momentum fraction x_a inside the proton P . The sum runs over all partons, which contribute to the partonic cross section σ , i.e. the gluon and (anti-)quarks in this thesis. The partonic cross section can be calculated in perturbation theory up to a given order by evaluating matrix elements squared, which have a diagrammatic representation in terms of Feynman graphs, multiply them with the flux factor of the incoming partons and integrate over the whole phase space of the final state particles:

$$\sigma = \int \frac{1}{4 p_1 p_2} |M(p_1 + p_2 \rightarrow k_1, \dots, k_m)|^2 \quad (3.2)$$

$$(2\pi)^4 \delta^{(4)} \left(p_1 + p_2 - \sum_{i=1}^m k_i \right) \frac{d^3 \mathbf{k}_1}{(2\pi)^3 2E_1} \cdots \frac{d^3 \mathbf{k}_m}{(2\pi)^3 2E_m} . \quad (3.3)$$

¹or lead ions, however lead ion collisions are not subject of this thesis

In this thesis the squark pair production cross section in the perturbative series in the strong coupling constant α_s up to next-to-leading order in the framework of SUSY QCD is calculated, i.e.

$$\sigma = \sigma^{\text{LO}} + \sigma^{\text{NLO}} . \quad (3.4)$$

The NLO corrections suffer from ultraviolet (UV) and infrared (IR) divergencies. The former are due to large momentum contributions to loop diagrams and the latter arise either in loop diagrams with virtual massless particles or in soft and collinear emissions of additional partons. The UV divergencies are canceled in the so-called renormalization procedure, which will be introduced in Section 3.2. According to the Kinoshita-Lee-Nauenberg (KLN) theorem [39, 40] IR divergencies cancel in the total result when sufficiently inclusive observables are taken into account. However, the IR singularities associated with initial state collinear radiation spoil the KLN cancellations since the initial state in Eq. (3.1) is fully determined. Fortunately, it has been shown that the factorization of these singularities is universal [41]. Therefore, they can be absorbed into a process-independent redefinition of the PDFs at the price of introducing an unphysical factorization scale μ_F in the partonic cross section and in the PDFs. In principle, the hadronic cross section should be independent of μ_F . However, the values of the PDFs cannot be calculated perturbatively but are extracted from experimental data via fits to fixed-order perturbative predictions. As a consequence, a dependence on an a priori arbitrary scale remains. The dynamical evolution of the PDFs with respect to this scale is yet again governed by perturbation theory in form of the Dokshitzer-Gribov-Lipatov-Altarelli-Parisi evolution equations [42–44]. When applying these equations to determine $f_a^P(x_a, Q^2)$, the PDF at a scale Q , for a given initial distribution $f_a^P(x_a, \mu_F^2)$, the leading logarithms $\alpha_s^n \log^n(Q^2/\mu_F^2)$ are resummed to all orders of perturbation theory. These logarithms can be sizable if the factorization scale μ_F is considerably different from the characteristic scale Q of the process under investigation. Therefore, if μ_F is set to the characteristic scale Q , the effect of these logarithms on the NLO prediction is not artificially enhanced.

3.2 Renormalization

The Lagrangian of the MSSM involves several free parameters like masses, couplings, mixing angles etc., which have to be determined experimentally. These are chosen such that they have an intuitive physical meaning at tree level which means that they are directly related to experimental quantities. Unfortunately, higher order corrections destroy this direct relation. The parameters of the original Lagrangian, the so-called bare parameters, differ from the corresponding physical quantities by UV divergent contributions. However, in renormalizable theories these divergencies cancel in physical quantities, thus allowing meaningful predictions. The renormalizability of non-abelian gauge theories with spontaneous symmetry breaking, like the MSSM, was proven by 't Hooft [45, 46].

In the counterterm approach the UV divergent bare parameters are expressed by finite renormalized parameters and divergent renormalization constants, the counterterms. In addition, the bare fields are replaced by renormalized fields. The counterterms are fixed by renormalization conditions which can be chosen arbitrarily but determine the relation between renormalized and physical parameters. The splitting of bare parameters into renormalized parameters and renormalization constants induces a splitting of the bare Lagrangian into a renormalized and a counterterm Lagrangian:

$$\mathcal{L}_0 = \mathcal{L} + \delta\mathcal{L} . \quad (3.5)$$

The renormalized Lagrangian \mathcal{L} has the same form as \mathcal{L}_0 but depends on renormalized parameters and fields instead of unrenormalized ones. The counterterm Lagrangian $\delta\mathcal{L}$ contains the counterterms and gives rise to counterterm diagrams which have to be added to the loop diagrams. Including the counterterm diagrams the renormalized one-particle irreducible two-point functions $\hat{\Gamma}$ can be obtained. For squarks, quarks and gluinos these are defined as

$$\hat{\Gamma}_{ij}^{\tilde{q}}(k^2) = i (k^2 - m_{\tilde{q}_i}^2) \delta_{ij} + i \hat{\Sigma}_{ij}^{\tilde{q}}(k^2) \quad (3.6)$$

$$\begin{aligned} \hat{\Gamma}_{ij}^q(k^2) &= i (\not{k} - m_{q_i}) \delta_{ij} \\ &+ i \left[\not{k} \hat{\Sigma}_{ij}^{q,L}(k^2) \mathcal{P}_L + \not{k} \hat{\Sigma}_{ij}^{q,R}(k^2) \mathcal{P}_R + m_{q_i} \hat{\Sigma}_{ij}^{q,Ls}(k^2) \mathcal{P}_L + m_{q_j} \hat{\Sigma}_{ij}^{q,Rs}(k^2) \mathcal{P}_R \right] \end{aligned} \quad (3.7)$$

$$\begin{aligned} \hat{\Gamma}_{\tilde{g}\tilde{g}}(k^2) &= i (\not{k} - m_{\tilde{g}}) \\ &+ i \left[\not{k} \Sigma_{\tilde{g}\tilde{g}}^L(k^2) \mathcal{P}_L + \not{k} \Sigma_{\tilde{g}\tilde{g}}^R(k^2) \mathcal{P}_R + m_{\tilde{g}} \Sigma_{\tilde{g}\tilde{g}}^{Ls}(k^2) \mathcal{P}_L + m_{\tilde{g}} \Sigma_{\tilde{g}\tilde{g}}^{Rs}(k^2) \mathcal{P}_R \right] \\ &= i (\not{k} - m_{\tilde{g}}) + i \left[\not{k} \hat{\Sigma}_{\tilde{g}\tilde{g}}(k^2) + m_{\tilde{g}} \hat{\Sigma}_{\tilde{g}\tilde{g}}^S(k^2) \right] , \end{aligned} \quad (3.8)$$

where \mathcal{P}_L and \mathcal{P}_R are chirality projectors. In the two-point function of the gluino, $\hat{\Gamma}_{\tilde{g}\tilde{g}}(k^2)$, it has been exploited that in the case of Majorana fermions the vector and scalar parts of the self energy can be combined. The counterterms can be chosen such that the finite renormalized parameters keep their intuitive physical meaning. This is the case in the so-called on-shell renormalization scheme [47, 48], which is used in this thesis for the renormalization of masses and fields. The renormalization conditions in this scheme are given by [49]

$$\widetilde{\text{Re}} \hat{\Gamma}_{ij}^{\tilde{q}}(m_{\tilde{q}_i}^2) = 0 \quad (3.9)$$

$$\lim_{k^2 \rightarrow m_{\tilde{q}_i}^2} \frac{1}{k^2 - m_{\tilde{q}_i}^2} \widetilde{\text{Re}} \hat{\Gamma}_{ii}^{\tilde{q}}(k^2) = i \quad (3.10)$$

$$\widetilde{\text{Re}} \hat{\Gamma}_{ij}^q(k^2) u_j(k)|_{k^2=m_{q_j}^2} = 0 \quad (3.11)$$

$$\lim_{k^2 \rightarrow m_{q_i}^2} \frac{\not{k} + m_{q_i}}{k^2 - m_{q_i}^2} \widetilde{\text{Re}} \hat{\Gamma}_{ii}^q(k^2) u_i(k) = i u_i(k) \quad (3.12)$$

$$\widetilde{\text{Re}} \hat{\Gamma}_{\tilde{g}\tilde{g}}(k^2) u(k)|_{k^2=m_{\tilde{g}}^2} = 0 \quad (3.13)$$

$$\lim_{k^2 \rightarrow m_{\tilde{g}}^2} \frac{\not{k} + m_{\tilde{g}}}{k^2 - m_{\tilde{g}}^2} \widetilde{\text{Re}} \hat{\Gamma}_{\tilde{g}\tilde{g}}(k^2) u(k) = i u(k) . \quad (3.14)$$

Here, the $u(k)$ are the spinors of the external particles and $\widetilde{\text{Re}}$ takes the real part of the loop integrals appearing in the self energies but not of potential complex parameters. These conditions ensure that the real parts of the poles of the propagators are given by the mass parameters of the Lagrangian, which are therefore the physical particle masses. Furthermore, they state that the renormalized one-particle irreducible two-point functions are diagonal if the external lines are on their mass shell and that the renormalized fields are properly normalized, i.e. that the residues of the renormalized propagators are equal to one.

For the remaining renormalization of the strong coupling constant as well as the quark and squark mixing matrices the $\overline{\text{MS}}$ -scheme [50] is used. In this scheme only the UV divergent terms together with some accompanying constants are included in the renormalization constants. Details concerning the renormalization of the mixing matrices are given in Chapter 4.3.1, whereas the procedure for the strong coupling constant is described in Chapter 5.3.

3.3 The Catani-Seymour Subtraction Formalism

The full NLO cross section for hadronic collisions receives contributions from real emissions of one additional parton as well as from virtual corrections. The former have to be evaluated in an $(m + 1)$ -particle phase space the latter in an m -particle phase space

$$\sigma^{NLO} = \int d\Phi_{m+1} d\sigma^R + \int d\Phi_m d\sigma^V, \quad (3.15)$$

where $d\sigma^R$ denotes the differential cross section for the real emissions and $d\sigma^V$ the one for the virtual corrections. Both integrals are separately IR divergent, although their sum is finite in inclusive physical observables due to the Kinoshita-Lee-Nauenberg theorem [39, 40]. Technically this causes difficulties for a numerical evaluation as the cancellation happens between phase spaces of different multiplicities. A standard algorithm in numerical calculations to keep track and deal with IR divergencies, which are regularized by dimensional regularization [51] (i.e. in $D = 4 - 2\epsilon$ dimensions), is the Catani-Seymour dipole formalism [52, 53]. The idea is to subtract a counterterm in one part of the calculation and add it back in another which leaves the total result unchanged:

$$\sigma^{NLO} = \int d\Phi_{m+1} [(d\sigma^R)_{\epsilon=0} - (d\sigma^A)_{\epsilon=0}] + \int d\Phi_m \left[d\sigma^V + \int d\Phi_1 d\sigma^A \right]_{\epsilon=0}. \quad (3.16)$$

This differential counterterm $d\sigma^A$ is an approximation of the differential real emission cross section $d\sigma^R$ in the sense that it has the same singular behavior. This means that $d\sigma^A$ acts as a local counterterm for $d\sigma^R$ and the difference of these two terms can be integrated numerically in four dimensions over the whole phase space. The subtracted term has to be added again and needs to be integrated together with the virtual contributions over the m -particle phase space. This is only possible if the integration of this term over the one-particle subspace can be performed analytically.

Then the poles can be extracted and canceled analytically against the poles from the virtual contributions. The remaining integration over the m -particle phase space can be carried out numerically.

The explicit form of $d\sigma^A$ is constructed from the knowledge about the soft and collinear structure of QCD amplitudes. They exhibit a simple factorization for collinear singularities. As a consequence, the counterterm is obtained as a sum over potentially collinear partons, the so-called *emitter pairs*. For soft singularities, however, only color-ordered amplitudes exhibit a simple factorization, which implies in general non-trivial color correlations. These color correlations are reflected by the reference to an additional, so-called *spectator* parton. The subtraction term is thus written schematically as a sum of individual dipoles, in the following form:

$$d\sigma^A = \sum_{\text{dipoles}} dV_{\text{dipole}} \otimes d\sigma^B . \quad (3.17)$$

Here, dV_{dipole} stands for the dipole factors which match the singular behaviour of $d\sigma^R$, whereas $d\sigma^B$ denotes the corresponding color projection of the Born-level cross section based on the so-called color linked Born amplitude squared (CLBS)

$$d\sigma^B \sim \left| \mathcal{M}_{m;a,b}^{I,J} \right|^2 . \quad (3.18)$$

This reduced Born amplitude is obtained by eliminating the additionally emitted parton from the real emission process. The color correlation between the emitter (I) and the spectator (J) parton is incorporated by inserting the color charge operators \mathbf{T}_I and \mathbf{T}_J associated with the emission of a gluon (with color index c). These color charges act on the color space of the reduced amplitude:

$$\begin{aligned} \left| \mathcal{M}_{m;a,b}^{I,J} \right|^2 &\equiv \quad m;a,b \langle 1, \dots, m; a, b \mid \mathbf{T}_I \cdot \mathbf{T}_J \mid 1, \dots, m; a, b \rangle_{m;a,b} \\ &= \frac{1}{n_c(a)n_c(b)} \left[\mathcal{M}_{m;a,b}^{a_1 \dots b_I \dots b_J \dots}(p_1, \dots, p_m; p_a, p_b) \right]^* T_{b_I a_I}^c T_{b_J a_J}^c \\ &\quad \mathcal{M}_{m;a,b}^{a_1 \dots a_I \dots a_J \dots}(p_1, \dots, p_m; p_a, p_b) . \end{aligned} \quad (3.19)$$

Here, a_i and b_i are color indices, p_1, \dots, p_m denote the momenta of the final and p_a, p_b the momenta of the initial state particles. Averaging over initial state colors introduces a factor of $1/n_c(a)n_c(b)$ for the initial state partons a and b carrying $n_c(a)$ and $n_c(b)$ colors. After the action of the color charge operators on the color space, the color charge matrices read

- for final state partons

$$T_{ba}^c = if_{bca} \quad \text{if the emitting parton is a gluon or gluino}$$

$$T_{\beta\alpha}^c = \begin{cases} t_{\beta\alpha}^c & \text{if the emitting parton is a (s)quark} \\ -t_{\alpha\beta}^c & \text{if the emitting parton is an anti-(s)quark} \end{cases}$$

- for initial state partons

$$T_{ba}^c = if_{bca} \quad \text{if the emitting parton is a gluon or gluino}$$

$$T_{\beta\alpha}^c = \begin{cases} -t_{\alpha\beta}^c & \text{if the emitting parton is a quark} \\ t_{\beta\alpha}^c & \text{if the emitting parton is an anti-quark} \end{cases} . \quad (3.20)$$

Here, $\alpha, \beta = 1, 2, 3$ are the indices of the fundamental and $a, b, c = 1, \dots, 8$ the indices of the adjoint representation. The color algebra relations needed in order to evaluate the products of these matrices in the color linked Born squared amplitudes are listed in Appendix A.

With an appropriate choice of dipoles the counterterm $d\sigma^A$ can be integrated analytically over the one-parton phase space

$$\int d\Phi_{m+1} d\sigma^A = \int d\Phi_m [d\sigma^B \otimes \mathbf{I}] + \int_0^1 dx \int d\Phi_m [d\sigma^B \otimes (\mathbf{P} + \mathbf{K})(x)] . \quad (3.21)$$

This integration yields the factor \mathbf{I} , which contains all the ϵ poles that are necessary to cancel the poles in the virtual contributions $d\sigma^V$, and additional singular terms, which are reabsorbed into the non-perturbative PDFs mentioned in Section 3.1. The last term in Eq. (3.21) is thus the (in four dimensions) finite collinear remainder which is left after initial state collinear singularities have been factorized into the PDFs. The functions \mathbf{P} and \mathbf{K} are finite in the limit $\epsilon \rightarrow 0$ and depend on the longitudinal momentum fraction x . The convolution of the Born-type cross section $d\sigma^B$ with the x -dependent functions \mathbf{P} and \mathbf{K} leads to an additional integration over x in the calculation of the finite collinear remainder. The final result of the subtraction procedure for the NLO cross section is hence given in terms of

$$\begin{aligned} \sigma^{NLO} &= \int d\Phi_{m+1} \left[(d\sigma^R)_{\epsilon=0} - \left(\sum_{\text{dipoles}} dV_{\text{dipole}} \otimes d\sigma^B \right)_{\epsilon=0} \right] \\ &+ \int d\Phi_m [d\sigma^V + d\sigma^B \otimes \mathbf{I}]_{\epsilon=0} + \int_0^1 dx \int d\Phi_m [d\sigma^B \otimes (\mathbf{P} + \mathbf{K})(x)]_{\epsilon=0} . \end{aligned} \quad (3.22)$$

This formalism has been applied to the calculation of squark pair production in hadronic collisions $pp \rightarrow \tilde{q}_i \tilde{q}_j$. Details concerning the expressions for the dipoles, the integrated dipoles and the finite collinear remainder are presented in Chapters 5.4 and 5.5.

Chapter 4

Light Stop Decay in the MSSM with Minimal Flavor Violation

4.1 Introduction

The predictions made by the SM are not only in excellent agreement with electroweak precision data but also show remarkable consistency with precision measurements in the quark flavor sector. These limits and constraints from K , D and B meson studies on flavor changing neutral currents (FCNC) have very strong implications [54–56]: The observed amount of flavor violation can be perfectly described by the Cabibbo-Kobayashi-Maskawa (CKM) mechanism of the SM. In that sense, possible New Physics beyond the SM cannot contain much more flavor violation than the SM. Contributions to flavor violation from New Physics at the TeV scale must be strongly suppressed and thus models with a generic flavor structure are forbidden. One of the best studied examples in this context is given by SUSY. However, the MSSM has in general many new flavor violating sources. This so-called New Physics Flavor Problem is solved if the model is subject to the principle of Minimal Flavor Violation (MFV) [57–60]. The MFV framework provides a solution, which leads to agreement with the precision measurements, by requiring that all flavor changing transitions are governed by the CKM matrix of the SM. Flavor mixing is then always proportional to the off-diagonal elements of the CKM matrix. As a consequence, no flavor changing neutral currents occur at tree level at the scale where this MFV condition is imposed.

In supergravity models MFV arises naturally, as these models provide flavor independent scalar mass terms at a high scale like the Planck scale M_P . In most of these models the lighter stop mass eigenstate \tilde{t}_1 is significantly lighter than the other squarks. If SUSY breaking is transmitted to the visible sector at some high scale, contributions from the large top Yukawa coupling to the renormalization group equations (RGE) tend to reduce the stop mass relative to the masses of the first generation squarks [24, 35]. This is even the case when all squarks have a common

mass at the SUSY breaking scale. Furthermore, the mixing between the weak eigenstates \tilde{t}_L and \tilde{t}_R is proportional to the mass of the top quark, and leads therefore to a large mass splitting between the stop mass eigenstates. This mixing will further reduce the mass of the lighter eigenstate. In scenarios with a very light stop and a small mass difference between this stop and the lightest neutralino $\tilde{\chi}_1^0$, which is assumed to be the LSP, the decay channels $\tilde{t}_1 \rightarrow b\tilde{\chi}_1^0 W$ and $\tilde{t}_1 \rightarrow t\tilde{\chi}_1^0$ are kinematically closed. Since the four-body decay $\tilde{t}_1 \rightarrow l\nu_l b\tilde{\chi}_1^0$ is strongly suppressed due to phase space, the two-body decay $\tilde{t}_1 \rightarrow c\tilde{\chi}_1^0$ is the dominant decay mode. With its $\tilde{t}_1 \rightarrow c$ transition, this FCNC decay is forbidden at tree level in the MFV framework. It is therefore mediated via one-loop diagrams with charged particles in the loops.

From the phenomenological point of view there are several reasons to be interested in light stops. In the context of the MSSM light stops are a necessary condition for successful electroweak baryogenesis, which requires a stop mass with about the top mass value or less [61–63]. One of the main motivations, as presented in Chapter 2.1, for postulating the existence of superparticles, has been to stabilize the electroweak hierarchy against radiative corrections. Since no signal of strongly interacting superparticles has been found yet at the LHC [16, 17], quite stringent bounds on their masses have been derived, leading to some tension with the fine-tuning argument. However, to one-loop order essentially only third generation (s)quarks contribute to the loop corrections to Higgs mass parameters. Thus with a light stop SUSY would still provide a solution to the fine-tuning problem. Recent studies, discussing the consequences of the potential discovery of the Higgs boson for the MSSM, point out that light stop scenarios are among the few regimes of the MSSM which are still allowed by all present experimental constraints [64] and that the hints for deviations from a SM-like Higgs boson can be explained best by an extremely mixed stop sector [65, 66].

Moreover, it has been shown that assuming $\tilde{t}_1 \rightarrow c\tilde{\chi}_1^0$ being the dominant decay mode, light stops can be discovered at the LHC, either based on the associate production of a $\tilde{t}_1\tilde{t}_1^*$ pair with a $b\bar{b}$ pair [67] or based on stop pair production in association with one hard jet [68, 69]. Finally, long stop lifetimes induced by the CKM-suppressed decay $\tilde{t}_1 \rightarrow c\tilde{\chi}_1^0$ can be exploited to test MFV. The flavor suppression needed for secondary vertices is unique to MFV models. By measuring the stop lifetime information on the size of the flavor changing coupling can be extracted under certain circumstances [70, 71].

Some time ago an approximate calculation of the FCNC decay $\tilde{t}_1 \rightarrow c\tilde{\chi}_1^0$ was provided [18]. The authors have assumed a vanishing tree level $\tilde{t}_1 - c - \tilde{\chi}_1^0$ coupling at the Planck scale and hence calculated the loop-induced decay. The UV divergencies have been subtracted by a soft counterterm at the Planck scale leading to a large logarithm $\log(M_P^2/M_W^2)$ at the weak scale, which has been set to the W mass M_W in their calculation. It has been argued that in view of this large logarithm the remaining non-logarithmic part of the one-loop diagrams can be neglected. As a consequence, their result for the decay width takes a rather simple form.

In the following the complete one-loop calculation of the FCNC decay $\tilde{t}_1 \rightarrow c\tilde{\chi}_1^0$ in the framework of MFV is presented [72]. The full renormalization program is

performed and the “finite”, i.e. non-logarithmic, terms arising from the loop integrals are kept. This procedure allows for the study of the importance of the neglected non-logarithmic pieces in the previous work.

To get a reliable result, the appearing large logarithms should be resummed. This corresponds to solving RGEs for the scalar soft SUSY breaking squark masses. However, the hypothesis of MFV is not renormalization group invariant [59]. Even though MFV is imposed at one scale, at any other scale FCNC couplings will be generated through renormalization group (RG) evolution. Since the weak interactions affect the squark and quark mass matrices differently, these matrices cannot be diagonalized simultaneously anymore and the stop state receives an admixture from the charm squark [73]. This induces a FCNC tree level coupling between $\tilde{t}_1 - c - \tilde{\chi}_1^0$ at any other scale than the scale μ_{MFV} of the MFV hypothesis. The RGE solution can be expanded in powers of the coupling constant α and written symbolically as

$$\alpha (A_1 \log + A_0) + \alpha^2 (B_2 \log^2 + B_1 \log + B_0) + \alpha^3 (C_3 \log^3 + \dots) + \mathcal{O}(\alpha^4) . \quad (4.1)$$

From this point of view, the logarithmic piece of our one-loop result is equivalent to the first term proportional to α in the line above, whereas the tree level decay with the FCNC coupling generated by the RG evolution includes the resummation of the large logarithms. The comparison of the exact one-loop result and the resummed tree level decay provides an estimate of the importance of the resummation of the large logarithms.

The outline of this part of the thesis is as follows: Section 4.2 is devoted to highlight flavor mixing aspects of the quark and squark sector in the SM and MSSM. The stop decay $\tilde{t}_1 \rightarrow c \tilde{\chi}_1^0$ at one-loop level is discussed in Section 4.3 including a detailed description of the renormalization procedure and a short presentation of the analytical results. Section 4.4 contains the numerical analysis of decay widths and branching ratios and the investigation of the scale dependence. Finally, in Section 4.5 the work is summarized.

4.2 Flavor Mixing in the SM and MSSM

As just mentioned in the introduction assuming MFV the FCNC decay $\tilde{t}_1 \rightarrow c \tilde{\chi}_1^0$ is forbidden at tree level at μ_{MFV} , the scale at which the principles of MFV hold. In order to understand which expressions enter the calculation of this decay and why it vanishes at tree level, a closer look on the flavor structure of the MSSM, especially in the context of MFV, is inevitable. Since in MFV all flavor changing transitions are governed by the CKM matrix of the SM a brief review of the SM quark flavor sector is useful.

In the SM the 3×3 unitary matrices $U^{u_{L,R}}$ and $U^{d_{L,R}}$ are defined as the matrices which rotate the left- and right-handed up- and down-type quark interaction eigenstates, $u_{L,R}$ and $d_{L,R}$, to their corresponding mass eigenstates, $u_{L,R}^m$ and $d_{L,R}^m$:

$$u_L^m = U^{u_L} u_L, \quad u_R^m = U^{u_R} u_R, \quad d_L^m = U^{d_L} d_L, \quad d_R^m = U^{d_R} d_R . \quad (4.2)$$

In other words, these matrices diagonalize the quark mass matrix. The CKM matrix is given by the combination

$$V^{\text{CKM}} = U^{uL} U^{dL\dagger} . \quad (4.3)$$

The CKM matrix is a 3×3 unitary matrix and describes the probability of a transition from one quark i to another quark j . These transitions are proportional to $|V_{ij}|^2$:

$$V^{\text{CKM}} = \begin{pmatrix} V_{ud} & V_{us} & V_{ub} \\ V_{cd} & V_{cs} & V_{cb} \\ V_{td} & V_{ts} & V_{tb} \end{pmatrix} . \quad (4.4)$$

Unitarity implies

$$\sum_i V_{ij} V_{ik}^* = \delta_{jk} \quad \text{and} \quad \sum_j V_{ij} V_{kj}^* = \delta_{ik} . \quad (4.5)$$

The second equation gives rise to the following combination

$$V_{cd} V_{td}^* + V_{cs} V_{ts}^* + V_{cb} V_{tb}^* = 0 , \quad (4.6)$$

which will be used in order to simplify the one-loop result of the decay $\tilde{t}_1 \rightarrow c\tilde{\chi}_1^0$. Only transitions from down-type quarks to up-type quarks, or vice versa, are allowed and thus no FCNC originating from transitions between up-type quarks of different generations (or down-type quarks of different generations) occur. Currently, the best determination of the magnitudes of the CKM matrix elements is [74]

$$V^{\text{CKM}} = \begin{pmatrix} 0.97427 \pm 0.00015 & 0.22534 \pm 0.00065 & 0.00351_{-0.00014}^{+0.00015} \\ 0.22520 \pm 0.00065 & 0.97344 \pm 0.00016 & 0.0412_{-0.0005}^{+0.0011} \\ 0.00867_{-0.00031}^{+0.00029} & 0.0404_{-0.0005}^{+0.0011} & 0.999146_{-0.000046}^{+0.000021} \end{pmatrix} . \quad (4.7)$$

While the diagonal matrix elements are close to 1, the off-diagonal elements lead to a strong suppression of processes involving the corresponding transitions. Apart from the flavor mixing defined by these matrices, no further flavor transitions are possible in the SM.

For the squark interaction eigenstate a six component vector

$$\tilde{q} = \begin{pmatrix} \tilde{q}_L \\ \tilde{q}_R \end{pmatrix} \quad (4.8)$$

is defined, where \tilde{q}_L and \tilde{q}_R are three component column vectors in generation space. The squared squark mass matrix can be written as a 2×2 Hermitian matrix of 3×3 blocks

$$\mathcal{M}_{\tilde{q}}^2 = \begin{pmatrix} \mathcal{M}_{\tilde{q}LL}^2 & \mathcal{M}_{\tilde{q}LR}^2 \\ \mathcal{M}_{\tilde{q}RL}^2 & \mathcal{M}_{\tilde{q}RR}^2 \end{pmatrix} . \quad (4.9)$$

In general, \mathcal{M}_q^2 contains a lot of new flavor violating sources. It is diagonalized by a 6×6 unitary matrix \tilde{W} which rotates the squark interaction eigenstates to their mass eigenstates \tilde{q}^m ,

$$\tilde{q}^m = \tilde{W} \tilde{q}. \quad (4.10)$$

The six component column vector \tilde{q}^m is defined to be ordered in mass, with \tilde{q}_1^m being the lightest squark. Equation (4.10) can then be rewritten as

$$\begin{aligned} \tilde{q}_s^m &= \tilde{W}_{si} \tilde{q}_{iL} + \tilde{W}_{s\ i+3} \tilde{q}_{iR} & (s = 1, \dots, 6, i = 1, 2, 3) \\ &\equiv (\tilde{W}_L \tilde{q}_L + \tilde{W}_R \tilde{q}_R)_s, \end{aligned} \quad (4.11)$$

where i denotes the generation index. Thus, the mass eigenstate squark field has been decomposed into left- and right-chiral interaction eigenstate squark fields.

The rotation of squarks by the same unitary matrices $U^{qL,R}$ as the quarks defines the super-CKM basis. In models with non-minimal flavor violation the squark mass matrix is flavor-mixed in this basis, in contrast to the quark mass matrix. In models with MFV at the scale μ_{MFV} , however, the squarks can be rotated by $U^{qL,R}$ to their flavor eigenstates in parallel to the quarks, and the super-CKM basis is at the same time the flavor eigenstate basis. This implies that any further rotation to the mass eigenstates does not mix squarks of different flavors, but only left- and right-chiral flavor eigenstates. Thus, suppressing generation indices, the flavor eigenstates in MFV are defined by

$$\tilde{q}'_L = U^{qL} \tilde{q}_L, \quad \tilde{q}'_R = U^{qR} \tilde{q}_R. \quad (4.12)$$

The squared mass matrix in the flavor eigenstate basis $(\tilde{q}'_L, \tilde{q}'_R)^T$ then reads

$$\mathcal{M}_{\tilde{q}}^2 = \begin{pmatrix} (\tilde{M}_{\tilde{q}_L}^2 + m_q^2) \mathbf{1}_3 & m_q (A_q - \mu_h r_q) \mathbf{1}_3 \\ m_q (A_q - \mu_h r_q) \mathbf{1}_3 & (\tilde{M}_{\tilde{q}_R}^2 + m_q^2) \mathbf{1}_3 \end{pmatrix}, \quad (4.13)$$

where $r_d = 1/r_u = \tan \beta$ for down- and up-type squarks. With $\tan \beta$ we denote the ratio of the vacuum expectation values of the two complex Higgs doublets. The parameter A_q denotes the trilinear coupling of the soft SUSY breaking part of the Lagrangian, μ_h the higgsino mass parameter and m_q the mass of the quark partner. Here, $\mathbf{1}_3$ is a 3×3 unit matrix in generation space. The parameters $\tilde{M}_{\tilde{q}_{L,R}}$ are given by the left- and right-handed scalar soft SUSY breaking masses $M_{\tilde{q}_{L,R}}$ and the D -terms,

$$\begin{aligned} \tilde{M}_{\tilde{q}_{L,R}}^2 &= M_{\tilde{q}_{L,R}}^2 + D_{\tilde{q}_{L,R}} \\ D_{\tilde{q}_L} &= M_Z^2 \cos 2\beta (I_q^3 - Q_q \sin^2 \theta_W) \\ D_{\tilde{q}_R} &= M_Z^2 \cos 2\beta Q_q \sin^2 \theta_W, \end{aligned} \quad (4.14)$$

where I_q^3 denotes the third component of the weak isospin, Q_q the electric charge, M_Z the Z boson mass and θ_W the Weinberg angle. The squared mass matrix $\mathcal{M}_{\tilde{q}}^2$

can be diagonalized by a 6×6 unitary matrix W which rotates the flavor eigenstates to their mass eigenstates,

$$\tilde{q}_s^m = W_{st} \begin{pmatrix} \tilde{q}'_L \\ \tilde{q}'_R \end{pmatrix}_t = W_{si} \tilde{q}'_{iL} + W_{s\ i+3} \tilde{q}'_{iR} \equiv (W_L \tilde{q}'_L + W_R \tilde{q}'_R)_s \quad (4.15)$$

$(s, t = 1, \dots, 6, i = 1, 2, 3)$.

By comparing Eqs. (4.15) and (4.12) with Eq. (4.11), it is evident that the 6×3 matrices $\tilde{W}_{L,R}$, which rotate the interaction eigenstates to the mass eigenstates, can be factorized into the 3×3 quark rotation matrices U^{qR} and U^{qL} , which rotate from the interaction to the flavor eigenstate basis, and the 6×3 flavor-diagonal matrices $W_{L,R}$, which transform flavor eigenstates into mass eigenstates,

$$\tilde{W}_L = W_L U^{qL} \quad \text{and} \quad \tilde{W}_R = W_R U^{qR}, \quad (4.16)$$

with $q = u, d$. The flavor-diagonal matrix W can be expressed in terms of mixing angles by

$$(W_L)_{ii} = (W_R)_{i+3\ i} = \cos \theta_{q_i} \quad , \quad (W_R)_{ii} = -(W_L)_{i+3\ i} = \sin \theta_{q_i}. \quad (4.17)$$

For the three quark generations i the relation between the flavor eigenstates $\tilde{q}'_{iL}, \tilde{q}'_{iR}$ and the squark mass eigenstates $\tilde{q}_s^m = (\tilde{q}_i^m, \tilde{q}_{i+3}^m)$ hence reads

$$\begin{aligned} \tilde{q}_i^m &= \tilde{q}'_{iL} \cos \theta_{q_i} + \tilde{q}'_{iR} \sin \theta_{q_i} \\ \tilde{q}_{i+3}^m &= -\tilde{q}'_{iL} \sin \theta_{q_i} + \tilde{q}'_{iR} \cos \theta_{q_i}. \end{aligned} \quad (4.18)$$

For better legibility, the generation indices will be suppressed from now on wherever possible, and the lighter and heavier squark mass eigenstates are generically called \tilde{q}_1 and \tilde{q}_2 . The mixing angles are then given by

$$\sin 2\theta_q = \frac{2m_q(A_q - \mu_h r_q)}{M_{\tilde{q}_1}^2 - M_{\tilde{q}_2}^2} \quad , \quad \cos 2\theta_q = \frac{\tilde{M}_{\tilde{q}_L}^2 - \tilde{M}_{\tilde{q}_R}^2}{M_{\tilde{q}_1}^2 - M_{\tilde{q}_2}^2}, \quad (4.19)$$

and the masses of the squark mass eigenstates read

$$M_{\tilde{q}_{1,2}}^2 = m_q^2 + \frac{1}{2} \left[\tilde{M}_{\tilde{q}_L}^2 + \tilde{M}_{\tilde{q}_R}^2 \mp \sqrt{(\tilde{M}_{\tilde{q}_L}^2 - \tilde{M}_{\tilde{q}_R}^2)^2 + 4m_q^2(A_q - \mu_h r_q)^2} \right]. \quad (4.20)$$

Since the mixing angles are proportional to the quark masses, the mixing is important in the stop sector and thus, as already mentioned in the introduction, can drive the lightest stop mass even lighter than the top quark mass.

The amplitude of the FCNC decay $\tilde{t}_1 \rightarrow c \tilde{\chi}_1^0$ at tree level is proportional to an off-diagonal matrix element of the flavor-diagonal matrix W . For that reason this process vanishes at tree level at the scale μ_{MFV} . At any other scale the squark mass matrix cannot be rotated to the flavor eigenstate basis by the matrices $U^{uL,R}$ and $U^{dL,R}$ any more. Therefore, the matrix W has to have flavor off-diagonal contributions inducing flavor violating tree level decays.

4.3 Light Stop Decay $\tilde{t}_1 \rightarrow c + \tilde{\chi}_1^0$ at One-Loop Level

Since the FCNC decay $\tilde{t}_1 \rightarrow c\tilde{\chi}_1^0$ is forbidden at tree level in the framework of the MSSM with MFV at the scale μ_{MFV} , it is mediated via loop diagrams. At one-loop level three types of diagrams contribute: Squark self energies, quark self energies and vertex diagrams. Generic diagrams illustrating these three contributions are depicted in Fig. 4.1. In MFV all flavor changing effects are governed by the CKM matrix of the SM. Consequently, all contributions to the decay at one-loop level are mediated by charged current loops, as can be inferred from the various diagrams listed in Fig. 4.2. Note that, in the calculation presented here the charm quark mass is set to¹

$$m_c = 0 . \quad (4.21)$$

Therefore, the \tilde{t}_1 self energies have only non-vanishing contributions for transitions into the left-handed charm squark \tilde{c}_L . The transitions into the right-handed charm squark, \tilde{c}_R , are zero for $m_c = 0$. This decay channel, though suppressed by small CKM matrix elements, is dominant for very light stops with a small mass difference to the lightest neutralino. Hence, for this calculation, scenarios where the light stop \tilde{t}_1 is the next-to-lightest supersymmetric particle (NLSP) and the lightest neutralino $\tilde{\chi}_1^0$ is the LSP, are considered.

The self energies and vertex corrections are divergent and have to be renormalized. The counterterms for the squark and quark self energies and for the vertex renormalization are shown in Fig. 4.3. The FCNC vertex does not arise at tree level. Its occurrence as counterterm at one-loop level is due to the fact that MFV is not RGE-invariant, since the weak interactions affect the squark and quark mass matrices differently [73]. Their simultaneous diagonalization cannot be maintained at higher orders and can only be consistently imposed at the scale μ_{MFV} .

For the calculation of the stop decay process an effective interaction vertex T is defined,

$$T \equiv g \bar{u}_c(k_2) (F_L \mathcal{P}_L + F_R \mathcal{P}_R) v_{\tilde{\chi}_1^0}(k_1) , \quad (4.22)$$

where $\bar{u}_c, v_{\tilde{\chi}_1^0}$ denote the charm and neutralino spinors and k_1, k_2 are the four-momenta of the outgoing neutralino and charm quark. Here, F_L and F_R are form factors associated with the chirality projectors \mathcal{P}_L and \mathcal{P}_R , respectively. They receive

¹In view of the smallness of the charm quark mass, $m_c = 1.28$ GeV, the numerical results are hardly affected by this choice.

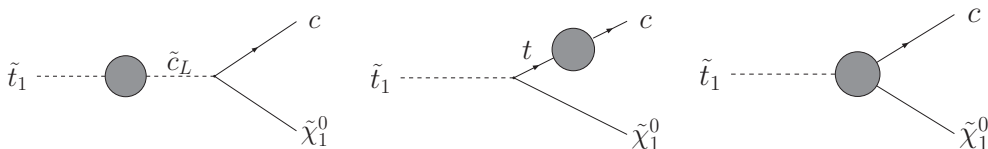


Figure 4.1: Generic diagrams contributing to the loop-decay $\tilde{t}_1 \rightarrow c\tilde{\chi}_1^0$.

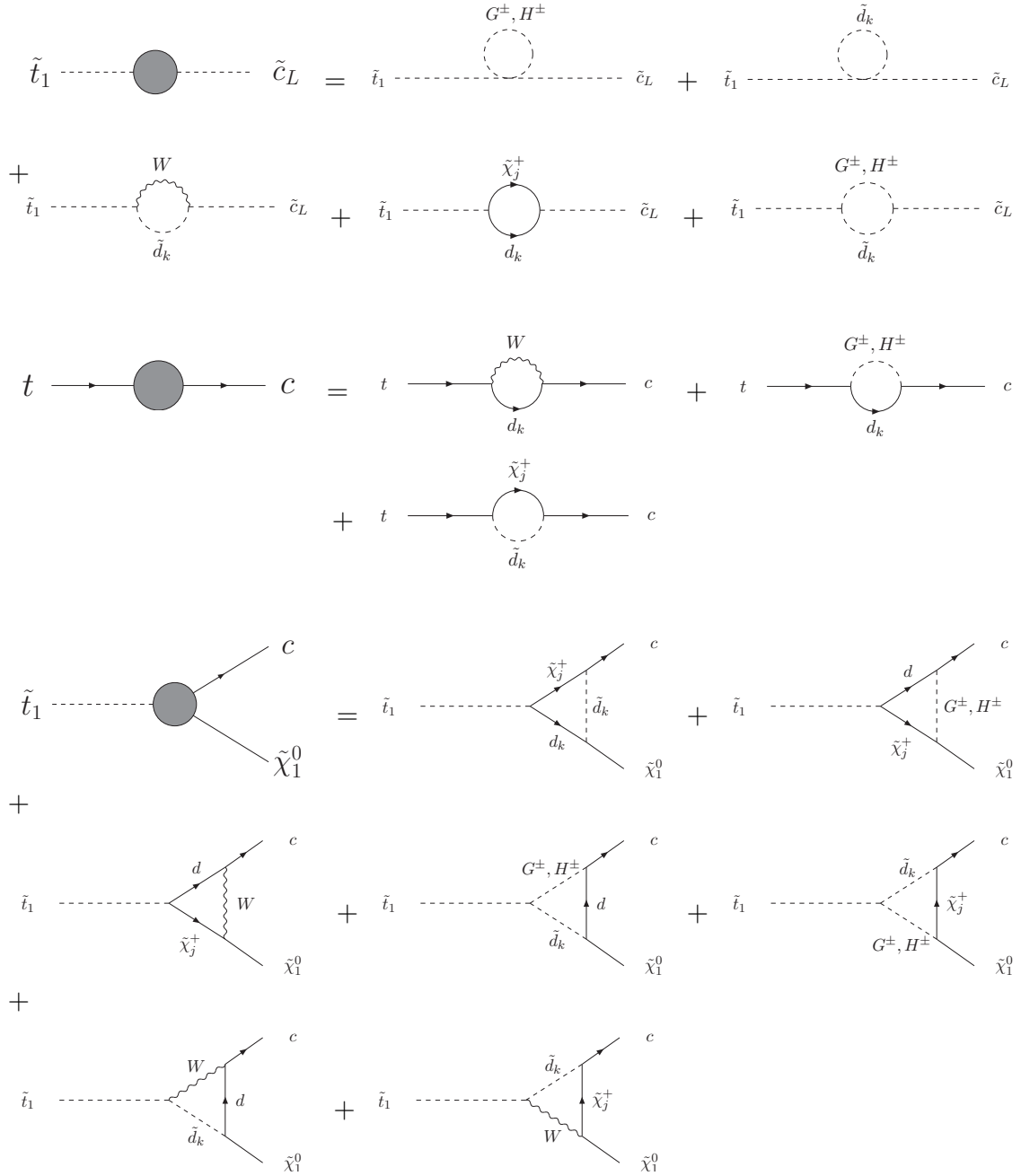


Figure 4.2: Generic diagrams contributing to the squark and quark self energy and the proper vertex correction.

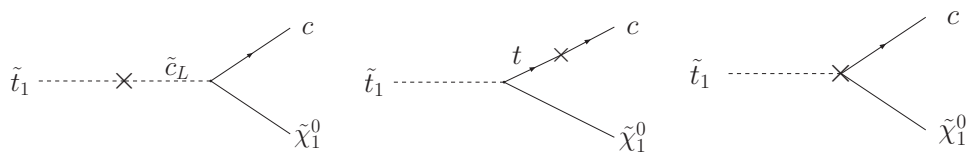


Figure 4.3: Counterterm diagrams.

contributions F^v from the vertex diagrams, F^{tc} , $F^{\tilde{t}_1\tilde{c}_L}$ from the quark and squark self energies and δF^v , δF^{tc} , $\delta F^{\tilde{t}_1\tilde{c}_L}$ from the vertex, the quark and squark wave function renormalization counterterms:

$$F_{L,R} = [F^{\tilde{t}_1\tilde{c}_L} + \delta F^{\tilde{t}_1\tilde{c}_L} + F^{tc} + \delta F^{tc} + F^v + \delta F^v]_{L,R}. \quad (4.23)$$

These contributions are specified in the following discussion of the counterterms which are needed for the renormalization procedure and in the presentation of the analytical results.

4.3.1 Counterterms and Renormalization

The loop diagrams in the self energies and vertex corrections contain momentum integrals which diverge due to contributions from large momenta. In order to be able to handle these UV divergencies, it is necessary to introduce a regularization scheme. In dimensional regularization [51] the number of space-time dimensions is lowered to $D = 4 - 2\epsilon$ and the UV singularities appear as poles in ϵ . In general SUSY is broken by dimensional regularization because it introduces a mismatch between fermionic and bosonic degrees of freedom. An alternative regularization scheme is dimensional reduction [75, 76], where no mismatch of fermionic and bosonic degrees of freedom is introduced. It has been verified explicitly in this calculation that the results obtained with both regularization schemes agree. Thus, the calculation performed in dimensional regularization does not need to be supplemented by a SUSY restoring counterterm.

The quark and squark fields are renormalized in the on-shell scheme introduced in Chapter 3.2. The bare quark $q^{(0)}$ and squark $\tilde{q}^{(0)}$ fields are related to the renormalized quark q and squark \tilde{q} fields by the renormalization constants $\delta Z^{\tilde{q}}$ and $\delta Z^{L,R}$

$$\tilde{q}^{(0)} = \left(1 + \frac{1}{2}\delta Z^{\tilde{q}}\right) \tilde{q} \quad \text{and} \quad q_{L,R}^{(0)} = \left(1 + \frac{1}{2}\delta Z^{L,R}\right) q_{L,R}. \quad (4.24)$$

Inserting the renormalized self energies into the on-shell renormalization conditions of Chapter 3.2, the field renormalization constants can be calculated from the unrenormalized quark and squark self energies. The off-diagonal part of the squark field renormalization constant in terms of the squark self energy reads

$$\delta Z_{st}^{\tilde{q}} = \frac{2}{m_{\tilde{q}_s}^2 - m_{\tilde{q}_t}^2} \text{Re}\Sigma_{st}^{\tilde{q}}(m_{\tilde{q}_t}^2) \quad s, t = 1, \dots, 6, \quad s \neq t. \quad (4.25)$$

Recalling the following structure of the quark self energy

$$\Sigma_{ij}(p^2) \equiv \not{p} \Sigma_{ij}^L(p^2) \mathcal{P}_L + \not{p} \Sigma_{ij}^R(p^2) \mathcal{P}_R + m_i \Sigma_{ij}^{Ls}(p^2) \mathcal{P}_L + m_j \Sigma_{ij}^{Rs}(p^2) \mathcal{P}_R, \quad (4.26)$$

the corrections to the off-diagonal chiral components of the quark field can be written as

$$\begin{aligned}
\delta Z_{ij}^L &= \frac{2}{m_{q_i}^2 - m_{q_j}^2} \left[m_{q_i}^2 \widetilde{\text{Re}}\Sigma_{ij}^{Ls}(m_{q_j}^2) + m_{q_j}^2 \widetilde{\text{Re}}\Sigma_{ij}^{Rs}(m_{q_j}^2) \right. \\
&\quad \left. + m_{q_j}^2 \widetilde{\text{Re}}\Sigma_{ij}^L(m_{q_j}^2) + m_{q_i} m_{q_j} \widetilde{\text{Re}}\Sigma_{ij}^R(m_{q_j}^2) \right] \\
\delta Z_{ij}^R &= \frac{2}{m_{q_i}^2 - m_{q_j}^2} \left[m_{q_i} m_{q_j} \widetilde{\text{Re}}\Sigma_{ij}^{Ls}(m_{q_j}^2) + m_{q_i} m_{q_j} \widetilde{\text{Re}}\Sigma_{ij}^{Rs}(m_{q_j}^2) \right. \\
&\quad \left. + m_{q_i} m_{q_j} \widetilde{\text{Re}}\Sigma_{ij}^L(m_{q_j}^2) + m_{q_j}^2 \widetilde{\text{Re}}\Sigma_{ij}^R(m_{q_j}^2) \right] \quad (4.27) \\
&\quad i, j = 1, 2, 3, \quad i \neq j.
\end{aligned}$$

After the renormalization of the quark and squark fields in the on-shell scheme, the contributions to the form factors of the effective interaction vertex in Eq. (4.22) from the self energies of the quarks and squarks and from their counterterms vanish:

$$\begin{aligned}
F^{\tilde{t}_1 \tilde{c}_L} + \delta F^{\tilde{t}_1 \tilde{c}_L} &= 0 \\
F^{tc} + \delta F^{tc} &= 0. \quad (4.28)
\end{aligned}$$

The divergencies in the one-loop vertex correction diagrams are left and need to be absorbed by the FCNC vertex counterterm. The general form of the vertex counterterm, depicted in Fig. 4.3, is derived in Appendix B. It arises from the flavor non-diagonal part of the field renormalization constants, from the renormalization of the quark and squark mixing matrices [77] and from the renormalization of the quark masses. Adjusted to the process of interest, the contributions of the vertex counterterm to the form factors are

$$g \delta F_R^v = -ig e_Z \left[\frac{1}{2} \delta Z_{ct}^{L\dagger} \cos \theta_t + \frac{1}{2} \delta Z_{\tilde{c}_L \tilde{t}_1}^{\tilde{q}} + \delta u_{ct}^{uL} \cos \theta_t + \delta \tilde{w}_{\tilde{c}_L \tilde{t}_1}^\dagger \right] \quad (4.29)$$

$$g \delta F_L^v = 0 \quad (4.30)$$

The constant e_Z summarizes the coupling factors

$$e_Z = \sqrt{2} \left[\frac{Z_{11}}{6} \tan \theta_W + \frac{1}{2} Z_{12} \right], \quad (4.31)$$

where Z_{11} and Z_{12} are matrix elements of the 4×4 Z matrix, which diagonalizes the neutralino mass matrix. The mixing matrix counterterms $\delta u^{uL,R}$ and $\delta \tilde{w}$ relate the bare quark and squark mixing matrices $U^{(0)}, \tilde{W}^{(0)}$ to the renormalized ones U^r, \tilde{W}^r :

$$\tilde{W}_{su}^{(0)} = (\delta_{st} + \delta \tilde{w}_{st}) \tilde{W}_{tu}^r, \quad s, t, u = 1, \dots, 6, \quad (4.32)$$

$$U_{ik}^{uL,R(0)} = (\delta_{ij} + \delta u_{ij}^{uL,R}) U_{jk}^{uL,Rr}, \quad i, j, k = 1, 2, 3, \quad (4.33)$$

The indices s, t, u denote the six squark mass eigenstates, and i, j, k are generation indices. Following the approach of [78], the MFV condition is imposed on the renormalized mixing matrices and hence they are demanded to be flavor-diagonal.

This leads to flavor non-diagonal counterterms $\delta u^{u_{L,R}}$ and $\delta \tilde{w}$. Furthermore, as the bare and renormalized mixing matrices are unitary, the counterterms must be anti-hermitian. The UV divergent part of both mixing matrix counterterms is determined such that it cancels the divergencies of the anti-hermitian part of the corresponding field renormalization constants [79, 80]

$$\delta \tilde{w} = \frac{1}{4}(\delta Z^{\tilde{q}} - \delta Z^{\tilde{q}\dagger}) \quad (4.34)$$

$$\delta u^{u_{L,R}} = \frac{1}{4}(\delta Z^{L,R} - \delta Z^{L,R\dagger}) . \quad (4.35)$$

The finite parts of these counterterms depend on the renormalization conditions. Absorbing also the finite part of the anti-hermitian field renormalization constants in general leads to a gauge-dependent on-shell renormalization scheme [81, 82]. Absorbing only the UV divergent part, proportional to

$$1/\epsilon + \log 4\pi - \gamma + \log \frac{\mu^2}{Q^2} \equiv \Delta + \log \frac{\mu^2}{Q^2} , \quad (4.36)$$

with γ being the Euler-Mascheroni constant, Q the renormalization and μ the 't Hooft scale, defines the $\overline{\text{MS}}$ renormalization scheme [50]. In the following this scheme is adopted and the MFV condition is imposed on the $\overline{\text{MS}}$ parameters at the scale $Q^2 = \mu_{MFV}^2$. Consequently, the result will depend on this scale [78]. The squark mixing matrix counterterm then reads

$$\delta \tilde{w}_{\tilde{c}_L \tilde{t}_1}^\dagger = \frac{1}{2} \left(\frac{\Sigma_{\tilde{c}_L \tilde{t}_1}^{\tilde{q}}(m_{\tilde{c}_L}^2) + \Sigma_{\tilde{c}_L \tilde{t}_1}^{\tilde{q}}(m_{\tilde{t}_1}^2)}{m_{\tilde{t}_1}^2 - m_{\tilde{c}_L}^2} \right)_{\overline{\text{MS}}} . \quad (4.37)$$

A gauge invariant prescription for the quark mixing matrix counterterm is given by [81]

$$\delta u_{ct}^{U_L} = -\frac{1}{2} [\Sigma_{tc}^L(0) + 2\Sigma_{tc}^{Ls}(0)]_{\overline{\text{MS}}} = -\frac{1}{2} \Sigma_{tc}^L(0)_{\overline{\text{MS}}} . \quad (4.38)$$

The scalar part of the quark self energy vanishes for zero momentum transfer and so does the quark field renormalization constant contributing to the vertex counterterm in Eq. (4.29)

$$\delta Z_{ct}^{L\dagger} = 2\Sigma_{tc}^{Ls}(m_c^2 = 0) = 0 . \quad (4.39)$$

Finally, the last renormalization constant needed for the vertex counterterm is the squark field renormalization constant, which according to Eq. (4.25) yields:

$$\delta Z_{\tilde{c}_L \tilde{t}_1}^{\tilde{q}} = \frac{2\Sigma_{\tilde{c}_L \tilde{t}_1}^{\tilde{q}}(m_{\tilde{t}_1}^2)}{m_{\tilde{c}_L}^2 - m_{\tilde{t}_1}^2} . \quad (4.40)$$

4.3.2 Analytical Results

By exploiting the unitarity relation of the CKM matrix in Eq. (4.6) as well as those of the chargino mixing matrices U and V , the contribution of the vertex diagrams to the form factors can be written as

$$g F_R^v = -ig \mathcal{F} \left[\Delta + \log \frac{\mu^2}{m_{\text{loop}}^2} + \text{finite terms} \right] \quad (4.41)$$

$$g F_L^v = 0, \quad (4.42)$$

where the short-hand notation

$$\mathcal{F} \equiv \frac{1}{16\pi^2} g^2 e_Z \left(\frac{V_{cb} V_{tb}^* m_b^2 \cos \theta_t}{2M_W^2 \cos^2 \beta} \right), \quad (4.43)$$

comprises common coupling factors, including the coupling constant g and the CKM matrix elements V_{cb} and V_{tb}^* . The left-handed form factor F_L is zero due to the choice of vanishing charm quark mass. The expression "finite terms" in Eq. (4.41) summarizes all terms in the result of the calculation, which are neither UV divergent nor depend on the logarithm of the 't Hooft scale, $\log \mu^2$. For reasons of legibility and in order to compare with the result derived in [18] a generic mass m_{loop} for all massive particles in the loops has been introduced. In the numerical analysis the exact result with different loop particle masses will be used. The contribution of the quark mixing matrix counterterm, defined in Eq. (4.38), to the vertex counterterm explicitly reads

$$-g e_Z \cos \theta_t (\delta u_{ct}^{U_L})_{\overline{\text{MS}}} = g \frac{\mathcal{F}}{2} \left[\Delta + \log \frac{\mu^2}{\mu_{\text{MFV}}^2} \right]. \quad (4.44)$$

The counterterm of the squark mixing matrix yields

$$-g e_Z (\delta \tilde{w}_{\tilde{c}_L \tilde{t}_1}^\dagger)_{\overline{\text{MS}}} = g \frac{\mathcal{F}}{2} \left(\frac{-m_{\tilde{t}_1}^2 - m_{\tilde{c}_L}^2 - 2\mathcal{A}}{m_{\tilde{t}_1}^2 - m_{\tilde{c}_L}^2} \right) \left[\Delta + \log \frac{\mu^2}{\mu_{\text{MFV}}^2} \right], \quad (4.45)$$

with

$$\mathcal{A} = -\mu_h^2 + A_b^2 + \tilde{M}_{b_R}^2 + \cos^2 \beta (M_W^2 (\tan^2 \beta - 1) + M_A^2 \tan^2 \beta) + m_t A_b \tan \theta_t. \quad (4.46)$$

It depends on the higgsino parameter μ_h , the soft SUSY breaking mass parameter \tilde{M}_{b_R} including D term contributions, the trilinear coupling A_b , the mixing angle β , the W boson mass and the pseudoscalar Higgs mass M_A . The contribution from the squark field renormalization constant $\delta Z_{\tilde{c}_L \tilde{t}_1}^{\tilde{q}}$ is given by

$$-g e_Z \frac{1}{2} (\delta Z_{\tilde{c}_L \tilde{t}_1}^{\tilde{q}}) = g \frac{\mathcal{F}}{2} \left(\frac{2m_{\tilde{t}_1}^2 + 2\mathcal{A}}{m_{\tilde{t}_1}^2 - m_{\tilde{c}_L}^2} \right) \left[\Delta + \log \frac{\mu^2}{m_{\text{loop}}^2} + \text{finite terms} \right]. \quad (4.47)$$

Since the latter has been renormalized in the on-shell scheme, it includes, as the vertex corrections before, 'finite terms', which do not depend on $\log \mu^2$. Inserting

Eqs. (4.39),(4.44),(4.45) and (4.47) in Eq. (4.29), the right-chiral part of the FCNC counterterm is then given by

$$g \delta F_R^v = ig \mathcal{F} \left[\Delta - \frac{m_{\tilde{c}_L}^2 + \mathcal{A}}{m_{\tilde{t}_1}^2 - m_{\tilde{c}_L}^2} \log \frac{\mu^2}{\mu_{\text{MFV}}^2} + \frac{m_{\tilde{t}_1}^2 + \mathcal{A}}{m_{\tilde{t}_1}^2 - m_{\tilde{c}_L}^2} \log \frac{\mu^2}{m_{\text{loop}}^2} + \text{finite terms} \right]. \quad (4.48)$$

Adding Eq. (4.41) to Eq. (4.48) we arrive at the following final result for the form factors, that contribute to Eq. (4.23):

$$g F_R = \frac{i}{16\pi^2} g^3 \sqrt{2} \left[\frac{Z_{11}}{6} \tan \theta_W + \frac{Z_{12}}{2} \right] \left(\frac{V_{cb} V_{tb}^* m_b^2 \cos \theta_t}{2M_W^2 \cos^2 \beta} \right) \times \left(\frac{m_{\tilde{c}_L}^2 - \mathcal{A}}{m_{\tilde{t}_1}^2 - m_{\tilde{c}_L}^2} \right) \log \left(\frac{\mu_{\text{MFV}}^2}{m_{\text{loop}}^2} \right) + \text{finite terms} \quad (4.49)$$

$$g F_L = 0. \quad (4.50)$$

Finally, the stop decay width in terms of the form factor in Eq. (4.49) is given by

$$\Gamma(\tilde{t}_1 \rightarrow c \tilde{\chi}_1^0) = \frac{g^2 m_{\tilde{t}_1}}{16\pi} \left(1 - \frac{m_{\tilde{\chi}_1^0}^2}{m_{\tilde{t}_1}^2} \right)^2 |F_R|^2. \quad (4.51)$$

On the one hand the form factor introduces a suppression by the CKM matrix elements $V_{cb} V_{tb}^*$, but on the other hand the logarithm, depending on the scale of MFV, can become very large. The finite terms, which do not depend on $\log \mu_{\text{MFV}}^2$, are then only subleading. Furthermore, as will be shown in the next section, the decay can gain importance in certain regions of parameter space.

If the finite terms in Eq. (4.49) are dropped, the approximate result given by Hikasa and Kobayashi in Ref. [18] should be reproduced. In fact, for $m_c = 0$ we can rewrite parts of the numerator in the second line of the form factor of Eq. (4.49)

$$m_{\tilde{c}_L}^2 - \mu_h^2 + c_\beta^2 (M_W^2 (\tan^2 \beta - 1) + M_A^2 \tan^2 \beta) = M_{H_d}^2 + M_{\tilde{q}_L}^2 + \frac{1}{3} M_Z^2 \sin^2 \theta_W \cos 2\beta, \quad (4.52)$$

where M_{H_d} denotes the mass parameter of the Higgs doublet H_d , which couples to down-type fermions. With this relation and by setting the MFV scale equal to the Planck scale, $\mu_{\text{MFV}} = M_P$, choosing M_W as generic loop particle mass and neglecting the finite terms, the form factor in Eq. (4.49) reproduces the approximate result $F_R^{H/K}$ of Ref. [18]:

$$g F_R^{H/K} = \frac{i}{16\pi^2} g^3 \sqrt{2} \left[\frac{Z_{11}}{6} \tan \theta_W + \frac{Z_{12}}{2} \right] \left(\frac{V_{cb} V_{tb}^* m_b^2 \cos \theta_t}{2M_W^2 \cos^2 \beta} \right) \left(\frac{1}{m_{\tilde{t}_1}^2 - m_{\tilde{c}_L}^2} \right) \times [M_{H_d}^2 + M_{\tilde{q}_L}^2 + A_b^2 + M_{\tilde{b}_R}^2 + m_t A_b \tan \theta_t] \log \left(\frac{M_P^2}{M_W^2} \right). \quad (4.53)$$

In the full one-loop calculation of the decay width in Eq. (4.51) the finite terms are included. Thus, the relevance of these contributions can be checked by comparison with the approximate decay width $\Gamma^{H/K}$, calculated with the form factor $F_R^{H/K}$:

$$\Gamma^{H/K}(\tilde{t}_1 \rightarrow c\tilde{\chi}_1^0) = \frac{g^2 m_{\tilde{t}_1}}{16\pi} \left(1 - \frac{m_{\tilde{\chi}_1^0}^2}{m_{\tilde{t}_1}^2}\right)^2 |F_R^{H/K}|^2. \quad (4.54)$$

This comparison will be discussed in detail in the following section.

4.4 Numerical Analysis

For the numerical analysis of the $\tilde{t}_1 \rightarrow c\tilde{\chi}_1^0$ decay the framework has to be chosen such, that MFV is ensured at a scale $\mu = \mu_{MFV}$. This is the case, when all soft SUSY breaking parameters are flavor-diagonal at this single scale. In particular, a common mass parameter $M_{\tilde{q}_L}$ for the soft SUSY breaking masses of the $SU(2)$ doublet has to be introduced, in order to make sure that the mass matrices for the up- and down-type squarks can be flavor diagonalized simultaneously. A framework which guarantees this is the mSUGRA model [27–30], where a hidden sector of spontaneous SUSY breaking terms is coupled to the MSSM only through flavor-blind gravitational-strength interactions. It is defined in terms of a small number of parameters at the GUT scale M_{GUT} , which is identified with the MFV scale in the following: $\mu_{MFV} = M_{GUT}$.

The scenarios have been chosen such, that they lead to a \tilde{t}_1 NLSP and a $\tilde{\chi}_1^0$ LSP. Then the decay channels $\tilde{t}_1 \rightarrow b\tilde{\chi}_1^0 W$ and $\tilde{t}_1 \rightarrow t\tilde{\chi}_1^0$ are kinematically forbidden. When the mass difference between the \tilde{t}_1 and $\tilde{\chi}_1^0$ is small enough, the FCNC decay

$$\tilde{t}_1 \rightarrow c\tilde{\chi}_1^0 \quad \sim |V_{cb}|^2 \approx |0.04|^2 \quad (4.55)$$

is dominating since the other possible decay modes are either suppressed by even smaller CKM matrix elements

$$\tilde{t}_1 \rightarrow u\tilde{\chi}_1^0 \quad \sim |V_{ub}|^2 \approx |0.004|^2 \quad (4.56)$$

or due to limited phase space for the four-body decay

$$\tilde{t}_1 \rightarrow \tilde{\chi}_1^0 b \bar{f} f. \quad (4.57)$$

The mass spectra and mixing angles have been calculated with the spectrum calculator **SPheno** [83, 84] and compared to **SOFTSUSY** [85]. Both codes include the option to perform two-loop RGE running with and without the inclusion of flavor violation and both support the SUSY Les Houches accord [86, 87]. Within this accord the gauge and Yukawa couplings as well as the soft SUSY breaking mass parameters and trilinear couplings are returned as running parameters in dimensional reduction at a scale Q , which has been chosen to be the scale of electroweak symmetry breaking (EWSB). As mentioned before, it has been verified that the calculation of the decay

width leads to the same result if dimensional reduction instead of dimensional regularization is applied. Consequently, the running parameters in dimensional reduction can be used. The mixing matrix elements and the SUSY particle pole masses have been taken at the scale of EWSB as well. The SM parameters have been chosen as

$$\begin{aligned}
M_Z &= 91.187 \text{ GeV} \\
\alpha_{em}^{-1\overline{\text{MS}}}(M_Z) &= 127.934 \\
\alpha_s^{\overline{\text{MS}}}(M_Z) &= 0.118 \\
m_b^{\overline{\text{MS}}}(m_b) &= 4.25 \text{ GeV} \\
M_t^{\text{pole}} &= 173.3 \text{ GeV} \\
m_\tau^{\text{pole}} &= 1.777 \text{ GeV} \\
|V_{tb}| &= 0.999 \\
|V_{cb}| &= 0.041 .
\end{aligned} \tag{4.58}$$

Apart from checking the importance of the finite terms in the exact one-loop calculation presented in the previous section for the decay widths and branching ratios, resummation effects due to the RG evolution from the GUT scale down to the EWSB scale are analyzed in the following section. The latter enter this analysis since the logarithm $\log \mu_{MFV}^2/m_{\text{loop}}^2$ in the result of the one-loop calculation (Eq. (4.49)) can become very large for $\mu_{MFV} = M_{GUT}$. In order to get a reliable result, the large logarithm must be resummed. The resummation is provided by the solution of the RGE for the quark and squark mixing matrices. The RG evolution of the corresponding soft-breaking terms generates small flavor off-diagonal entries in the squark mixing matrix \tilde{W} , which give rise to an FCNC tree level decay. In this "flavor violating" case, denoted by FV in the following no flavor-eigenstates exist any more. However, the lightest up-type squark state \tilde{u}_1 can be identified to correspond to \tilde{t}_1 . This is possible since both are required to be the lightest up-type squark and the flavor violating effects introduced through RG evolution are small. The form factor F_R^{FV} of the FCNC tree level decay is given by the right-handed part of the FCNC $\tilde{u}_1 - c - \tilde{\chi}_1^0$ coupling²,

$$F_R^{FV} = -i \sqrt{2} \left(\frac{Z_{11}}{6} t_W + \frac{Z_{12}}{2} \right) (\tilde{W}_L)_{\tilde{u}_1 c} , \tag{4.59}$$

with the squark mixing matrix \tilde{W}_L defined in Eq. (4.11). This leads to the partial decay width

$$\Gamma^{\text{FV}}(\tilde{u}_1 \rightarrow c \tilde{\chi}_1^0) = \frac{g^2 m_{\tilde{u}_1}}{16\pi} \left(1 - \frac{m_{\tilde{\chi}_1^0}^2}{m_{\tilde{u}_1}^2} \right) |F_R^{\text{FV}}|^2 , \tag{4.60}$$

which will also be compared to the decay width of the exact one-loop result. Furthermore, the behavior of the different form factors and decay widths is studied for decreasing scales of MFV. All numerical results stated in the following have been obtained with the program *SUSY-HIT* [88, 89], where the formula for the loop-induced flavor changing stop decay has been implemented and will be available with a future

²The left-handed part is negligibly small for $m_c = 0$.

release. Actually, two independent implementations have been developed by the authors of [72] in order to provide a cross check for the results.

Analysis for $\mu_{\text{MFV}} \approx 10^{16}$ GeV

The analysis is accomplished for two different mSUGRA scenarios with soft-breaking terms at the GUT scale $M_{\text{GUT}} \approx 2.3 \cdot 10^{16}$ GeV, which is identified with the MFV scale. The boundary conditions at $\mu_{\text{MFV}} = M_{\text{GUT}}$ are

$$\begin{aligned}
 (1) \quad & M_0 = 200 \text{ GeV} \quad M_{1/2} = 230 \text{ GeV} \quad A_0 = -920 \text{ GeV} \\
 & \tan \beta = 10 \quad \text{sign}(\mu_h) = + \\
 (2) \quad & M_0 = 200 \text{ GeV} \quad M_{1/2} = 230 \text{ GeV} \quad A_0 = -895 \text{ GeV} \\
 & \tan \beta = 10 \quad \text{sign}(\mu_h) = + .
 \end{aligned} \tag{4.61}$$

The masses are obtained by RGE evolution from the GUT scale down to the electroweak scale. The running is performed at two-loop order without the inclusion of explicit flavor violation in the squark sector. The most relevant masses are

$$\begin{aligned}
 (1) \quad & m_{\tilde{t}_1} = 104 \text{ GeV} \quad m_{\tilde{\chi}_1^0} = 92 \text{ GeV} \quad m_{\tilde{\chi}_1^+} = 175 \text{ GeV} \\
 (2) \quad & m_{\tilde{t}_1} = 130 \text{ GeV} \quad m_{\tilde{\chi}_1^0} = 92 \text{ GeV} \quad m_{\tilde{\chi}_1^+} = 175 \text{ GeV} .
 \end{aligned} \tag{4.62}$$

The second scenario has a larger $m_{\tilde{t}_1} - m_{\tilde{\chi}_1^0}$ difference compared to scenario (1), whereas the mass difference between \tilde{t}_1 and the lightest chargino $\tilde{\chi}_1^+$ is smaller. Since the four-body decays are dominated by a chargino exchange diagram [90], in scenario (2) the four-body decays should be more important leading to a smaller branching ratio of the loop-induced flavor changing decay.

For these scenarios the partial stop decay width into charm and neutralino, calculated with the exact one-loop formula, is compared to the approximate result by [18]. For the latter, we take M_W as generic loop particle mass, *cf.* Eq. (4.53). The widths and form factors are given in Table 4.1. Note, that as anticipated the partial width in the first scenario is ~ 6 times smaller than in the second scenario due the smaller

$\tilde{t}_1 \rightarrow c\tilde{\chi}_1^0$	$\Gamma^{1\text{-loop}}[\text{GeV}]$	$\Gamma^{\text{H/K}}[\text{GeV}]$	$ F_R^{1\text{-loop}} $	$ F_R^{\text{H/K}} $
Scenario (1)	$9.322 \cdot 10^{-10}$	$1.004 \cdot 10^{-9}$	$1.486 \cdot 10^{-4}$	$1.542 \cdot 10^{-4}$
Scenario (2)	$5.862 \cdot 10^{-9}$	$6.446 \cdot 10^{-9}$	$1.460 \cdot 10^{-4}$	$1.531 \cdot 10^{-4}$

Table 4.1: The partial widths and form factors for the decay $\tilde{t}_1 \rightarrow c\tilde{\chi}_1^0$ in scenario (1) and (2), calculated with the exact one-loop formula, ($\Gamma^{1\text{-loop}}$, $F_R^{1\text{-loop}}$), and with the approximate formula of Ref. [18], ($\Gamma^{\text{H/K}}$, $F_R^{\text{H/K}}$).

branching ratio	$\text{BR}(\tilde{t}_1 \rightarrow \tilde{\chi}_1^0 c)$	$\text{BR}(\tilde{t}_1 \rightarrow \tilde{\chi}_1^0 u)$	$\text{BR}(\tilde{t}_1 \rightarrow \tilde{\chi}_1^0 b f \bar{f}')$
Scenario (1)	0.9944	0.0056	$4.587 \cdot 10^{-5}$
Scenario (2)	0.9443	0.0053	0.0504

Table 4.2: The \tilde{t}_1 branching ratios for different final states for scenario (1) and (2).

$m_{\tilde{t}_1} - m_{\tilde{\chi}_1^0}$ difference and hence reduced phase space. The exact and approximate decay width differ in both scenarios by $\mathcal{O}(10)\%$. In fact, the finite terms extracted from the one-loop formula turn out to contribute with $\sim 3 - 5\%$ to F_R , Eq. (4.49). This difference translates into the 10% effect in the decay width.

For the calculation of the branching ratios, also the partial width for the \tilde{t}_1 decay into an u -quark and neutralino, $\tilde{t}_1 \rightarrow u \tilde{\chi}_1^0$, as well as the four-body decay width are needed. The former is suppressed by two orders of magnitude compared to the $c \tilde{\chi}_1^0$ final state due to the small CKM matrix element $|V_{ub}| \approx 0.004$ which enters quadratically in the decay width. The branching ratios are listed in Table 4.2. As expected, the stop four-body decay is more important in scenario (2) leading to a change of the branching ratio of interest, $\text{BR}(\tilde{t}_1 \rightarrow \tilde{\chi}_1^0 c)$, at the few per-cent level. The difference in the branching ratio $BR(\tilde{t}_1 \rightarrow c \tilde{\chi}_1^0)$ calculated in the exact and approximate approach is negligible, however.

As stated before, the large logarithms in the one-loop decay formula should be resummed. To get an estimate of the importance of the resummation effects, the loop-induced decay is compared to the FCNC tree level stop decay into charm and neutralino with flavor off-diagonal elements in the squark mixing matrix. The input parameters for the FCNC tree level decay formula in Eq. (4.60) are obtained with the spectrum calculator **SPheno** [83, 84]. The scenarios in Eq. (4.61) have been chosen such that in the case of FCNC transitions at tree level the mass of the lightest up-type squark state \tilde{u}_1 corresponds roughly to the mass of the light stop \tilde{t}_1 . The $\tilde{\chi}_1^0$ and $\tilde{\chi}_1^+$ masses are almost unchanged.

The form factors and partial widths are shown in Table 4.3. As can be inferred from the table, there is a factor ~ 4.4 between the right-handed form factor calculated

	$ F_R^{1\text{-loop}} $	$ F_R^{\text{FV}} $	$\Gamma^{1\text{-loop}}$ [GeV]	Γ^{FV} [GeV]
Scenario (1)	$1.486 \cdot 10^{-4}$	$3.361 \cdot 10^{-5}$	$9.322 \cdot 10^{-10}$	$4.766 \cdot 10^{-11}$
Scenario (2)	$1.460 \cdot 10^{-4}$	$3.306 \cdot 10^{-5}$	$5.862 \cdot 10^{-9}$	$3.006 \cdot 10^{-10}$

Table 4.3: The right-handed form factors and partial decay widths of the lightest up-type squark into charm and neutralino for loop-induced (1-loop) and the FCNC tree level decay (FV).

Scenario (2)	$\text{BR}(\tilde{t}_1 \rightarrow \tilde{\chi}_1^0 c)$	$\text{BR}(\tilde{t}_1 \rightarrow \tilde{\chi}_1^0 u)$	$\text{BR}(\tilde{t}_1 \rightarrow \tilde{\chi}_1^0 b f \bar{f}')$
Exact 1-loop	0.9443	0.0053	0.0504
	$\text{BR}(\tilde{u}_1 \rightarrow \tilde{\chi}_1^0 c)$	$\text{BR}(\tilde{u}_1 \rightarrow \tilde{\chi}_1^0 u)$	$\text{BR}(\tilde{t}_1 \rightarrow \tilde{\chi}_1^0 b f \bar{f}')$
FCNC TL	0.4884	0.0032	0.5084

Table 4.4: The \tilde{t}_1 branching ratios for the loop-induced (Exact 1-loop) and the FCNC tree level decay (FCNC TL).

at the one-loop level and the one derived from RG evolution including FCNC at tree level. As expected, resummation effects turn out to be important for a large scale $\mu_{\text{MFV}} = M_{\text{GUT}}$ ³. The partial widths, which depend quadratically on the right-handed form factor, differ by a factor ~ 20 .

For comparison the calculation has been performed with the decay spectra and mixing angles evaluated by **SOFTSUSY**. The squark mixing matrix elements agree within 10^{-2} accuracy with the results of **SPheno**. The mixing matrix element $(\tilde{W}_L)_{\tilde{u}_1 c}$, which enters in the form factor F_R^{FV} Eq. (4.59), is $\mathcal{O}(10^{-4})$ and differs in the two spectrum calculators, as the two codes implement the one-loop corrections to the squark mass matrices differently. **SOFTSUSY** corrects only the flavor-diagonal entries of the squark mass matrices, while **SPheno** implements a full one-loop calculation, so that differences in the flavor off-diagonal entries are to be expected [92]. For the **SOFTSUSY** parameter values, this results in a ratio between loop-induced decay and FCNC tree level decay of ~ 2.7 for the two scenarios, compared to the ratio ~ 4.4 found with the **SPheno** parameter values. All in all, the results with both spectrum calculators show the importance of the resummation effects.

The consequences of these resummation effects on the \tilde{t}_1 branching ratio into the charm plus neutralino final state are of phenomenological interest. To quantify this, the partial decay width for the decay into the up-quark and the lightest neutralino, as well as the four-body stop decay width, calculated with FCNC tree level couplings, are needed. The decay width into the up-quark can be determined from the corresponding resummed flavor off-diagonal matrix element $\tilde{W}_{\tilde{u}_1 u_L}$. However, the calculation for the competing four-body stop decay width including tree level FCNC couplings is not available at present. But the additional FCNC contributions are expected to be small due to the suppression by CKM matrix elements, so the existing calculation is used for the following comparison of branching ratios. This means, that the decay width of the four-body decay is supposed to remain unchanged for the calculation of the branching ratios with and without FCNC tree level couplings. The results are presented in Table 4.4 for scenario (2). The resummation effects, which have already been shown to reduce the partial decay width

³This result is in agreement with the discussion in Ref. [91] where resummation effects in the coupling $\tilde{t}_1 - c - \tilde{\chi}_1^0$ have been found to be large.

of the decay $\tilde{t}_1 \rightarrow c\tilde{\chi}_1^0$ by a factor ~ 20 , can lead to a significant decrease of the corresponding branching ratio by a factor of ~ 0.5 . This is the case as long as the partial decay width of the four-body decay (Γ_3) is not too small and cannot be neglected compared to the loop-induced decay width of $\tilde{t}_1 \rightarrow c\tilde{\chi}_1^0$ (Γ_1). This is true for scenario (2):

$$\begin{aligned} BR(\tilde{t}_1 \rightarrow \tilde{\chi}_1^0 c) &= \frac{\Gamma_1}{\Gamma_1 + \Gamma_2 + \Gamma_3} \\ &> \frac{\Gamma_1}{\Gamma_1 + 20\Gamma_2 + 20\Gamma_3} = BR(\tilde{u}_1 \rightarrow \tilde{\chi}_1^0 u) . \end{aligned} \quad (4.63)$$

Here, Γ_2 is the decay-width of $\tilde{t}_1 \rightarrow u\tilde{\chi}_1^0$. On the contrary, in scenario (1) the four-body decay is suppressed due to phase space and consequently the branching ratios remain almost unchanged in the case with and without FCNC tree level couplings. The branching ratio of the decay into the up-quark final state is always suppressed by two orders of magnitude. The drastically reduced branching ratio of $\tilde{t}_1 \rightarrow \tilde{\chi}_1^0 c$ or $\tilde{u}_1 \rightarrow \tilde{\chi}_1^0 u$, respectively, is no longer in any agreement with the assumption of the branching ratio $BR(\tilde{t}_1 \rightarrow \tilde{\chi}_1^0 c) = 1$, which has been used in phenomenological analyses [67–69] as well as experimental searches [36, 37] so far. In summary, in order to get correct predictions for the flavor changing light stop decay for large scales of MFV, resummation effects have to be included. To further improve on this decay, the next step would be the calculation of the full one-loop corrections to the FCNC tree level stop decay including the off-diagonal squark mixing matrix elements from RGE evolution in the whole calculation.

Analysis for $\mu_{\text{MFV}} \leq M_{\text{GUT}}$

In the previous section the importance of resummation effects has been discussed. With decreasing μ_{MFV} and hence smaller $\log \mu_{\text{MFV}}^2$, the non-resummed one-loop result should approach the resummed FCNC tree level result. Furthermore, the approximate formula of Ref. [18], which is a good approximation of the exact one-loop result for large scales, is expected to be worse with decreasing MFV scale. In order to verify this behavior, scenarios with different μ_{MFV} varied between $10^3 \text{ GeV} \leq \mu_{\text{MFV}} \leq 10^{16} \text{ GeV}$ have been chosen. The soft SUSY breaking input parameters in each scenario are adjusted such, that the masses for \tilde{t}_1 and $\tilde{\chi}_1^0$ remain almost unchanged. Consequently, the differences in the partial decay widths will not be due to phase space effects. The scenarios are constrained by the requirement that \tilde{t}_1 is the NLSP and $\tilde{\chi}_1^0$ is the LSP, so that the decay $\tilde{t}_1 \rightarrow c\tilde{\chi}_1^0$ dominates. The relevant particle masses for the different scenarios vary within

$$m_{\tilde{t}_1} = 105 \dots 116 \text{ GeV} \quad \text{and} \quad m_{\tilde{\chi}_1^0} = 92 \dots 104 \text{ GeV} , \quad (4.64)$$

with the $\tilde{t}_1 - \tilde{\chi}_1^0$ mass difference ranging between

$$m_{\tilde{t}_1} - m_{\tilde{\chi}_1^0} = 9 \dots 15 \text{ GeV} . \quad (4.65)$$

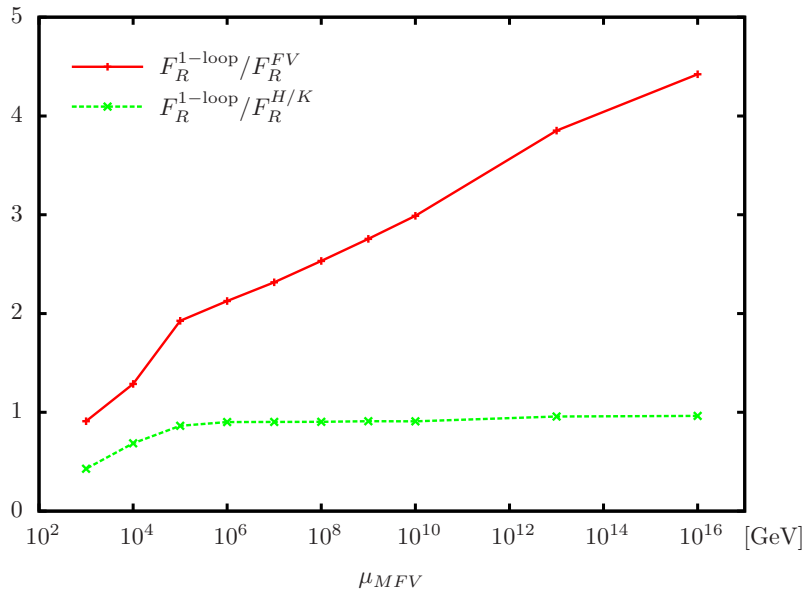


Figure 4.4: Ratio between the right-handed form factor of the MFV loop decay F_R^{1-loop} and the form factor of the FV tree level decay F_R^{FV} (red/full) and ratio between the MFV loop-decay form factor and the approximate form factor $F_R^{H/K}$ (green/dashed) as function of the MFV scale μ_{MFV} .

The various scenarios have not been required to fulfill Dark Matter constraints and/or constraints from electroweak precision data. The main emphasis has been to achieve approximately constant masses for the NLSP and LSP. In Fig. 4.4 the ratio of the non-resummed right-handed form factor F_R^{1-loop} in the loop-induced decay to F_R^{FV} in the FCNC tree level decay as well as the ratio of F_R^{1-loop} to the approximate form factor $F_R^{H/K}$ as a function of the MFV scale are shown.⁴ The values at the highest scale of MFV depicted in this plot coincide with the results discussed in the previous section. In this scenario the non-resummed one-loop result and the resummed FCNC tree level result differ by the factor ~ 4.4 . As expected, these two results approach each other with decreasing scales of MFV, since the resummation effects become less relevant. On the other hand, the approximate one-loop result reproduces the exact one-loop result down to low scales. Starting from $\mu_{MFV} = 10^5$ GeV the finite terms become relevant. At $\mu_{MFV} = 10^3$ GeV neglecting the finite terms in $F_R^{H/K}$ leads to a factor ~ 2 between the approximate and the exact one-loop form factor.

Figure 4.5 shows the partial widths as functions of μ_{MFV} for the approximate, for the exact one-loop decay and for the FCNC tree level resummed decay. In accordance with the behavior of the right-handed form factors, at high scales the exact one-loop and the approximate result agree up to the effect of the non-logarithmic terms on the partial width, which is at the 10% level. The one-loop and the resummed tree

⁴Note that the line connecting the different points uniquely serves to guide the eye.

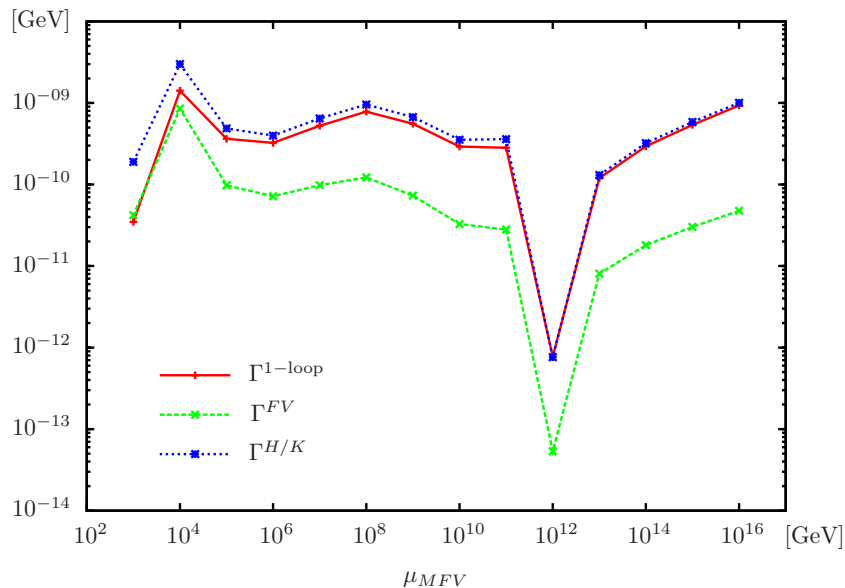


Figure 4.5: Partial decay width $\Gamma(\tilde{t}_1 \rightarrow c\tilde{\chi}_1^0)$ calculated assuming MFV, Γ^{1-loop} (red/full), calculated with the approximate formula, $\Gamma^{H/K}$ (blue/dotted), and calculated at tree level including FV, Γ^{FV} (green/dashed), as function of μ_{MFV} .

level decay agree at low scales where the resummation effects of the large logarithms can be neglected, whereas the deviations are large for high scales. An interesting feature is the size of the decay width. It does not only depend on the size of the logarithm, but also on the coefficient of the logarithmic term, which is given in terms of the soft SUSY breaking parameters, particle masses and mixing angles, *cf.* Eqs. (4.46) and (4.49). As explained above, for each value of the scale μ_{MFV} a different set of boundary conditions $M_0, m_{1/2}, A_0, \tan\beta, \text{sign}(\mu)$ has been chosen such that the \tilde{t}_1 and $\tilde{\chi}_1^0$ masses remain approximately unchanged. This leads to a different coefficient of the logarithmic term for each μ_{MFV} . For $\mu_{MFV} = 10^{12}$ GeV, for example, the parameter set and resulting masses and mixing angles are such that the coefficient becomes rather small, so that the partial width is less than 10^{-12} GeV. However, due to the large value of μ_{MFV} the logarithmic contribution still dominates over the finite terms, so that there is good agreement between the exact one-loop and approximate result. For small values of μ_{MFV} the partial width can be as large as a few 10^{-11} GeV since the factor, which multiplies the logarithm, turns out to be large for the chosen parameter set.

As mentioned in the introduction FV couplings can be tested by means of this stop decay [70, 71]. Small decay widths of less than 10^{-12} GeV, which is the case for certain parameter sets especially when taking resummation effects into account, lead to stop life times in the range of picoseconds and therefore to stops which hadronize before they decay. This raises the possibility of observing a secondary vertex. The suppression needed for a secondary vertex is unique to MFV models. Thus, observing such a vertex would already be a strong support to the MFV principle. After

the decomposition of the neutralino into higgsino and gaugino and the left-right decomposition of the stop is known, measuring the stop lifetime could even provide information on the size of flavor changing couplings.

4.5 Conclusion and Outlook

In this part of the thesis the complete calculation of the loop-induced FCNC decay $\tilde{t}_1 \rightarrow c\tilde{\chi}_1^0$ in the framework of MFV has been presented. The so-called finite terms, which do not depend on the logarithm of the scale μ_{MFV} , where the MFV principle holds, and which have been neglected in a previous work by Hikasa and Kobayashi have been taken into account. The full renormalization program including a gauge-independent renormalization of the quark and squark mixing matrices has been accomplished.

The loop-induced decay has been compared to the approximate result derived earlier by Hikasa and Kobayashi. It has been found that these finite terms contribute to the partial width with about 10%. The approximation becomes worse with decreasing scales of MFV, since in the calculation by Hikasa and Kobayashi the scale, at which the FCNC tree level coupling vanishes, has been fixed to the Planck scale.

The exact one-loop result, and also the approximate formula, however, do not resum the large logarithms. The resummation is done by solving the renormalization group equations. Since MFV is not RG-invariant, flavor changing off-diagonal elements are induced in the squark mixing matrices which lead to FCNC couplings at tree level. The resulting FCNC decay at tree level can be compared to the effective loop-induced coupling. The resummation effects turn out to be important for large scales of MFV. The exact one-loop result and the formula by Hikasa and Kobayashi only give an approximate value of the light stop decay width into charm and neutralino when large scales μ_{MFV} are assumed. Depending on the scenario, the branching ratios of the stop can be affected drastically, leading to a significant deviation from the value $BR(\tilde{t}_1 \rightarrow c\tilde{\chi}_1^0) = 1$, which has been used so far in all phenomenological studies and experimental analyses. The reason for this is that in the corresponding scenario resummation effects have reduced the decay width of $\tilde{t}_1 \rightarrow c\tilde{\chi}_1^0$ by a factor ~ 20 . The search for scalar top quark partners is currently of great phenomenological interest. Since these results can change the assumptions made so far, resummation effects should be taken into account in future analyses, when models with SUSY breaking at high scales are investigated.

The next important step to further improve the prediction for the phenomenologically important light stop decay will be the full calculation of the one-loop corrections to the FCNC tree level decay with resummation effects, including the full flavor structure and the relevant QCD corrections.

Chapter 5

Squark Pair Production at NLO

5.1 Introduction

The search for SUSY particles is one of the major experimental endeavors of high-energy physics at the moment. In the MSSM with conserved R-parity SUSY particles can only be produced in pairs. Since the pair production of squarks and gluinos proceeds via the strong interaction, these channels have typically the largest production cross sections of all SUSY particles. The search for SUSY particles and the determination of their properties at the LHC is based on the analysis of the cascade decay chains in which SUSY particles are produced. On the one hand the shapes of distributions are widely used for phenomenological studies, e.g. for spin determination of SUSY particles by using lepton charge asymmetry [93] or the discrimination of different BSM models [94]. Experimental analyses exploit the kinematic endpoints of mass distributions to determine masses and combinations of masses of the SUSY particles in the decay chains. On the other hand calculations of higher-order corrections have been shown to have a sizable impact on the shape of the distributions, especially near kinematic edges [95]. In this context precise theoretical predictions are crucial for a proper understanding of the distributions, for setting accurate exclusion limits and, in case of a discovery, for the determination of the properties of the new particles.

First LO cross section predictions for pair production of strongly interacting SUSY particles in hadron collisions have been calculated some time ago [96–99]. The calculation of the NLO SUSY QCD corrections has been performed in [20, 100–102] assuming all squarks to be degenerate in mass (except for stop pair production, where all squarks apart from the stop have been assumed to be degenerate in mass). The NLO corrections have been found to be positive and in general large, between 5% and 90% depending on the process and parameters. Not only the large corrections, but also the reduction of the dependence of the total production cross section on the unphysical factorization and renormalization scales to typically 20% to 30% makes the inclusion of the NLO corrections inevitable in phenomenological studies. In the past years a lot of effort has been put in calculating results beyond NLO, taking

into account resummation and threshold effects [103–111]. These corrections can increase the inclusive cross section by 2% to 10% and lead to a further reduction of the scale uncertainty. Furthermore, electroweak contributions have been considered at LO [112, 113] and at NLO [114–120]. These corrections can be sizable but strongly depend on the model parameters and the flavor and chirality of the produced squarks.

The LO cross sections and NLO corrections in SUSY QCD can be calculated with the publicly available computer program `Prospino2` [121]. Since the program is based on the calculations in [20] the NLO corrections can only be evaluated for degenerate squark masses. Furthermore, these corrections are implemented such, that the various subchannels, characterized by different flavor and chirality combinations, are always summed up. Results for individual subchannels can be returned, but these are obtained by scaling the exactly calculated LO cross section for the subchannel with the ratio of the total NLO cross section and the total LO cross section, the so-called K -factor. This approach is based on the assumption that the K -factors do not vary in the different subchannels. Along with the NLO corrections to the total cross section also differential distributions in transverse momentum and rapidity at NLO for the produced SUSY particles have been presented in [20]. It has been found that in these distributions, for the scenarios considered, the NLO corrections have hardly any other effect than scaling the LO distribution by the global K -factor. Based on these results it has been assumed that differential K -factors are flat.

Within this part of the thesis the calculation of squark pair production for squarks of the first two generations at NLO in SUSY QCD without any assumptions on the squark masses is presented. All subchannels are treated individually and the results are implemented in a parton-level Monte-Carlo program, which allows to calculate arbitrary distributions at NLO. As first examples of possible applications of this Monte-Carlo program two problems are addressed. First, it is investigated whether the assumption that the K -factor is constant in the various subchannels is correct. Moreover, it is analyzed whether the differential K -factors are flat in further scenarios and distributions than the ones presented in [20]. The squark pair production is understood as the first step towards the calculation and implementation of all squark and gluino production channels at NLO in a fully flexible partonic Monte-Carlo program. Anticipating to include SUSY QCD corrections also in the decay stages of the produced particles, squark-squark production constitutes an excellent channel for setting up the framework for this project. Since squarks are scalar particles, no spin correlations have to be taken into account when decays of the squarks are added. Additionally, as illustrated in [19], squark pair production is the dominant channel in the higher mass region for squarks and gluinos, which is probed in the current and upcoming searches at LHC. Recently, a calculation of squark pair production with a subsequent decay of each squark into a quark and the lightest neutralino with NLO corrections in production and decay has been published [122]. However, since the methods used to handle and cancel the soft and collinear divergencies in the virtual and real corrections are different - the calculation presented here applies the Catani-Seymour subtraction formalism whereas in [122] phase space slicing has

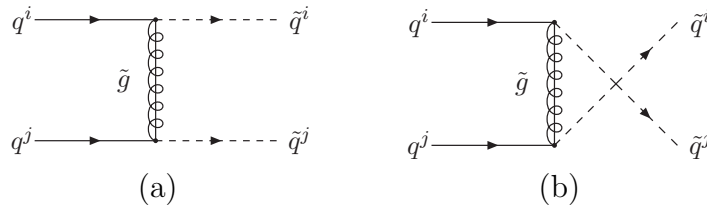


Figure 5.1: Feynman diagrams contributing to LO squark pair production via t -channel (a) or u -channel (b) exchange of a gluino. The latter does not contribute to the production of differently flavored squarks.

been used - both calculations are completely independent and can be exploited for additional cross checks of the phenomenologically important results they provide.

This chapter of the thesis is organized as follows: In Section 5.2 squark pair production at LO is discussed, the notation is set and four different categories of sub-channels are introduced. Section 5.3 is devoted to the presentation of the virtual corrections and the explanation of the renormalization program. The real emission matrix elements and the different contributions to the subtraction counterterm of the Catani-Seymour dipole formalism introduced in Chapter 3.3 are described in detail in Section 5.4. The following Section 5.5 contains the integrated dipoles which are needed to cancel the IR divergencies in the virtual contributions. Finally, the numerical results are presented in Section 5.6. All tests and comparisons which have been made to validate the code are discussed in detail. The calculation and its results are summarized in Section 5.7, where also an outlook on planned related projects is given.

5.2 Squark Pair Production at LO

In order to set the notation and introduce the chirality and flavor structure of the squark pair production process it is useful to discuss the LO process. The momenta of the initial state quarks with flavor indices i and j are always denoted by p_a and p_b , while the momenta of the final state squarks are k_1 and k_2 :

$$q^i(p_a) + q^j(p_b) \rightarrow \tilde{q}_{L,R}^i(k_1) + \tilde{q}_{L,R}^j(k_2) . \quad (5.1)$$

The Feynman diagrams contributing to this process are depicted in Fig. 5.1. The set of Lorentz-invariant, kinematical variables used for the description of the process is given by

$$s = (p_a + p_b)^2 = (k_1 + k_2)^2 \quad (5.2)$$

$$t = (k_1 - p_a)^2 = (k_2 - p_b)^2 \quad (5.3)$$

$$u = (k_1 - p_b)^2 = (k_2 - p_a)^2 . \quad (5.4)$$

The charge conjugated process is not listed explicitly, but will be considered in the calculations of the hadronic cross section and distributions. Since we take only

squarks of the first two generations ($\tilde{u}, \tilde{d}, \tilde{c}, \tilde{s}$) into account in the final state, the quarks in the initial state are assumed to be massless. The amplitudes depend on the flavors and chiralities of the particles and can be categorized into four different subchannels.

- **Same chirality, same flavor**

The matrix element squared, averaged over initial state colors and spins and summed over final state colors reads for pair produced squarks of same chirality and same flavor

$$\overline{|\mathcal{M}_{q^i q^i \rightarrow \tilde{q}^i \tilde{q}^i}|^2} = \frac{1}{2} \cdot \frac{1}{4 \cdot 9} 8g_s^4 m_{\tilde{g}}^2 s \left[\frac{1}{(t - m_{\tilde{g}}^2)^2} + \frac{1}{(u - m_{\tilde{g}}^2)^2} - \frac{2}{3} \frac{1}{(t - m_{\tilde{g}}^2)(u - m_{\tilde{g}}^2)} \right]. \quad (5.5)$$

Since in this case the squarks in the final state are identical an additional statistical factor of 1/2 has to be added on the right side of this equation.

- **Different chirality, same flavor**

For squarks of different chiralities but same flavors and in the limit of vanishing quark masses no interference term between the u - and t -channel arises in the corresponding matrix element squared:

$$\overline{|\mathcal{M}_{q^i q^i \rightarrow \tilde{q}_L^i \tilde{q}_R^i}|^2} = \frac{1}{4 \cdot 9} 8g_s^4 \left[\frac{tu - m_{\tilde{q}_L}^2 m_{\tilde{q}_R}^2}{(t - m_{\tilde{g}}^2)^2} + \frac{tu - m_{\tilde{q}_L}^2 m_{\tilde{q}_R}^2}{(u - m_{\tilde{g}}^2)^2} \right]. \quad (5.6)$$

- **Same chirality, different flavor**

In case the two squarks in the final state have different flavors, no u -channel exchange diagram is possible any more, since all couplings are assumed to be flavor conserving. Therefore, for different flavors and same chiralities of the squarks the matrix element squared is

$$\overline{|\mathcal{M}_{q^i q^j \rightarrow \tilde{q}^i \tilde{q}^j}|^2} = \frac{1}{4 \cdot 9} 8g_s^4 m_{\tilde{g}}^2 \left[\frac{s}{(t - m_{\tilde{g}}^2)^2} \right]. \quad (5.7)$$

- **Different chirality, different flavor**

For different flavors and different chiralities the matrix element yields

$$\overline{|\mathcal{M}_{q^i q^j \rightarrow \tilde{q}_L^i \tilde{q}_R^j}|^2} = \frac{1}{4 \cdot 9} 8g_s^4 \left[\frac{tu - m_{\tilde{q}_L}^2 m_{\tilde{q}_R}^2}{(t - m_{\tilde{g}}^2)^2} \right]. \quad (5.8)$$

In order to obtain the hadronic cross section the squared matrix element has to be integrated over the 2-particle phase space, multiplied by a flux factor and folded with the PDFs as described in Section 3.1.

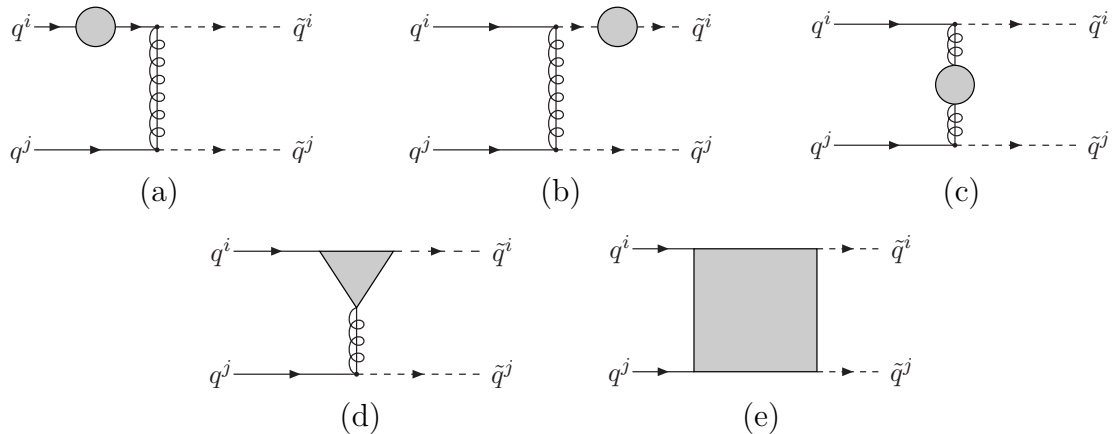


Figure 5.2: Generic Feynman diagrams for virtual corrections like quark (a), squark (b), gluino (c) self energies, vertex corrections (d) and box diagrams (e).

5.3 The Virtual Corrections

The virtual SUSY QCD corrections to squark pair production include gluino, quark and squark self energies, vertex corrections and box diagrams. Generic Feynman diagrams for these corrections are depicted in Fig. 5.2. Of course, also the lower quark and squark lines are affected by the self energy contributions, as well as the lower quark-squark-gluino vertex receives vertex corrections. The individual Feynman diagrams contributing to the quark, squark and gluino self energies, the vertex correction diagrams and the box diagrams are listed in Fig. 5.3. It is important to point out that the diagrams in the last line of this figure do not contribute when both squarks have different flavors. Note that from now on the chirality index is suppressed.

The loop diagrams in the self energies and vertex corrections contain momentum integrals which diverge due to contributions from large momenta. Though these divergencies cancel in the final result after renormalization, it is necessary to introduce a regularization prescription to be able to handle those UV divergencies. Dimensional regularization [51] is a convenient regularization scheme because it respects all gauge symmetries. By lowering the number of space-time dimensions over which one integrates to $D = 4 - 2\epsilon$, the UV divergencies appear as poles in ϵ . But dimensional regularization breaks SUSY because it introduces a mismatch between fermionic and bosonic degrees of freedom. In this scheme all 4-vectors including vector fields are continued to D space time dimensions. That means that the gluon represented by a massless gauge field has $D - 2$ degrees of freedom while its superpartner, the gluino, represented by a Majorana spinor field has only 2 degrees of freedom. Since the matching of fermionic and bosonic degrees of freedom follows from the SUSY algebra, SUSY is broken by this mismatch. The invariance under SUSY transformations enforces the strong gauge coupling g_s and the SUSY Yukawa coupling \hat{g}_s to be equal in all orders of perturbation theory. At one-loop level, when calculating in dimensional regularization, this relation is violated and needs to be restored by adding a finite counterterm. This counterterm can be determined by

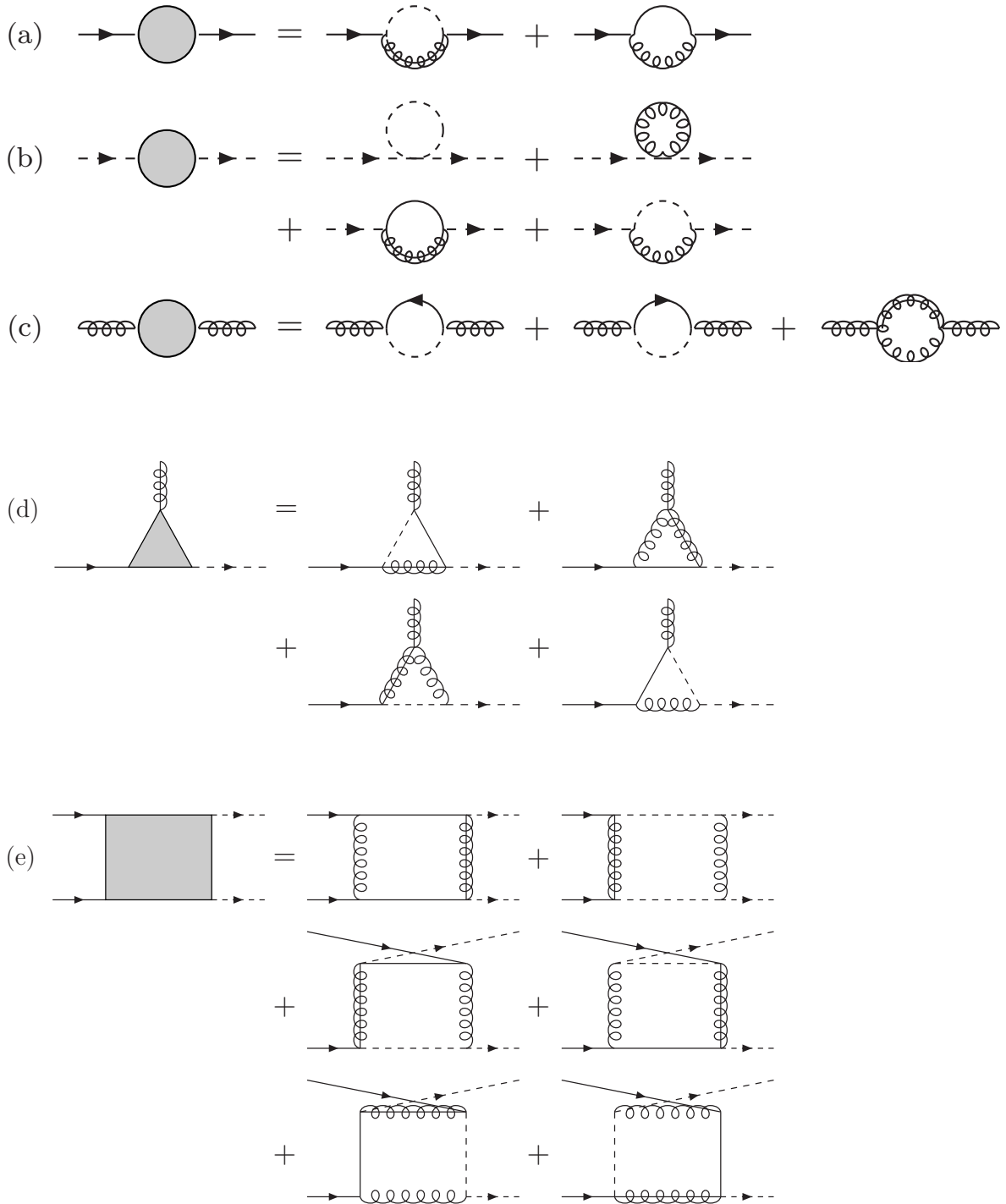


Figure 5.3: Feynman diagrams contributing to quark (a), squark (b) and gluino (c) self energies, vertex corrections (d) and box diagrams (e). The box diagrams in the last line do not contribute when both squarks have different flavors.

comparing the effective vertices in the SUSY limit at small momentum transfer. SUSY can be restored by adding this counterterm to the Yukawa coupling [20]

$$\hat{g}_s = g_s \left(1 + \frac{\alpha_s}{3\pi}\right). \quad (5.9)$$

An alternative renormalization scheme is dimensional reduction [75, 76]. In this scheme no mismatch between bosonic and fermionic degrees of freedom is introduced and SUSY is preserved. As a result both couplings are identical order by order. The transition between these two schemes is well known and involves a finite shift [123]. In the following we use the dimensional regularization scheme supplemented by the finite shift of the Yukawa coupling in Eq. (5.9). On the one hand SUSY is preserved by this procedure and the definition of the strong gauge coupling corresponds to the usual SM measurements [74] on the other hand.

In squark pair production the UV divergencies in the virtual corrections can be absorbed by introducing renormalization constants for the non-vanishing squark and gluino masses

$$m_{\tilde{q}}^2{}^{(0)} = m_{\tilde{q}}^2 + \delta m_{\tilde{q}}^2 \quad (5.10)$$

$$m_{\tilde{g}}^{(0)} = m_{\tilde{g}} + \delta m_{\tilde{g}}, \quad (5.11)$$

the quark, squark and gluino fields

$$q_{L,R}^{(0)} = \left(1 + \frac{1}{2} \delta Z^{q;L,R}\right) q_{L,R} \quad (5.12)$$

$$\tilde{q}^{(0)} = \left(1 + \frac{1}{2} \delta Z^{\tilde{q}}\right) \tilde{q} \quad (5.13)$$

$$\tilde{g}^{(0)} = \left(1 + \frac{1}{2} \delta Z^{\tilde{g}}\right) \tilde{g} \quad (5.14)$$

and the coupling constant

$$g_s^{(0)} = g_s + \delta g_s. \quad (5.15)$$

The renormalization constants are fixed by renormalization conditions. For the mass and the field renormalization constants we choose on-shell renormalization conditions as introduced explicitly in Chapter 3.2. By inserting the renormalized self energies into these conditions it is possible to calculate the renormalization constants from the unrenormalized quark, squark and gluino self energies. The self energy of the squarks is denoted by $\Sigma_{ij}^{\tilde{q}}(p^2)$, the structure of the quark self energy reads here

$$\begin{aligned} \Sigma_{ij}^q(p^2) &= \not{p} \Sigma_{ij}^{q,L}(p^2) \mathcal{P}_L + \not{p} \Sigma_{ij}^{q,R}(p^2) \mathcal{P}_R + m_{q_i} \Sigma_{ij}^{q,Ls}(p^2) \mathcal{P}_L + m_{q_j} \Sigma_{ij}^{q,Rs}(p^2) \mathcal{P}_R \\ &= \not{p} \Sigma_{ij}^{q,L}(p^2) \mathcal{P}_L + \not{p} \Sigma_{ij}^{q,R}(p^2) \mathcal{P}_R. \end{aligned} \quad (5.16)$$

The last two terms in the first line of Eq. (5.16) vanish since we take only the quarks of the first two generations into account and treat them as massless. The gluino self energy is according to Eq. (3.9) decomposed to

$$\Sigma_{\tilde{g}\tilde{g}}(p^2) = \not{p} \Sigma_{\tilde{g}\tilde{g}}(p^2) + m_{\tilde{g}} \Sigma_{\tilde{g}\tilde{g}}^s(p^2). \quad (5.17)$$

With these definitions the renormalization constants introduced in Eqs. (5.10)-(5.14) can be expressed as

$$\delta m_{\tilde{q}}^2 = \widetilde{\text{Re}} \Sigma_{ii}^{\tilde{q}}(m_{\tilde{q}_i}^2) \quad (5.18)$$

$$\delta m_{\tilde{g}} = m_{\tilde{g}} \widetilde{\text{Re}} [\Sigma_{\tilde{g}\tilde{g}}(m_{\tilde{g}}^2) + \Sigma_{\tilde{g}\tilde{g}}^s(m_{\tilde{g}}^2)] \quad (5.19)$$

$$\delta Z_{ii}^{q;L,R} = -\widetilde{\text{Re}} \Sigma_{ii}^{q;L,R}(m_{q_i}) \quad (5.20)$$

$$\delta Z_{ii}^{\tilde{q}} = -\widetilde{\text{Re}} \partial \Sigma_{ii}^{\tilde{q}}(m_{\tilde{q}_i}^2) \quad (5.21)$$

$$\delta Z^{\tilde{g}} = -\widetilde{\text{Re}} \Sigma_{\tilde{g}\tilde{g}}(m_{\tilde{g}}^2) - 2m_{\tilde{g}}^2 \widetilde{\text{Re}} [\partial \Sigma_{\tilde{g}\tilde{g}}(m_{\tilde{g}}^2) + \partial \Sigma_{\tilde{g}\tilde{g}}^s(m_{\tilde{g}}^2)] \quad (5.22)$$

where $\partial \Sigma$ is an abbreviation for the partial derivative of the respective self energy

$$\partial \Sigma(m^2) = \frac{\partial \Sigma(p^2)}{\partial p^2} \Big|_{p^2=m^2} . \quad (5.23)$$

The non-diagonal quark and squark field renormalization constants vanish for quark masses equal to zero and mixing matrices of the first two generations equal to the unity matrix.

For the strong coupling renormalization constant we work in the $\overline{\text{MS}}$ -scheme [50], where only the $1/\epsilon$ -UV poles along with some universal constants are absorbed. It is determined via the transverse part of the gluon self energy

$$\delta g_s = \frac{1}{2} \delta Z_g \quad g_s = \frac{1}{2} \left(-\widetilde{\text{Re}} \partial \Sigma_{gg}(0) \right) \quad g_s . \quad (5.24)$$

The longitudinal part of the gluon self energy vanishes due to a Ward identity. The renormalization constant of the strong coupling is in this scheme

$$\delta g_s^{\overline{\text{MS}}} = -\frac{\alpha_s}{8\pi} \beta_0 \Delta \quad g_s , \quad (5.25)$$

with

$$\Delta = 1/\epsilon - \gamma + \log 4\pi \quad (5.26)$$

denoting the pole and constants that have been absorbed. Here, γ is the Euler-Mascheroni constant. The one-loop beta function coefficient β_0 in this counterterm contains contributions from SM as well as SUSY particles. These contribute to the gluon self energy diagrams and thus to the running of the strong coupling. The strong coupling depends on the renormalization scale and this scale dependence is governed to one-loop level by

$$Q^2 \frac{dg_s(Q^2)}{dQ^2} = -g_s(Q^2) \frac{\alpha_s(Q^2)}{8\pi} \beta_0 . \quad (5.27)$$

The contributions of the different particles to the one-loop beta function coefficient are in detail

$$\begin{aligned} \beta_0 &= \left[11 - \frac{2}{3} \cdot 5 \right] + \left[-2 - \frac{2}{3} - \frac{1}{6} \cdot 12 \right] \\ &= \beta_0^L + \beta_0^H . \end{aligned} \quad (5.28)$$

The first term in the line above stands for the contribution of the gluon and the five light quarks, the second one for the contributions of the heavy particles, the gluino, the top quark and the twelve squarks. However, the experimental value of α_s is given within non-SUSY QCD with only five active quark flavors [74]. In order to match the experimental value of α_s the heavy particles are decoupled from the running of α_s . The relation between these two schemes involves the subtraction of the logarithms of the masses of the heavy particles¹

$$\delta g_s^{\overline{\text{MS}}_5} = \delta g_s^{\overline{\text{MS}}} g_s - \frac{\alpha_s}{8\pi} \left[2 \log \frac{m_{\tilde{g}}^2}{Q^2} + \frac{2}{3} \log \frac{m_t^2}{Q^2} + \sum_{i=1,12} \frac{1}{6} \log \frac{m_{\tilde{q}_i}^2}{Q^2} \right] g_s . \quad (5.29)$$

This technique assures that only the gluon and the five light quarks contribute to the running of α_s :

$$\begin{aligned} Q^2 \frac{d g_s^{\overline{\text{MS}}_5}(Q^2)}{d Q^2} &= -g_s(Q^2) \frac{\alpha_s(Q^2)}{8\pi} \left[\beta_0 + 2 + \frac{2}{3} + \frac{1}{6} \cdot 12 \right] \\ &= -g_s(Q^2) \frac{\alpha_s(Q^2)}{8\pi} \beta_0^L . \end{aligned} \quad (5.30)$$

This decoupling is not strictly necessary but then the contributions from the heavy particles have to be taken into account as a relation between the experimental value and the coupling constant used in the calculation. In order to avoid this the calculation was worked out including this decoupling.

The code for the LO amplitude and the virtual corrections has been generated with the `Mathematica` packages `FeynArts` [128, 129] and `FormCalc` [130, 131]. The former generates and visualizes Feynman diagrams and amplitudes, the latter reads diagrams generated with `FeynArts` and calculates tree-level and one-loop Feynman diagrams. `FormCalc` writes out a Fortran subroutine to compute the squared matrix element for a given process. The one-loop integrals in the calculation are evaluated by the program package `LoopTools` [130] which is based on an interface to the scalar one-loop functions of the program `FF` [132].

`FeynArts` provides a model file with the Feynman rules of the MSSM. In contrast to the model file of the SM, in the MSSM model file no counterterms are specified. These have been added according to the renormalization procedure described above. It has been checked explicitly that this procedure renders the calculation UV finite by adding up all contributions proportional to the $1/\epsilon$ poles.

After canceling all UV divergencies by renormalization the IR divergencies are still left. They will be canceled against the IR divergencies from the real emission diagrams by applying the Catani-Seymour subtraction formalism as described in Section 3.3.

¹Decoupling relations for the strong coupling α_s are known to two-loop order for a degenerate supersymmetric mass spectrum [124–126] and to three-loop order for several different assumptions on the masses of the MSSM [127].

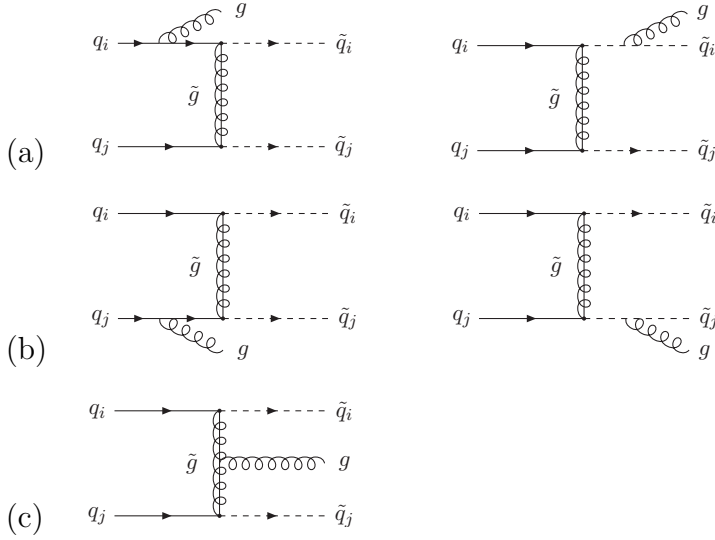


Figure 5.4: Feynman diagrams contributing to real emission matrix elements with qq initial states and an emitted gluon. Diagrams which lead to soft and collinear divergencies are depicted in (a) and (b), the diagram in (c) is IR finite.

5.4 The Real Emission and Subtraction Dipoles

The matrix elements of the real emission of one additional parton can be classified in two different topologies. The first topology contains diagrams with two quarks in the initial state and the additionally emitted particle being a gluon:

$$q_i(p_a) q_j(p_b) \rightarrow \tilde{q}_i(k_1) \tilde{q}_j(k_2) g(k_3) . \quad (5.31)$$

These diagrams are shown in Fig. 5.4. The second topology comprises diagrams with a quark and a gluon in the initial state and an emitted, massless antiquark. These diagrams are depicted in Fig. 5.5. Apart from implementing

$$g(p_a) q_i(p_b) \rightarrow \tilde{q}_i(k_1) \tilde{q}_j(k_2) \bar{q}_j(k_3) \quad (5.32)$$

it is important to include for $i \neq j$ also

$$g(p_a) q_j(p_b) \rightarrow \tilde{q}_i(k_1) \tilde{q}_j(k_2) \bar{q}_i(k_3) \quad (5.33)$$

in order to account for all possible initial state configurations.

Both topologies for real emission of an antiquark or a gluon comprise diagrams which lead to IR divergencies. In the diagrams with qq initial states the gluon, being a massless particle, can be emitted from on-shell external particles, either as being attached to one of the squarks in the final or to one of the quarks in the initial state. This configuration is called softly divergent when the energy of the emitted gluon is too small to be identified experimentally as an isolated jet, i.e. when the gluon is soft. Additionally, the gluon attached to the two massless propagators of

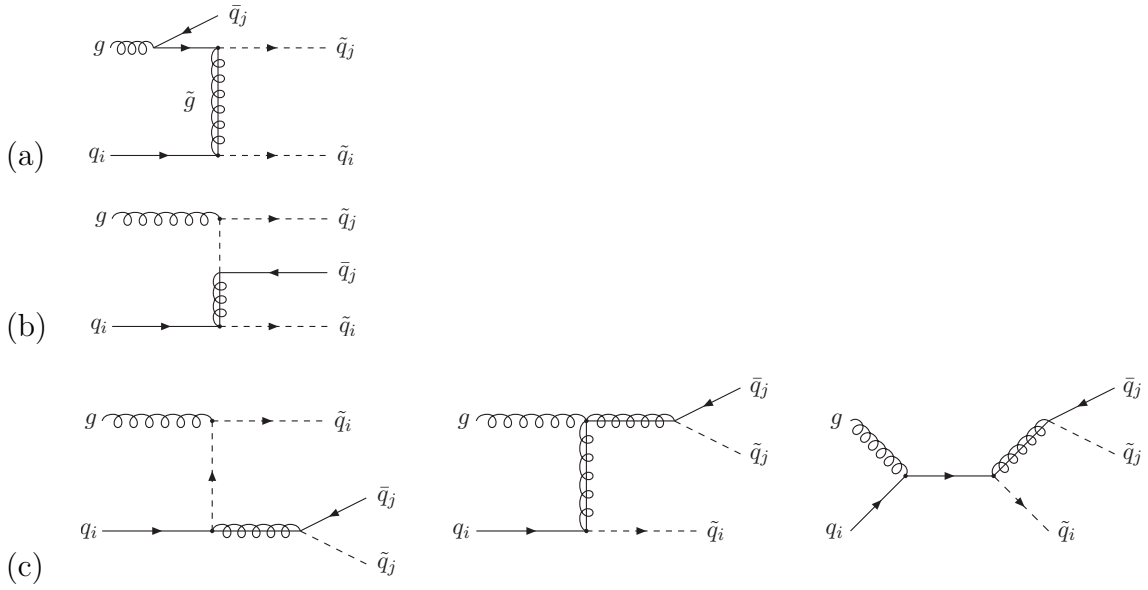


Figure 5.5: Feynman diagrams contributing to real emission matrix elements with qq initial states. The diagram in (a) gives rise to collinear singularities. The diagrams in (b) and (c) are IR finite. The diagrams in (c) can contribute to resonant production of squarks and gluinos.

the quarks in the initial state gives rise to collinear divergencies. These emerge when the angle between the emitted parton and the emitter parton is too small to separate these two particles from each other. Collinear divergencies appear only for massless propagators and are screened by massive emitters. Diagrams with qq initial states, which lead to soft and collinear divergencies, are collected in Fig. 5.4 (a) and (b). In the diagrams with qq initial states the emitted, massless antiquark can also be attached to the massless propagators in the initial state, resulting in further collinear divergencies. The corresponding diagram is shown in Fig. 5.5 (a).

The diagrams in Fig. 5.5 (c) have to be handled with care in parameter regions where the gluino is heavier than one or both squarks of the final state. In this case, these diagrams contribute to the resonant production of a squark in association with a gluino. This resonant production channel basically corresponds to LO squark-gluino production and a subsequent decay of the on-shell gluino into a squark and an antiquark. In order to avoid double-counting these contributions have to be subtracted consistently from squark-squark production. Although not discussed further in this thesis, since the relevant parameter regions are not taken into account in the numerical analysis, consistent subtraction procedures exist for different processes in the literature [20, 133, 134].

Both kinds of divergencies, soft and collinear, are subtracted by the Catani-Seymour dipoles in the counterterm $d\sigma^A$ as already sketched in Chapter 3.3. The expressions for the real emission matrix elements, dipoles and integrated dipoles, which will be introduced in the next section, have been generated using the **SuperAutoDipole** package [135, 136]. **SuperAutoDipole** itself provides an interface with the program

MadGraph [137, 138], which automatically provides a code for the squared matrix elements of the real emission diagrams by calling the HELAS subroutines based on the helicity amplitude formalism [139].

The dipoles needed to render the real emission matrix elements finite are organized in pairs of potentially collinear partons with an additional reference to a spectator parton. For diagrams with two quarks in the initial state this gives rise to twelve individual dipoles: The emitted gluon can be collinear to the initial state or soft to the final state particles and in each case any of the other three particles can serve as spectator parton. For diagrams with a quark and a gluon in the initial state only three dipoles are necessary: The emitted antiquark can only become collinear to the initial state gluon while the other three particles can act as the spectator parton, again. Hence, we have

$$d\sigma_{qq}^A = \sum_{i=1}^{12} \mathcal{D}_i^{qq} \quad d\sigma_{qg}^A = \sum_{i=1}^3 \mathcal{D}_i^{qg} . \quad (5.34)$$

In the following we discuss the individual dipoles contributing to the counterterms in Eq. (5.34).

Initial state singularities with initial state spectators

The first category of dipoles covers initial state emitter pairs with another initial state particle taken to be the spectator. For qq initiated processes with initial and final momenta assigned as in Eq. (5.31) the first combination reads

$$\begin{aligned} \mathcal{D}^{q_i(p_a)g(k_3),q_j(p_b)} &= -\frac{1}{2p_a k_3} \frac{1}{x_{3,ab}} 8\pi\alpha_s C_F \cdot \left[\frac{2}{1-x_{3,ab}} - (1+x_{3,ab}) \right] \\ &\cdot \left| \mathcal{M}^{a,b}(\tilde{p}_a, p_b, \tilde{k}_1, \tilde{k}_2) \right|^2 . \end{aligned} \quad (5.35)$$

The first line on the right side of Eq. (5.35) consists of the dipole factors which match the singular behavior of the corresponding real emission matrix element. The constant $C_F = \frac{4}{3}$ is a color factor and $x_{3,ab}$ a momentum fraction parameter defined as

$$x_{3,ab} = \frac{p_a p_b - k_3 p_a - k_3 p_b}{p_a p_b} . \quad (5.36)$$

In the second line of Eq. (5.35) $|\mathcal{M}^{a,b}(\tilde{p}_a, p_b, \tilde{p}_1, \tilde{p}_2)|^2$ denotes the color linked Born amplitude squared (see Eq. (3.19)) evaluated with a set of Born-type kinematics which is deduced from the 3-particle real emission kinematics according to

$$\tilde{p}_a^\mu = x_{3,ab} p_a^\mu \quad \tilde{p}_b^\mu = p_b^\mu \quad (5.37)$$

and

$$\tilde{k}_i^\mu = k_i^\mu - \frac{2k_i(K + \tilde{K})}{(K + \tilde{K})^2} (K + \tilde{K})^\mu + \frac{2k_i K}{K^2} \tilde{K}^\mu \quad (5.38)$$

with

$$K^\mu = p_a^\mu + p_b^\mu - k_3^\mu \quad \tilde{K}^\mu = \tilde{p}_a^\mu + p_b^\mu . \quad (5.39)$$

This transformation to the so-called tilde kinematics is performed in such a way that the momentum of the additional final state parton vanishes. In this special case the momentum of the spectator p_b is kept unchanged whereas apart from the momentum of the emitter p_a the momenta of the final state particles are altered in order to correctly implement four-momentum conservation in the underlying Born process

$$\tilde{p}_a + p_b - \tilde{k}_1 - \tilde{k}_2 = 0 , \quad (5.40)$$

as well as the on-shell conditions

$$\begin{aligned} \tilde{p}_a^2 &= p_b^2 = 0 \\ \tilde{k}_1^2 &= m_{\tilde{q}_i}^2 \\ \tilde{k}_2^2 &= m_{\tilde{q}_j}^2 . \end{aligned} \quad (5.41)$$

The expressions in Eqs. (5.35)-(5.39) can also be applied without any change to the initial-initial dipoles $\mathcal{D}^{g(p_a)\tilde{q}_j(k_3),q_i(p_b)}$ and $\mathcal{D}^{g(p_a)\tilde{q}_i(k_3),q_j(p_b)}$ in the processes (5.32) and (5.33) with a gluon in the initial state.

The gluon in the qq initiated processes can also be emitted by the second parton in the initial state. Thus a second dipole absorbs the divergencies stemming from this configuration. It is obtained by a trivial interchange of the initial state momenta

$$\begin{aligned} \mathcal{D}^{q_j(p_b)g(k_3),q_i(p_a)} &= -\frac{1}{2p_b k_3} \frac{1}{x_{3,ab}} 8\pi\alpha_s C_F \cdot \left[\frac{2}{1-x_{3,ab}} - (1+x_{3,ab}) \right] \\ &\cdot \left| \mathcal{M}^{b,a}(p_a, \tilde{p}_b, \tilde{k}_1, \tilde{k}_2) \right|^2 , \end{aligned} \quad (5.42)$$

just as the corresponding tilde kinematics

$$\tilde{p}_a^\mu = p_a^\mu \quad \tilde{p}_b^\mu = x_{3,ab} p_b^\mu \quad (5.43)$$

and

$$\tilde{K}^\mu = p_a^\mu + \tilde{p}_b^\mu . \quad (5.44)$$

Initial state singularities with final state spectators

The second category of dipoles is responsible for initial state singularities with a final state parton as spectator. The first dipole for the qq initiated processes is

$$\begin{aligned} \mathcal{D}_{\tilde{q}_i(k_1)}^{q_i(p_a)g(k_3)} &= -\frac{1}{2p_a k_3} \frac{1}{x_{31,a}} 8\pi\alpha_s C_F \cdot \left[\frac{2}{1-x_{31,a}+u_3} - (1+x_{31,a}) \right] \\ &\cdot \left| \mathcal{M}^{a,1}(\tilde{p}_a, p_b, \tilde{k}_1, k_2) \right|^2 \end{aligned} \quad (5.45)$$

with the parameters $x_{31,a}$ and u_3 defined as

$$x_{31,a} = \frac{k_1 p_a + k_3 p_a - k_3 k_1}{(k_1 + k_3) p_a} \quad u_3 = \frac{k_3 p_a}{(k_1 + k_3) p_a} . \quad (5.46)$$

In this case for the reduced kinematics only the momenta of the emitter and the spectator are transformed according to

$$\tilde{p}_a^\mu = x_{31,a} p_a^\mu \quad \tilde{k}_1^\mu = k_1^\mu + k_3^\mu - (1 - x_{31,a}) p_a^\mu . \quad (5.47)$$

Another possible combination for an initial-final dipole is obtained by choosing the other squark in the final state as spectator. The expression and the kinematics for this dipole, $\mathcal{D}_{\tilde{q}_j(k_2)}^{q_i(p_a)g(k_3)}$, are obtained from the above formulas by an interchange of the final state momenta k_1 and k_2 .

Since in the processes with two quarks in the initial state the gluon can also become collinear to the second quark in the initial state two more dipoles arise

$$\mathcal{D}_{\tilde{q}_i(k_1)}^{q_j(p_b)g(k_3)} \quad \text{and} \quad \mathcal{D}_{\tilde{q}_j(k_2)}^{q_j(p_b)g(k_3)} .$$

Their expressions and kinematics follow from Eqs. (5.45)-(5.47) by interchanging p_a and p_b or k_1 and k_2 , respectively.

This category completes potential dipole combinations for the processes with qg initial states. The dipoles

$$\mathcal{D}_{\tilde{q}_i(k_1)}^{g(p_a)\tilde{q}_j(k_3)} \quad \text{and} \quad \mathcal{D}_{\tilde{q}_i(k_1)}^{g(p_a)\tilde{q}_i(k_3)}$$

as well as their versions with the second squark chosen to be the spectator

$$\mathcal{D}_{\tilde{q}_j(k_2)}^{g(p_a)\tilde{q}_j(k_3)} \quad \text{and} \quad \mathcal{D}_{\tilde{q}_j(k_2)}^{g(p_a)\tilde{q}_i(k_3)}$$

can also be calculated from the formulas listed above by trivial interchanges of momenta.

Final state singularities with initial state spectators

The third category of dipoles renders configurations with final state singularities and initial state spectators finite. The first out of four possible dipoles is:

$$\begin{aligned} \mathcal{D}_{g(k_3)\tilde{q}_i(k_1)}^{q_i(p_a)} &= -\frac{1}{2p_a k_3} \frac{1}{x_{31,a}} 8\pi\alpha_s C_F \cdot \left[\frac{2}{2 - x_{31,a} - \tilde{z}_1} - 2 - \frac{m_{\tilde{q}_i}^2}{k_3 k_1} \right] \\ &\cdot \left| \mathcal{M}^{1,a}(\tilde{p}_a, p_b, \tilde{k}_1, k_2) \right|^2 . \end{aligned} \quad (5.48)$$

The parameters $x_{31,a}$ and \tilde{z}_1 in these dipoles are composed of the momenta of the contributing particles in the following way

$$x_{31,a} = \frac{k_3 p_a + k_1 p_a - k_3 k_1}{(k_1 + k_3) p_a} \quad \tilde{z}_1 = \frac{p_a k_1}{(k_1 + k_3) p_a} . \quad (5.49)$$

The reduced kinematics entering the color linked Born amplitude in Eq. (5.48) involves transformations for the momenta of the spectator and emitter parton

$$\tilde{p}_a^\mu = x_{31,a} p_a^\mu \quad \tilde{k}_1^\mu = k_1^\mu + k_3^\mu - (1 - x_{31,a}) p_a^\mu . \quad (5.50)$$

Another three dipoles of this category arise by changing the spectator from $q_i(p_a)$ to $q_j(p_b)$ and/or the emitter from $\tilde{q}_i(k_1)$ to $\tilde{q}_j(k_2)$

$$\mathcal{D}_{g(k_3)\tilde{q}_i(k_1)}^{q_j(p_b)}, \quad \mathcal{D}_{g(k_3)\tilde{q}_j(k_2)}^{q_i(p_a)} \quad \text{and} \quad \mathcal{D}_{g(k_3)\tilde{q}_j(k_2)}^{q_j(p_b)} . \quad (5.51)$$

Final state singularities with final state spectators

The last category of dipoles contributes to the cancellation of final state singularities with reference to a final state spectator. Since only the two final state squarks are taken into account in this category there are only two dipoles, the first of which reads

$$\mathcal{D}_{g(k_3)\tilde{q}_i(k_1),\tilde{q}_j(k_2)} = -\frac{1}{2k_1k_3} 8\pi\alpha_s C_F \cdot \left[\frac{2}{1-\tilde{z}_1(1-y_{31,2})} - \frac{\tilde{v}_{31,2}}{v_{31,2}} \left(2 + \frac{m_{\tilde{q}_i}^2}{k_1k_3} \right) \right] \cdot \left| \mathcal{M}^{1,2}(p_a, p_b, \tilde{k}_1, \tilde{k}_2) \right|^2. \quad (5.52)$$

The parameters which are directly defined by the momenta of the particles in the process are

$$\tilde{z}_1 = \frac{k_1k_2}{(k_1+k_3)k_2} \quad \text{and} \quad y_{31,2} = \frac{k_1k_3}{k_1k_3+k_2k_3+k_1k_2}. \quad (5.53)$$

For the definition of the relative velocities $\tilde{v}_{31,2}$ and $v_{31,2}$ we need to introduce the sum of the four-momenta of the final state particles

$$Q^\mu = k_1^\mu + k_2^\mu + k_3^\mu \quad (5.54)$$

as well as the rescaled squark masses

$$\mu_1 = \frac{m_{\tilde{q}_i}}{\sqrt{Q^2}} \quad \text{and} \quad \mu_2 = \frac{m_{\tilde{q}_j}}{\sqrt{Q^2}}. \quad (5.55)$$

The relative velocity $\tilde{v}_{31,2}$ between \tilde{k}_1 and \tilde{k}_2

$$\tilde{v}_{31,2} = \frac{\sqrt{\lambda(1, \mu_1^2, \mu_2^2)}}{1 - \mu_1^2 - \mu_2^2} \quad (5.56)$$

is expressed in terms of the triangular function

$$\lambda(x, y, z) = x^2 + y^2 + z^2 - 2xy - 2xz - 2yz. \quad (5.57)$$

The relative velocity $v_{31,2}$ between $k_1 + k_3$ and k_2 is a function of $y_{31,2}$ and reads explicitly

$$v_{31,2} = \frac{\sqrt{[2\mu_2^2 + (1 - \mu_1^2 - \mu_2^2)(1 - y_{31,2})]^2 - 4\mu_2^2}}{(1 - \mu_1^2 - \mu_2^2)(1 - y_{31,2})}. \quad (5.58)$$

The reduced kinematics for final-final dipoles requires transformations of the final state momenta

$$\tilde{k}_1^\mu = k_1^\mu + k_3^\mu - \frac{y_{31,2}}{1 - y_{31,2}} k_2^\mu \quad \tilde{k}_2^\mu = \frac{1}{1 - y_{31,2}} k_2^\mu. \quad (5.59)$$

The second dipole in this category

$$\mathcal{D}_{g(k_3)\tilde{q}_i(k_2),\tilde{q}_j(k_1)} \quad (5.60)$$

can be straightforwardly calculated from the expressions above by replacing k_1 by k_2 and vice versa.

5.5 The Integrated Dipoles

Having subtracted the counterterm from the real emission matrix elements the cancellation takes place among the virtual corrections

$$\int d\Phi_2 [d\sigma^V + \int d\Phi_1 d\sigma^A] . \quad (5.61)$$

With the choice of dipoles as published in [52, 53] and described in the previous section, the counterterm can be integrated analytically over the one-parton phase space. This integration yields the so-called **I**-terms and **PK**-terms:

$$\int d\Phi_1 d\sigma^A = [d\sigma^B \otimes \mathbf{I}] + \int_0^1 dx [d\sigma^B \otimes (\mathbf{P}(x, \mu_F^2) + \mathbf{K}(x))] . \quad (5.62)$$

The **I** operator contains all IR poles multiplying the Born-level matrix element and the **P** and **K** operators give rise to a finite collinear remainder and involve an integration over x , the longitudinal momentum fraction after the splitting in the initial state. In the following subsections these two contributions to the integrated dipoles are presented in more detail.

5.5.1 I terms

The **I**-terms are obtained from the LO expression by replacing the LO matrix element squared by

$${}_{m;a,b} \langle 1, \dots, m; a, b | \mathbf{I} | 1, \dots, m; a, b \rangle_{m;a,b} . \quad (5.63)$$

The insertion operator **I** depends on the color charges, momenta and masses of the particles in the initial (a, b) and final ($1, \dots, m$; here: $m = 2$) state of the process. It further depends on the 't Hooft scale μ and on the regularization parameter ϵ . The expansion of the following expressions in ϵ gives rise to terms with $1/\epsilon^2$ and $1/\epsilon$ poles, which are necessary to cancel the corresponding terms in the virtual corrections:

$$\begin{aligned} \mathbf{I}_{m+a+b}(p_a, p_b, k_1, m_1, k_2, m_2) = & \\ & \mathbf{I}_m(k_1, m_1, k_2, m_2) + \mathbf{I}_a(p_a, k_1, m_1, k_2, m_2) + \mathbf{I}_b(p_b, k_1, m_1, k_2, m_2) \\ & - \frac{\alpha_s}{2\pi} \frac{(4\pi)^\epsilon}{\Gamma(1-\epsilon)} \left(\frac{1}{\mathbf{T}_a^2} \mathbf{T}_a \cdot \mathbf{T}_b \left[\left(\frac{\mu^2}{s_{ab}} \right)^\epsilon \left(\frac{\mathbf{T}_a^2}{\epsilon^2} + \frac{\gamma_a}{\epsilon} \right) - \mathbf{T}_a^2 \frac{\pi^2}{3} + \gamma_a + K_a \right] + (a \leftrightarrow b) \right) . \end{aligned} \quad (5.64)$$

The contribution to this operator from the integrated final-final dipoles is

$$\begin{aligned} \mathbf{I}_m(k_1, m_1, k_2, m_2) = & - \frac{\alpha_s}{2\pi} \frac{(4\pi)^\epsilon}{\Gamma(1-\epsilon)} \sum_j \frac{1}{\mathbf{T}_j^2} \sum_{k \neq j} \mathbf{T}_j \cdot \mathbf{T}_k \\ & \times \left[\mathbf{T}_j^2 \left(\frac{\mu^2}{s_{jk}} \right)^\epsilon \left(\mathcal{V}_j(s_{jk}, m_j, m_k) - \frac{\pi^2}{3} \right) + \Gamma_j(\mu, m_j) \right. \\ & \left. + \gamma_j \log \frac{\mu^2}{s_{jk}} + \gamma_j + K_j + \mathcal{O}(\epsilon) \right] , \end{aligned} \quad (5.65)$$

where the sum runs over possible final state emitter partons (j) and final state spectators (k). The contribution from final-initial and initial-final dipoles is

$$\begin{aligned} \mathbf{I}_a(p_a, k_1, m_1, k_2, m_2) = & -\frac{\alpha_s}{2\pi} \frac{(4\pi)^\epsilon}{\Gamma(1-\epsilon)} \sum_j \{ \\ & \frac{1}{\mathbf{T}_j^2} \mathbf{T}_j \cdot \mathbf{T}_a \left[\mathbf{T}_j^2 \left(\frac{\mu^2}{s_{ja}} \right)^\epsilon \left(\mathcal{V}_j(s_{ja}, m_j, 0) - \frac{\pi^2}{3} \right) + \Gamma_j(\mu, m_j) \right. \\ & \quad \left. + \gamma_j \log \frac{\mu^2}{s_{ja}} + \gamma_j + K_j \right] \\ & + \frac{1}{\mathbf{T}_a^2} \mathbf{T}_a \cdot \mathbf{T}_j \left[\mathbf{T}_a^2 \left(\frac{\mu^2}{s_{aj}} \right)^\epsilon \left(\mathcal{V}_a(s_{aj}, 0, m_j) - \frac{\pi^2}{3} \right) + \frac{\gamma_a}{\epsilon} \right. \\ & \quad \left. + \gamma_a \log \frac{\mu^2}{s_{aj}} + \gamma_a + K_a \right] \} , \end{aligned} \quad (5.66)$$

with j denoting either a final state emitter or spectator parton.

The color charge operators act on the color space of the Born amplitude and the same rules as introduced in Eqs. (3.19) and (3.20) apply. As a consequence the same color linked Born amplitudes squared as in the dipoles of the previous section enter also the calculation of the \mathbf{I} -terms. Since the initial state particles in the Born process are two quarks, the constants γ_a and K_a are always equal to

$$\gamma_q = \frac{3}{2} C_F, \quad K_q = \left(\frac{7}{2} - \frac{\pi^2}{6} \right) C_F. \quad (5.67)$$

The constants γ_j and K_j refer to the final state squarks,

$$\gamma_{\bar{q}} = 2C_F, \quad K_{\bar{q}} = \left(4 - \frac{\pi^2}{6} \right) C_F. \quad (5.68)$$

The dependence on the momenta is hidden in the kinematical variable $s_{xy} = 2 p_x p_y$, where p_x and p_y are the momenta of the 2-particle phase space which are also used to evaluate the LO production process and the virtual corrections.

The functions Γ_j , which are singular in four dimensions, depend on the flavor of parton j and on the parton masses, just as the kernels \mathcal{V}_j and \mathcal{V}_a which additionally depend on the momenta. Both functions are listed in Appendix C.

The program `SuperAutoDipole` [135, 136] generates a Fortran code for the \mathbf{I} -terms as functions of the momenta and masses of the partons. It provides a flag in order to separately extract the coefficients of the $1/\epsilon^2$ and $1/\epsilon$ poles as well as the finite parts. In principle the program `LoopTools`, which has been used to evaluate the virtual corrections, provides the same feature for the coefficients of the poles of the loop diagrams. By combining these two tools it is basically possible to compare the coefficients of the poles for every phase space point during the numerical evaluation of the process and check whether the cancellation of the divergencies in the virtual corrections works.

However, it has to be taken into account that in the code generated by `LoopTools` the term

$$\frac{(4\pi)^\epsilon}{\Gamma(1-\epsilon)} = 1 + \epsilon [\log 4\pi - \gamma] + \epsilon^2 \left[\frac{1}{2}(\log^2 4\pi + \gamma^2) - \frac{\pi^2}{12} - \gamma \cdot \log 4\pi \right] + \mathcal{O}(\epsilon^3) \quad (5.69)$$

has been factored out. In order to achieve agreement between the coefficients of the poles from the virtual corrections and the \mathbf{I} -terms this factor has to be added back in by hand. This changes the coefficient C_{-1} of the $1/\epsilon$ poles and the finite part C_0 of the virtual corrections calculated by the `LoopTools` software:

$$\begin{aligned} & \left(C_{-2} \frac{1}{\epsilon^2} + C_{-1} \frac{1}{\epsilon} + C_0 \right) \times \\ & \left(1 + \epsilon [\log 4\pi - \gamma] + \epsilon^2 \left[\frac{1}{2}(\log^2 4\pi + \gamma^2) - \frac{\pi^2}{12} - \gamma \cdot \log 4\pi \right] \right) = \\ & \left(C_0 + C_{-1} [\log 4\pi - \gamma] + C_{-2} \left[\frac{1}{2}(\log^2 4\pi + \gamma^2) - \frac{\pi^2}{12} - \gamma \cdot \log 4\pi \right] \right) + \\ & \left(C_{-1} + C_{-2} [\log 4\pi - \gamma] \right) \frac{1}{\epsilon} + C_{-2} \frac{1}{\epsilon^2} . \end{aligned} \quad (5.70)$$

With this modification the cancellation of IR divergencies from the virtual corrections by subtracting the integrated Catani-Seymour dipoles can be carried out successfully.² Validation and explicit tests of this subtraction procedure will be discussed in Section 5.6.1.

5.5.2 \mathbf{PK} terms

The remaining initial-state collinear divergencies can be reabsorbed into the non-perturbative PDFs. The finite terms that remain after canceling all IR divergencies can be calculated by the \mathbf{P} and \mathbf{K} operators. Their contribution to the partonic cross section is:

$$\begin{aligned} \sigma_{\text{coll}}^{a,b} &= \int_0^1 dx \int d\Phi_m(x) \left(\mathbf{P}^{a,q}(x, xp_a, p_b, k_1, k_2, \mu_F^2) + \mathbf{K}^{a,q}(x) \right) \otimes d\sigma_{q,b}^B(xp_a, p_b, k_1, k_2) \\ &+ \int_0^1 dx \int d\Phi_m(x) \left(\mathbf{P}^{a,q}(x, p_a, xp_b, k_1, k_2, \mu_F^2) + \mathbf{K}^{a,q}(x) \right) \otimes d\sigma_{q,b}^B(p_a, xp_b, k_1, k_2) . \end{aligned} \quad (5.71)$$

At hadron-level the corresponding cross section is obtained by the standard convolution with the PDFs

$$\sigma_{\text{coll}} = \sum_{a,b} \int \int dx_a dx_b f_a(x_a, \mu_F^2) f_b(x_b, \mu_F^2) \sigma_{\text{coll}}^{a,b} , \quad (5.72)$$

²Furthermore, in some scalar integrals where a UV and an IR pole cancel each other, like *e.g.* in the $B_0(0,0,0)$ function, the pole structure had to be restored by hand in `LoopTools`.

summing over possible initial state partons a and b originating from splittings in the initial state. In the case of squark pair production where the Born matrix element has only one initial state configuration, two quarks namely, only two splittings are possible:

$$g \rightarrow q\bar{q} \quad \text{and} \quad q \rightarrow gq . \quad (5.73)$$

Therefore the cross section of the finite collinear remainder can be written as sum of these two contributions

$$\begin{aligned} \sigma_{\text{coll}} &= \int \int dx_a dx_b f_g(x_a, \mu_F^2) f_q(x_b, \mu_F^2) \sigma_{\text{coll}}^{g,q} \\ &+ \int \int dx_a dx_b f_q(x_a, \mu_F^2) f_q(x_b, \mu_F^2) \sigma_{\text{coll}}^{q,q} . \end{aligned} \quad (5.74)$$

It is convenient to absorb the partonic finite collinear terms into modified PDFs and express the cross section in the compact form

$$\begin{aligned} \sigma_{\text{coll}} &= \int \int dx_a dx_b \int d\Phi_2(p_a, p_b, k_1, k_2) \frac{1}{\hat{s}} \times \\ &\left(\tilde{f}_{q_i}(x_a, \mu_F^2) f_{q_j}(x_b, \mu_F^2) + f_{q_i}(x_a, \mu_F^2) \tilde{f}_{q_j}(x_b, \mu_F^2) \right) \otimes |\mathcal{M}(p_a, p_b, k_1, k_2)|^2 \\ &+ (a \leftrightarrow b) . \end{aligned} \quad (5.75)$$

Here, \hat{s} denotes the square of the partonic center-of-mass energy and the symbol \otimes together with $|\mathcal{M}(p_a, p_b, k_1, k_2)|^2$ stands for properly defined convolutions with the corresponding color linked Born amplitudes squared, already introduced during the discussion of the subtraction dipoles in Section 5.4 and integrated dipoles in Section 5.5.1.

The modified PDFs \tilde{f}_q are defined as an integral over the longitudinal momentum fraction after the splitting in the initial state and a sum of contributing initial PDFs, in this case the quark and gluon PDFs

$$\begin{aligned} \tilde{f}_q(\tilde{x}_a) &= \frac{\alpha_s}{2\pi} \int_{\tilde{x}_a}^1 \frac{dx}{x} \left\{ A_1(x, \tilde{x}_a) \left(f_q\left(\frac{\tilde{x}_a}{x}\right) - x f_q(\tilde{x}_a) \right) \right. \\ &+ A_2(x, \tilde{x}_a) \sum_{j=1,2} \left(f_q\left(\frac{\tilde{x}_a}{x}\right) \log\left(1 - x + \frac{m_j^2}{s_{ja}^{(x)}}\right) - x f_q(\tilde{x}_a) \log\left(1 - x + \frac{m_j^2}{s_{ja}^{(1)}}\right) \right) \\ &+ B(x, \tilde{x}_a) f_q\left(\frac{\tilde{x}_a}{x}\right) \\ &+ \left. C(x, \tilde{x}_a) f_g\left(\frac{\tilde{x}_a}{x}\right) \right\} \\ &+ \frac{\alpha_s}{2\pi} (D_1(\tilde{x}_a) + D_2(\tilde{x}_a)) f_q(\tilde{x}_a) . \end{aligned} \quad (5.76)$$

The index j in the second line denotes one of the squarks in the final state, so that m_j is the mass of this squark. The kinematical variables $s_{ja}^{(x)}$ and $s_{ja}^{(1)}$ involve the initial (a) and final (j) state momenta

$$s_{ja}^{(x)} = 2 \frac{p_a p_j}{x} \quad \text{and} \quad s_{ja}^{(1)} = 2 p_a p_j . \quad (5.77)$$

The derivation of the coefficients $A_1(x, \tilde{x}_a)$, $A_2(x, \tilde{x}_a)$, $B(x, \tilde{x}_a)$, $C(x, \tilde{x}_a)$, $D_1(\tilde{x}_a)$ and $D_2(\tilde{x}_a)$ is rather lengthy and thus presented in detail in Appendix C.

Implementing the finite collinear remainder terms in the numerical evaluation as part of the 2-particle phase space, as described above, has a drawback. The code slows down dramatically as for every phase space point an additional integration over the longitudinal momentum fraction x has to be carried out. To reduce the computing time it is convenient to perform the integration over the 3-particle phase space rather than over the 2-particle one with an additional integration over x . The numerical evaluation can be speeded up by taking advantage of the fact that the phase space factorizes. The following relation between the 2- and 3-particle phase space

$$\frac{1}{2p_a p_b} d\Phi_3(p_a, p_b, k_1, k_2, k_3) = \int_0^1 dx d\Phi_2(xp_a, p_b, \tilde{k}_1, \tilde{k}_2) \frac{1}{16\pi^2} \int_0^{1-x} d\tilde{v}_i \quad (5.78)$$

maps the Born-level phase space into the real emission phase space by utilizing the reduced kinematics which has already been introduced for the dipoles with initial state singularities and initial state spectators in Section 5.4. The idea is to consider the 2-particle phase space kinematics with which the finite collinear terms have been evaluated so far in this section as the reduced kinematics of the initial-initial dipole. Therefore, the longitudinal momentum fraction is in this context defined as

$$x = x_{3,ab} = \frac{p_a p_b - p_a k_3 - p_b k_3}{p_a p_b} \quad (5.79)$$

transforming the initial state momentum p_a to its value in the reduced kinematics by

$$\tilde{p}_a^\mu = x_{3,ab} p_a^\mu . \quad (5.80)$$

Interpreting the Born kinematics in the first term of Eq. (5.75) as the initial-initial tilde kinematics, this term reads

$$\begin{aligned} \sigma_{\text{coll},1} &= \int \int d\tilde{x}_a dx_b \int d\Phi_2(\tilde{p}_a, p_b, \tilde{k}_1, \tilde{k}_2) \frac{1}{2\tilde{p}_a p_b} \cdot \\ &\quad \tilde{f}_{q_i}(\tilde{x}_a, \mu_F^2) f_{q_j}(x_b, \mu_F^2) \otimes \left| \mathcal{M}(\tilde{p}_a, p_b, \tilde{k}_1, \tilde{k}_2) \right|^2 . \end{aligned} \quad (5.81)$$

In order to transform this expression to the 3-particle phase space three steps have to be performed. First of all, an artificial integration over x has to be introduced for the D_1 and D_2 coefficients in the parametrization of the modified PDF in Eq. (5.76)

$$1 = \frac{1}{1 - \tilde{x}_a} \int_{\tilde{x}_a}^1 dx . \quad (5.82)$$

Furthermore an integral over the variable \tilde{v}_i , which is not present in the integrand, has to be inserted

$$1 = \int_0^{1-x} d\tilde{v}_i \frac{1}{1-x} . \quad (5.83)$$

Finally, the substitution $\tilde{x}_a \rightarrow x x_a$ has to be done, transforming the relevant integrations to

$$\int_0^1 d\tilde{x}_a \int_{\tilde{x}_a}^1 \frac{dx}{x} \quad \rightarrow \quad \int_0^1 dx_a \int_0^1 dx . \quad (5.84)$$

With these modifications the transformation in Eq. (5.78) can be applied and the modified PDF becomes

$$\begin{aligned} \sigma_{\text{coll},1} = & \int_0^1 \int_0^1 dx_a dx_b \frac{\int d\Phi_3(p_a, p_b, k_1, k_2, k_3)}{(2p_a p_b) (2x p_a p_b)} \frac{16\pi^2}{1-x} f_q(x_b) \\ & \left\{ A_1(x, x x_a) (f_q(x_a) - x f_q(x x_a)) \right. \\ & + A_2(x, x x_a) \left(f_q(x_a) \log \left(1 - x + \frac{m_j^2}{s_{ja}^{(1)}} \right) - x f_q(x x_a) \log \left(1 - x + \frac{m_j^2}{s_{ja}^{(x)}} \right) \right) \\ & + B(x, x x_a) f_q(x_a) + C(x, x x_a) f_g(x_a) \\ & \left. + \frac{x}{1 - x x_a} (D_1(x x_a), D_2(x c_a)) f_q(x x_a) \right\} \otimes \left| \mathcal{M}(\tilde{p}_a, p_b, \tilde{k}_1, \tilde{k}_2) \right|^2 . \quad (5.85) \end{aligned}$$

Apart from saving computing time, this factorization of the phase space allows for consistency checks of the program, since the finite collinear cross section can be determined either as part of the 2-particle or as part of the 3-particle phase space. Details concerning this test will be presented in Section 5.6.1.

5.6 Numerical Evaluation

The complete NLO calculation, as described in the previous chapters, has been implemented in a Fortran program in order to perform the phase space integration and the convolution with the PDFs numerically by means of statistical Monte-Carlo methods.

The integration routine used for this purpose is `MONACO`, which is a modified version of the Fortran subroutine `VEGAS` [140]. It is part of the Monte Carlo program `VBFNLO` [141–143]. The `VEGAS` algorithm evaluates the integrand N times by mapping random numbers $x_i \in [0, 1]$ on the integration variables. The expectation value for the result of the integral is estimated by the arithmetic average of the evaluations. In order to reduce the variance for the result a technique called importance-sampling is used, i.e. more points are sampled into regions where the integrand is large. This procedure is repeated in subsequent iterations. In the first iteration the integration domain is split up equally into a rectangular grid of hypercubes with a constant density of sample points x_i . From iteration to iteration the grid subdivision is modified in order to concentrate more hypercubes, and thus more sample points, in regions where the integrand is large.

For the convolution with PDFs the CTEQ PDF-sets are used. The LO cross section as well as the corresponding differential distributions are evaluated with the CTEQ6L1 PDF-set [144]. The NLO cross section and the NLO distributions, on

the other hand, are calculated with the latest CTEQ10 NLO PDF-sets [145]. The strong coupling constant $\alpha_s^{\overline{MS_5}}(Q^2)$ is taken from the PDF-sets. For the calculation of the LO cross section the value of $\alpha_s^{\overline{MS_5}}(Q^2)$ corresponds to the running coupling at one-loop order, while in the calculation of the NLO corrections the running coupling up to two-loop order is needed. The coupling satisfies the following renormalization group equation

$$Q^2 \frac{d\alpha_s^{\overline{MS_5}}(Q^2)}{dQ^2} = -b_0 \alpha_s^{2, \overline{MS_5}}(Q^2) - b_1 \alpha_s^{3, \overline{MS_5}}(Q^2) - \dots \quad (5.86)$$

with the one-loop and two-loop coefficients

$$b_0 = \frac{33 - 2 \cdot 5}{12 \pi} \quad \text{and} \quad b_1 = \frac{153 - 19 \cdot 5}{24 \pi^2}. \quad (5.87)$$

A convenient approximate analytic solution to the RGE in Eq. (5.86) is given to one-loop order by

$$\alpha_s^{\overline{MS_5}}(Q^2) = \frac{1}{b_0 \log\left(\frac{Q^2}{\Lambda_{\text{QCD}}^2}\right)}. \quad (5.88)$$

It is parametrized in terms of the constant Λ_{QCD} , an integration constant which corresponds to the non-perturbative scale of QCD. In Eq. (5.88) it amounts to

$$\Lambda_{\text{QCD}} = 165 \text{ MeV}. \quad (5.89)$$

The approximate solution of Eq. (5.86) to two-loop order reads

$$\alpha_s^{\overline{MS_5}}(Q^2) = \frac{1}{b_0 \log(Q^2/\Lambda_{\text{QCD}}^2)} \left[1 - \frac{b_1}{b_0^2} \frac{\log(\log(Q^2/\Lambda_{\text{QCD}}^2))}{\log(Q^2/\Lambda_{\text{QCD}}^2)} \right] \quad (5.90)$$

with

$$\Lambda_{\text{QCD}} = 226 \text{ MeV}. \quad (5.91)$$

An alternative to the use of formulas (5.88) and (5.90) is to solve the RGE in Eq. (5.86) exactly, numerically [146]. In this case no scale Λ_{QCD} has to be introduced but an initial condition $\alpha_s(\mu)|_{\mu=M_Z} = \alpha_s(M_Z)$ is used to solve the differential equation. Equation (5.88) leads to $\alpha_s(M_Z) = 0.130$ and Eq. (5.90) yields $\alpha_s(M_Z) = 0.118$.

The factorization scale μ_F is set together with the renormalization scale Q in the virtual corrections to a characteristic energy scale of the squark pair production process, which has been chosen to be the average mass $\mu_F = Q = \overline{m_{\tilde{q}}}$ of all light-flavor squarks of the SUSY parameter scenario used for the evaluation.

If not stated otherwise, e.g. in comparisons to previous works, a SUSY parameter scenario is investigated which is in agreement with all direct SUSY searches at the LHC as described in Chapter 2.3.1. Within the framework of mSUGRA the boundary conditions for the renormalization group running at the GUT scale are

	\tilde{u}_L	\tilde{c}_L	\tilde{t}_1	\tilde{u}_R	\tilde{c}_R	\tilde{t}_2
	1796.4	1796.4	1283.6	1756.9	1756.9	1601.7
\tilde{g}	\tilde{d}_L	\tilde{s}_L	\tilde{b}_1	\tilde{d}_R	\tilde{s}_R	\tilde{b}_2
1598.7	1797.9	1797.9	1581.9	1753.1	1753.1	1742.2

Table 5.1: Masses of the squarks and gluino given in GeV within “scenario 1” defined in Eq. (5.92).

given by five parameters. These read for the point chosen here for the analysis of phenomenological results

$$\begin{aligned} \text{Scenario 1 : } M_0 = 1150 \text{ GeV} \quad M_{1/2} = 690 \text{ GeV} \quad A_0 = 0 \text{ GeV} \\ \tan \beta = 10 \quad \text{sign}(\mu_h) = + \quad . \end{aligned} \quad (5.92)$$

The renormalization group running and the calculation of physical on-shell particle masses is done with the spectrum calculator `SOFTSUSY` [85]. The SM input parameters needed are according to [74]

$$\begin{aligned} M_Z &= 91.187 \text{ GeV} \\ \alpha_{em}^{-1\overline{\text{MS}}}(M_Z) &= 127.934 \\ m_b^{\overline{\text{MS}}}(m_b) &= 4.2 \text{ GeV} \\ M_t^{\text{pole}} &= 173.5 \text{ GeV} \\ m_\tau^{\text{pole}} &= 1.777 \text{ GeV} . \end{aligned}$$

Most relevant for the calculation of squark pair production at NLO are the masses of the squarks as well as the mass of the gluino. These are listed in Table 5.1. With the right-handed light-flavor squarks having masses slightly above 1750 GeV and the left-handed light-flavor squarks of almost 1800 GeV. The renormalization and factorization scale for this scenario are set to 1776 GeV.

5.6.1 Tests and Comparisons

In order to check the various parts of the implementation of the calculation and in order to exclude possible error sources, numerous internal tests have been performed. Among these is the check whether the Catani-Seymour dipoles cancel the real emission contributions in the singular regions, the check whether the \mathbf{I} terms of the integrated dipoles render the correct coefficients of the $1/\epsilon$ and $1/\epsilon^2$ terms and the check whether the cross section of the finite collinear remainder coincides in the implementations as part of the 2-particle and as part of the 3-particle phase space. To further validate the code these tests have been supplemented, as far as possible, by a comparison of the results for the LO and NLO cross section to results obtained with the program `Prospino2` [20].

To confirm the cancellation of the IR divergencies in the real emission matrix elements by the Catani-Seymour subtraction dipoles, the ratio of the squared real emission matrix element $|M^R|^2$ over the sum of the corresponding dipoles is investigated. As the dipoles act as local counterterms, they should cancel the divergencies in the real emission matrix elements in the singular regions, which are characterized by small energies of the emitted parton and/or by small angles between massless partons. The ratio of the real emission matrix element over the sum of dipoles is shown in Fig. 5.6 for processes with two quarks in the initial state and in Fig. 5.7 for processes with a quark and a gluon in the initial state for about one million phase space points each. In both figures the ratio is plotted in dependence of the product of one initial state momentum and the momentum of the emitted parton, which is a gluon in the $q\bar{q}$ initiated processes and an antiquark in the qg initiated processes. For large values far away from the singular region the contributions from real emissions and dipoles differ, whereas in the soft and collinear regions, i.e. in the limit $p_q \cdot p_g \rightarrow 0$ and $p_g \cdot p_{\bar{q}} \rightarrow 0$, respectively, the subtraction dipoles exactly cancel the real emission matrix elements resulting in a ratio of one. This is precisely the expected behavior of the subtraction dipoles.

The **I**-terms of the integrated dipoles can be written schematically as

$$C_{-2} \frac{1}{\epsilon^2} + C_{-1} \frac{1}{\epsilon} + C_0, \quad (5.93)$$

where C_{-2}, C_{-1} and C_0 are process and kinematics dependent coefficients. The coefficient C_{-2} should obey the following simple relation [147]

$$C_{-2} = \frac{\alpha_s}{2\pi} |M_{Born}|^2 \cdot 2 C_F. \quad (5.94)$$

Figure 5.8 demonstrates that this relation is fulfilled in the calculation at every phase space point: The ratio of the coefficient C_{-2} and the squared Born matrix element multiplied by the factor $2\pi/\alpha_s$ always yields the constant $2 C_F = 8/3$, independent of the details of the phase space point they are evaluated at. A similar but more complicated relation [147] holds for the coefficient of the $1/\epsilon$ term in Eq. (5.93). During the evaluation of the NLO corrections it is checked explicitly that at every phase space point the contributions to the coefficients of the poles from the virtual corrections and **I**-terms cancel, therefore only the finite parts of both contribute to the NLO cross section and distributions.

The **PK**-terms, the finite terms which remain after all IR divergencies have been canceled, can be determined either as part of the 2-particle or as part of the 3-particle phase space. In the 2-particle phase space implementation an additional integration over x , the longitudinal momentum fraction in the initial state, has to be performed. This slows down the code drastically but can be mended when the 2-particle phase space with this additional integration is mapped into the 3-particle phase space. Both implementations should yield the same result for the finite collinear cross section. By calculating the cross sections for this part of the calculation with both

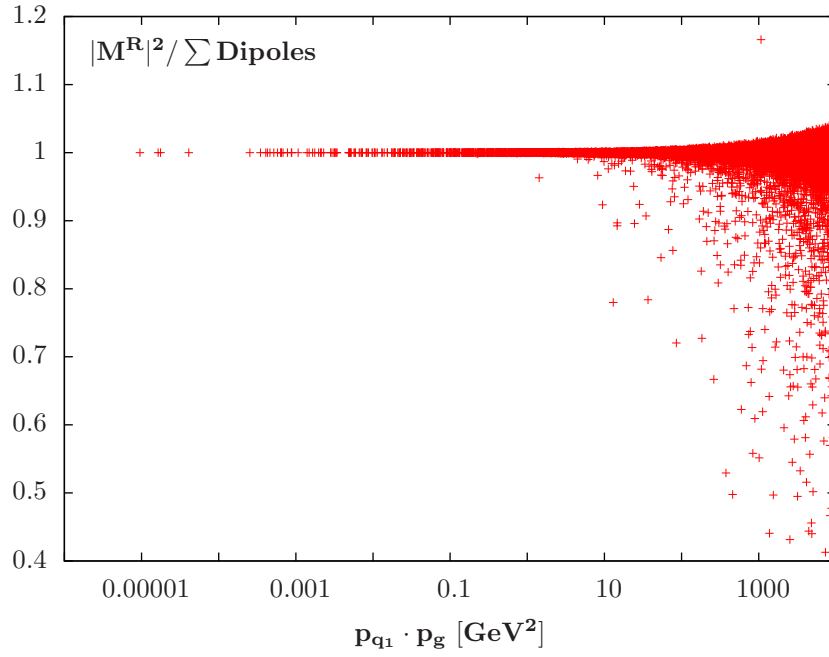


Figure 5.6: Ratio of real emission matrix elements squared and corresponding dipoles for qq initial states.

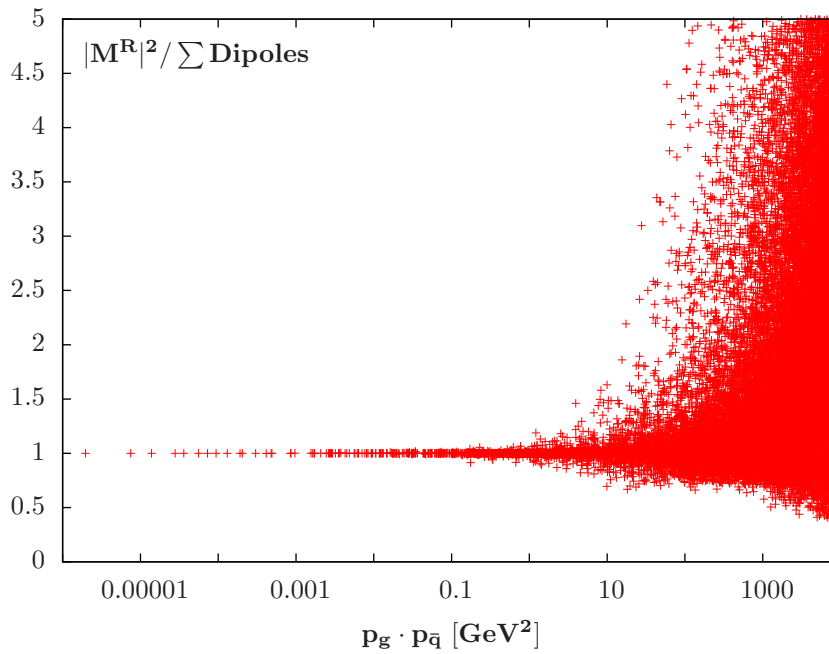


Figure 5.7: Ratio of real emission matrix elements squared and corresponding dipoles for qq initial states.

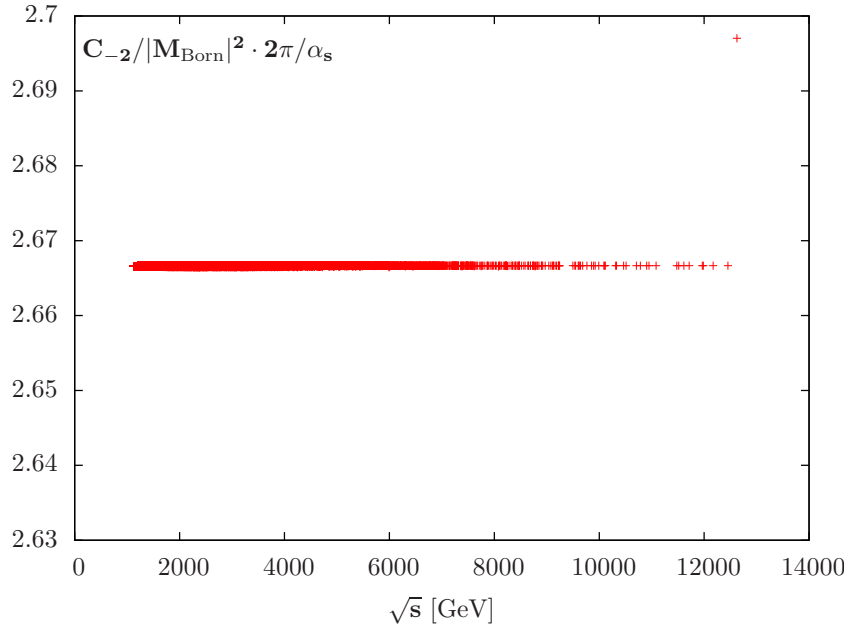


Figure 5.8: Ratio of coefficient of $1/\epsilon^2$ poles over the squared Born matrix elements evaluated at different phase space points characterized by different partonic center-of-mass energies \sqrt{s} .

methods for different parameter points it can be checked whether the finite collinear remainders have been implemented consistently. Figure 5.9 shows the ratio of the finite collinear remainder cross section calculated in the 2-particle phase space and the one calculated in the 3-particle phase space including error bars. Both contributions have been evaluated with input parameters based on the scenario defined in Eq. (5.92) and with all the corresponding masses in Table 5.1 apart from the mass of the left-handed up-type squark $m_{\tilde{u}_L}$ which has been varied by hand between 1650 and 2100 GeV. Both cross sections agree within their small statistical errors, originating from the Monte-Carlo integration, leading to a ratio which is in agreement with one within the error calculated according to error propagation. Since the implementation of the finite collinear terms as part of the 3-particle phase space is about ~ 1100 times faster than the 2-particle phase space implementation in the following only the former one is used.

The program `Prospino2` computes NLO cross sections efficiently for the production of SUSY particles at hadron colliders based on the calculations accomplished in [20]. However, some simplifications have been assumed which have to be taken into account for a consistent comparison of results. While the LO cross section for squark pair production is calculated correctly and separately for the various flavor and chirality combinations, the NLO corrections are always summed over the subchannels assuming a common mass for all squarks. The so-called K -factor, i.e. the ratio between the NLO and LO cross section

$$K = \frac{\sigma_{NLO}}{\sigma_{LO}}, \quad (5.95)$$

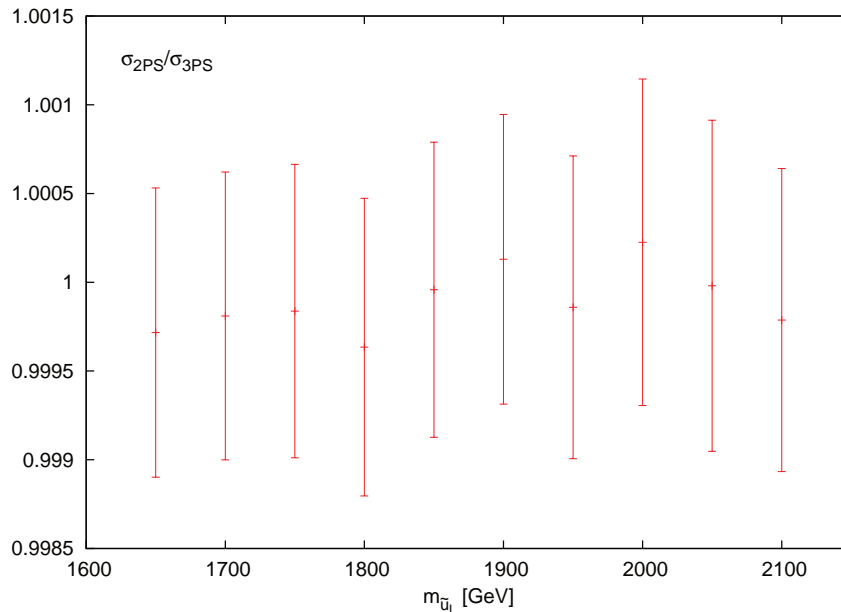


Figure 5.9: Ratio of cross sections of the finite collinear remainders evaluated in 2-particle and 3-particle phase space. The error bars are calculated according to error propagation of the errors of the two cross sections in the different phase spaces.

is determined for the total cross sections, with all subchannels summed up. Results for the NLO cross sections of different subchannels are returned but have been obtained by scaling the LO cross sections by the K -factor obtained from the total cross sections at LO and NLO. Thus, it is assumed that the K -factor does not change for different flavor and chirality combinations. Since **Prospino2** reads Les Houches SUSY spectrum files but calculates an average squark mass for the evaluation of the NLO corrections, it is most sensible to compare results for a scenario with degenerate squark masses. For that purpose “scenario 1” of Eq. (5.92) and Table 5.1 has been altered by setting all squark masses to

$$m_{\tilde{q}} = 1800 \text{ GeV} . \quad (5.96)$$

This scenario is denoted “scenario 2” in the following. Additionally, **Prospino2** uses CTEQ6 PDFs throughout, i.e. the CTEQ6L1 set for the LO and the CTEQ6M set for the NLO cross section. Adopting these changes, results for a cross-check against **Prospino2** at a center-of-mass energy of 8 TeV can be produced. In case of degenerate squark masses several of the 36 subchannels yield the same result. For example $\tilde{u}_L\tilde{u}_L$ and $\tilde{u}_R\tilde{u}_R$ have the same cross section and so have $\tilde{u}_L\tilde{d}_R$ and $\tilde{u}_R\tilde{d}_L$. This holds for several combinations of the four squarks of the first two generations. As a consequence, only 20 out of the 36 possible channels have cross sections that differ from each other. The LO and NLO cross sections for these with the corresponding K -factors in comparison to the ones obtained with **Prospino2** are listed in Table 5.2. As everywhere else in this work the charge conjugated processes are included in every subchannel. In the last line of Table 5.2 the sum of all subchannels,

channel	σ_{LO} [fb]	σ_{NLO} [fb]	K	$\sigma_{\text{LO}}^{\text{Prospino}}$ [fb]	$\sigma_{\text{NLO}}^{\text{Prospino}}$ [fb]	K^{Prospino}
$\tilde{u}_L \tilde{u}_L$	$6.18 \cdot 10^{-2}$	$6.82 \cdot 10^{-2}$	1.10	$6.18 \cdot 10^{-2}$	$7.18 \cdot 10^{-2}$	1.16
$\tilde{u}_L \tilde{d}_L$	$3.90 \cdot 10^{-2}$	$4.72 \cdot 10^{-2}$	1.21	$3.90 \cdot 10^{-2}$	$4.53 \cdot 10^{-2}$	1.16
$\tilde{u}_L \tilde{c}_L$	$2.47 \cdot 10^{-4}$	$8.39 \cdot 10^{-4}$	3.40	$2.47 \cdot 10^{-4}$	$2.87 \cdot 10^{-4}$	1.16
$\tilde{u}_L \tilde{s}_L$	$6.33 \cdot 10^{-4}$	$1.12 \cdot 10^{-3}$	1.77	$6.33 \cdot 10^{-4}$	$7.35 \cdot 10^{-4}$	1.16
$\tilde{d}_L \tilde{d}_L$	$2.90 \cdot 10^{-3}$	$3.47 \cdot 10^{-3}$	1.19	$2.90 \cdot 10^{-3}$	$3.37 \cdot 10^{-3}$	1.16
$\tilde{d}_L \tilde{c}_L$	$4.63 \cdot 10^{-5}$	$1.80 \cdot 10^{-4}$	3.90	$4.64 \cdot 10^{-5}$	$5.38 \cdot 10^{-5}$	1.16
$\tilde{d}_L \tilde{s}_L$	$1.15 \cdot 10^{-4}$	$2.33 \cdot 10^{-4}$	2.02	$1.15 \cdot 10^{-4}$	$1.34 \cdot 10^{-4}$	1.16
$\tilde{c}_L \tilde{c}_L$	$1.77 \cdot 10^{-7}$	$1.98 \cdot 10^{-6}$	1.12	$1.77 \cdot 10^{-7}$	$2.05 \cdot 10^{-7}$	1.16
$\tilde{c}_L \tilde{s}_L$	$1.17 \cdot 10^{-6}$	$7.65 \cdot 10^{-7}$	6.52	$1.17 \cdot 10^{-6}$	$1.36 \cdot 10^{-6}$	1.16
$\tilde{s}_L \tilde{s}_L$	$9.55 \cdot 10^{-7}$	$3.19 \cdot 10^{-6}$	3.34	$9.56 \cdot 10^{-7}$	$1.11 \cdot 10^{-6}$	1.16
$\tilde{u}_L \tilde{u}_R$	$3.27 \cdot 10^{-2}$	$3.83 \cdot 10^{-2}$	1.17	$3.27 \cdot 10^{-2}$	$3.80 \cdot 10^{-2}$	1.16
$\tilde{u}_L \tilde{d}_R$	$6.79 \cdot 10^{-3}$	$8.31 \cdot 10^{-3}$	1.22	$6.79 \cdot 10^{-3}$	$7.89 \cdot 10^{-3}$	1.16
$\tilde{u}_L \tilde{c}_R$	$3.84 \cdot 10^{-5}$	$1.50 \cdot 10^{-4}$	3.89	$3.84 \cdot 10^{-5}$	$4.46 \cdot 10^{-5}$	1.16
$\tilde{u}_L \tilde{s}_R$	$9.56 \cdot 10^{-5}$	$1.91 \cdot 10^{-4}$	1.99	$9.55 \cdot 10^{-5}$	$1.11 \cdot 10^{-4}$	1.16
$\tilde{d}_L \tilde{d}_R$	$1.29 \cdot 10^{-3}$	$1.68 \cdot 10^{-3}$	1.30	$1.29 \cdot 10^{-3}$	$1.50 \cdot 10^{-3}$	1.16
$\tilde{d}_L \tilde{c}_R$	$6.79 \cdot 10^{-6}$	$2.98 \cdot 10^{-5}$	4.39	$6.79 \cdot 10^{-6}$	$7.89 \cdot 10^{-6}$	1.16
$\tilde{d}_L \tilde{s}_R$	$1.62 \cdot 10^{-5}$	$3.69 \cdot 10^{-5}$	2.28	$1.62 \cdot 10^{-5}$	$1.88 \cdot 10^{-5}$	1.16
$\tilde{c}_L \tilde{c}_R$	$7.10 \cdot 10^{-8}$	$1.01 \cdot 10^{-6}$	14.28	$7.10 \cdot 10^{-8}$	$8.24 \cdot 10^{-8}$	1.16
$\tilde{c}_L \tilde{s}_R$	$1.61 \cdot 10^{-7}$	$1.25 \cdot 10^{-6}$	7.74	$1.61 \cdot 10^{-7}$	$1.87 \cdot 10^{-7}$	1.16
$\tilde{s}_L \tilde{s}_R$	$3.54 \cdot 10^{-8}$	$1.52 \cdot 10^{-6}$	4.28	$3.54 \cdot 10^{-8}$	$4.11 \cdot 10^{-8}$	1.16
Sum	$2.57 \cdot 10^{-1}$	$3.00 \cdot 10^{-1}$	1.16	$2.57 \cdot 10^{-1}$	$2.99 \cdot 10^{-1}$	1.16

Table 5.2: LO and NLO cross sections and K -factors for individual subchannels and the sum of all 36 subchannels in comparison to **Prospino2**. Charge conjugated processes are included. The values have been obtained for “scenario 2” of Eq. (5.96) and a center-of-mass energy of 8 TeV.

taking into account the ones not listed in the lines above, is stated.

As can be inferred from the table the LO cross sections for the individual subchannels as well as the LO cross section for all subchannels are in perfect agreement. The NLO total cross sections agree within their errors and consequently the total K -factors are the same. While `Prospino2` assumes that this total K -factor is constant in the various subchannels, calculating the NLO cross sections for the subchannels individually shows that this assumption is just a rough one. However, the (huge) K -factors for subchannels involving \tilde{c} and \tilde{s} quarks have to be considered critically. Evaluating the LO process, $c c \rightarrow \tilde{c}_L \tilde{c}_R$ for example, with the CTEQ6L1 set and with the CTEQ6M set yields already a difference of a factor 10 just in the LO cross sections. In order to verify that this effect is unambiguously stemming from large differences in the LO and NLO PDF sets for charm quarks, the ratio of these has been plotted³ in Fig. 5.10 for a factorization scale of $Q = 2$ TeV in dependence of x , the quark momentum fraction of the proton momentum. For momentum fractions lower than $x = 0.1$ the LO CTEQ6L1 set and the NLO CTEQ6M set differ in a range of 10 – 20%, whereas for x values about 0.6 the PDFs differ by a factor of 4. The same behavior can be observed for strange quark PDF sets, which differ for large values of x by a factor 2.2. Since the PDFs for charm and strange quarks are derived from the gluon PDFs by taking into account the gluon splitting into a quark-antiquark pair, this difference can be traced back to the large gluon PDF uncertainties for large values of x , as evident from Fig. 10 in [144]. For squark pair production with squark masses around 2 TeV at a center-of-mass energy of 8 TeV rather large momentum fractions are necessary for partonic center-of-mass energies exceeding the kinematic production threshold. The last statement can be exemplified by recalling the relation between the partonic center-of-mass energy \hat{s} and the center-of-mass energy s in the proton-proton system

$$\begin{aligned} \hat{s} &= x_1 x_2 s \\ (4 \text{ TeV})^2 &\leq x_1 x_2 (8 \text{ TeV})^2 \\ x_1 x_2 &\geq 0.25, \end{aligned} \tag{5.97}$$

with x_1 and x_2 being the momentum fractions of the two partons. Taking these arguments into account it becomes clear where the large differences in the LO cross sections evaluated with CTEQ6L1 and CTEQ6M and thus the huge K -factors in channels with \tilde{c} and \tilde{s} squarks originate from. Since the values of the charm and strange quark PDFs are at least two orders of magnitude smaller than the up and down quark PDFs [144], the corresponding cross sections are small and hardly contribute to the total cross section: The 10 subchannels which have only up and down quark contributions make up 98.2 % of the total cross section. Disregarding therefore the large K -factors in subchannels with \tilde{c} and \tilde{s} squarks for the moment, the remaining K -factors for subchannels with up and down quarks in the initial state still vary in the range of 1.10 – 1.30. Therefore, an independent treatment of subchannels seems reasonable, as in general squarks of different chiralities and thus different channels have different masses, decays and kinematic distributions.

³Thanks to Karol Kovařík for providing this plot.

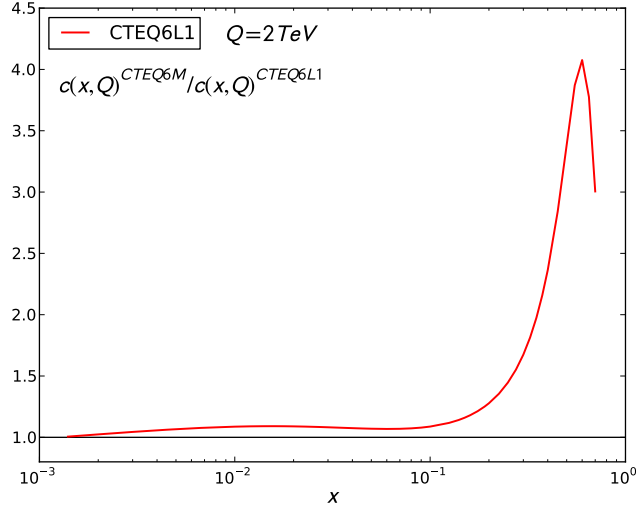


Figure 5.10: Ratio of CTEQ6M and CTEQ6L1 PDF sets for the charm quark at the factorization scale of 2 GeV in dependence of the proton momentum fraction parameter x .

Apart from the internal tests of the code and the comparison to `Prospino2` all building blocks of the program as well as various results have been checked against an independent implementation of squark pair production in the `POWHEG BOX` [134, 148]. The only commonly used part in the implementation in the `POWHEG BOX` and the parton level Monte-Carlo program described in this thesis are the `FormCalc` and `LoopTools` routines for the calculation and evaluation of the virtual corrections. The Born matrix elements, the color linked Born matrix elements and the real emissions have been calculated and implemented independently. Furthermore, in the `POWHEG BOX` a different subtraction method for dealing with the IR divergencies in the calculation is used. In contrast to the Catani-Seymour subtraction procedure presented in this thesis, the `POWHEG BOX` relies on the method proposed by Frixione, Kunszt and Signer (FKS) [149, 150]. All matrix elements have been checked for a multitude of phase space points yielding perfect agreement. LO and NLO cross sections have been compared for all 36 subchannels for different parameter scenarios with the outcome that all results agree within their statistical errors. Finally, differential distributions for several observables, which will be specified in the following section, have been plotted and agree up to anticipated statistical fluctuations.

5.6.2 Phenomenological Results

Before investigating the effects of the NLO corrections on differential distributions, the scale dependence of the total cross sections shall be analyzed. Since the factorization and renormalization scales are unphysical, their variation in the LO and NLO cross sections can provide a rough estimate on the remaining theoretical uncertainties due to higher order corrections. In the ideal case, the scale dependence

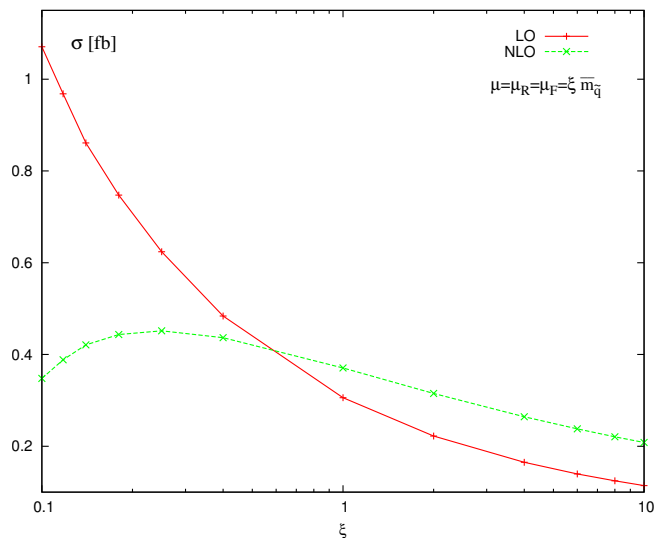


Figure 5.11: Scale dependence of the LO and NLO total cross section.

of the LO cross section is larger than the scale dependence of the next-to-leading order cross section, which is larger than the scale dependence of the next-to-next-to-leading order cross section and so on. In this sense, the scale dependence can be taken as a measure of the precision of the prediction. However, this estimate merely gives an indication and cannot be regarded as the true theoretical uncertainty on the cross section. Nonetheless, by analyzing the scale dependence a rough picture on the remaining uncertainty due to neglected higher order corrections can be given. Figure 5.11 reflects the scale dependence of the LO and NLO cross sections of squark pair production at the LHC for a center-of-mass energy of 8 TeV calculated with input parameters according to “scenario 1” of Eq. (5.92) and Table 5.1. The renormalization (Q) and factorization scale (μ_F) have been set to a common value, which is varied by a factor of 10 in both directions around the central value given by the average squark mass $\overline{m_{\bar{q}}} = 1776$ GeV. The NLO cross section exhibits clearly a much flatter scale dependence than the LO cross section. Varying the latter by a factor of two around 1776 GeV results in a dependence of about $\pm 50\%$. In the NLO cross section the scale dependence in the same range reduces to $\pm 15\%$. The dependence on the factorization scale is very weak and the residual scale dependence is dominated by the renormalization scale dependence of α_s . The cross sections at the central scale amount to

$$\sigma^{LO} = 0.306 \text{ fb} \quad \sigma^{NLO} = 0.371 \text{ fb}, \quad (5.98)$$

implying a K -factor of

$$K = 1.21 \quad (5.99)$$

and thus an enhancement of the LO cross section due to the NLO corrections by 21%.

In the rest of this section the effects of the NLO corrections on differential distributions shall be presented. These effects are exemplified based on the two observables:

- The invariant mass of the squark pair in the final state

$$M^{\text{inv}} = \sqrt{(p_{\tilde{q}_i} + p_{\tilde{q}_j})^2} \quad (5.100)$$

- The transverse momentum of each squark in the final state

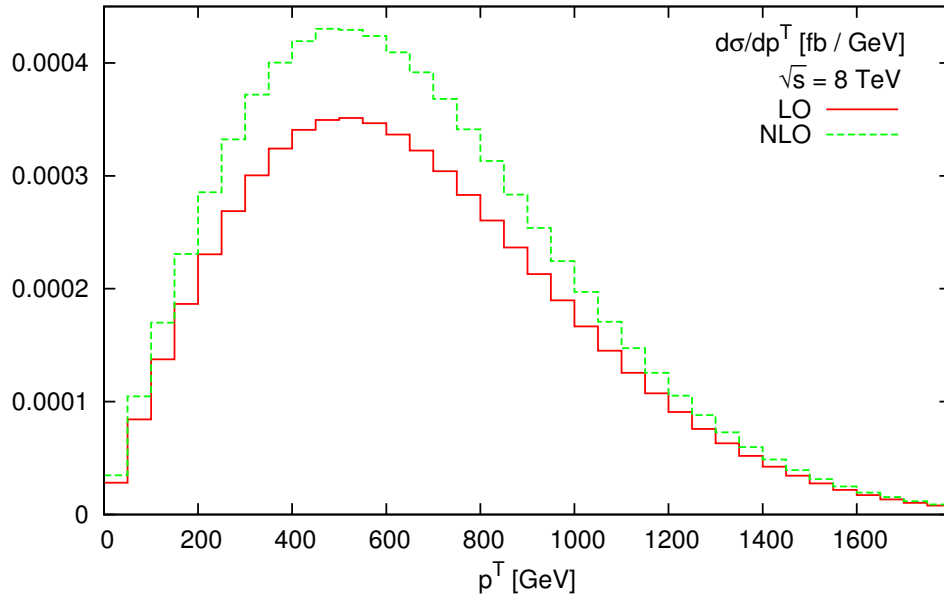
$$p_{\tilde{q}_i}^T = \sqrt{p_{\tilde{q}_i,x}^2 + p_{\tilde{q}_i,y}^2} . \quad (5.101)$$

Differential distributions in transverse momentum p^T at production level have already been shown in [20], where the NLO corrections for degenerate squark masses have been calculated. In Fig. 5.12 (a) the p^T distribution is shown for the NLO calculation described in this thesis evaluated for “scenario 1” at a center-of-mass energy of 8 TeV. As an example for further distributions at production level, which have not been available at NLO so far⁴, the invariant mass distribution is depicted in Fig. 5.12 (b).

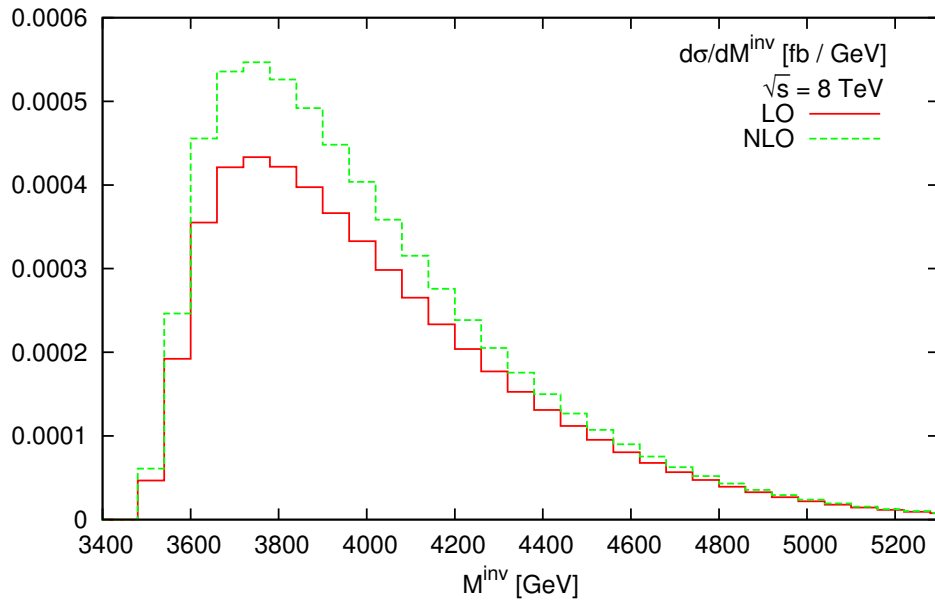
The effects of the NLO corrections on the shapes of distributions can be visualized by normalizing the distributions to unity, i.e. by dividing the LO distributions by the LO cross section and the NLO distributions by the NLO cross section. If the K -factor was flat, which means that the NLO distributions coincide with the LO distribution scaled by the K -factor of the total cross section, the normalized LO and NLO distributions would match exactly.

In [20] it was found that the normalized p^T -distributions are hardly affected by the transition from LO to NLO. These results have been obtained with a common squark mass of $m_{\tilde{q}} = 600$ GeV, a gluino mass of $m_{\tilde{g}} = 500$ GeV and a top quark mass of $m_t = 175$ GeV for the factorization and renormalization scale $Q = m_{\tilde{q}}$ at a center-of-mass energy of $\sqrt{s} = 14$ TeV. Adopting these parameters in the present calculation the distributions of [20] have been reproduced. For the scenario analyzed here, the normalized distributions are shown in Fig. 5.13. The p^T distribution exhibits similar and small effects as already found for this distribution in [20]. The shape of the invariant mass distribution is affected more by the NLO corrections. These effects can be quantified by determining the differential K -factor, defined as the NLO differential cross section divided by the LO differential cross section. The differential K -factor for the p^T and invariant mass distributions is also depicted in Fig. 5.13 underneath the distributions. For the p^T distribution it varies in a range of 10 %, while in the case of the invariant mass distribution the variation takes place in a range of 20 %. For comparison the figures with the differential K -factor also include the constant K -factor from the total cross sections, depicted by the dashed line. In both cases rescaling the LO distributions by the global K -factor would overestimate the tail of the distributions and underestimate the threshold regions.

⁴Recently, in [122] several distributions for squark pair production have been published. However, full decay chains have been considered and the effects of the NLO corrections for distributions at production level have not been shown.



(a)



(b)

Figure 5.12: LO and NLO p_q^T (a) and invariant mass $M_{q\bar{q}}^{\text{inv}}$ (b) distributions for a center-of-mass energy of 8 TeV.

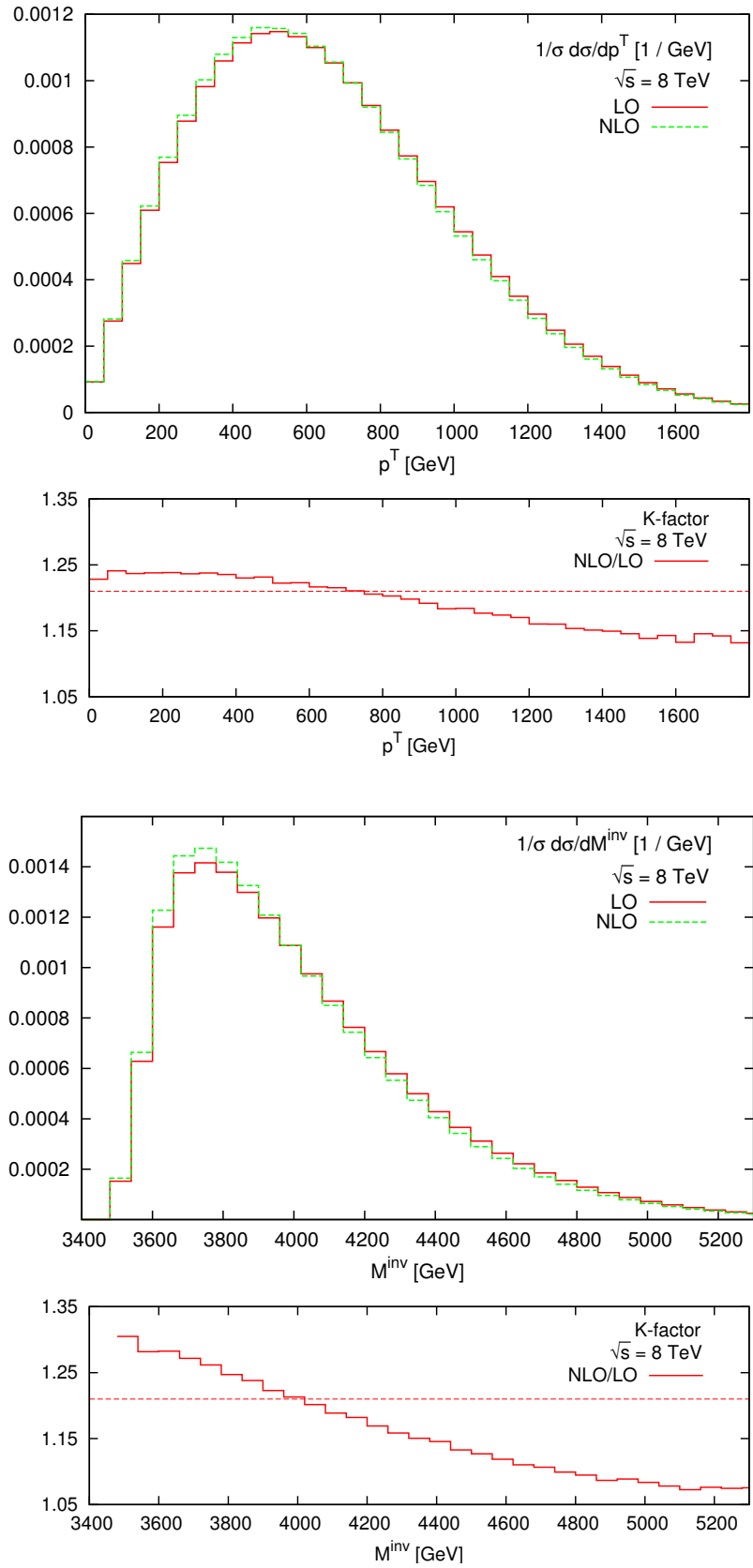


Figure 5.13: Normalized p_q^T (upper) and $M_{\tilde{q}\tilde{q}}^{\text{inv}}$ (lower) distributions and corresponding differential (full) and global (dashed) K -factors for a center-of-mass energy of 8 TeV.

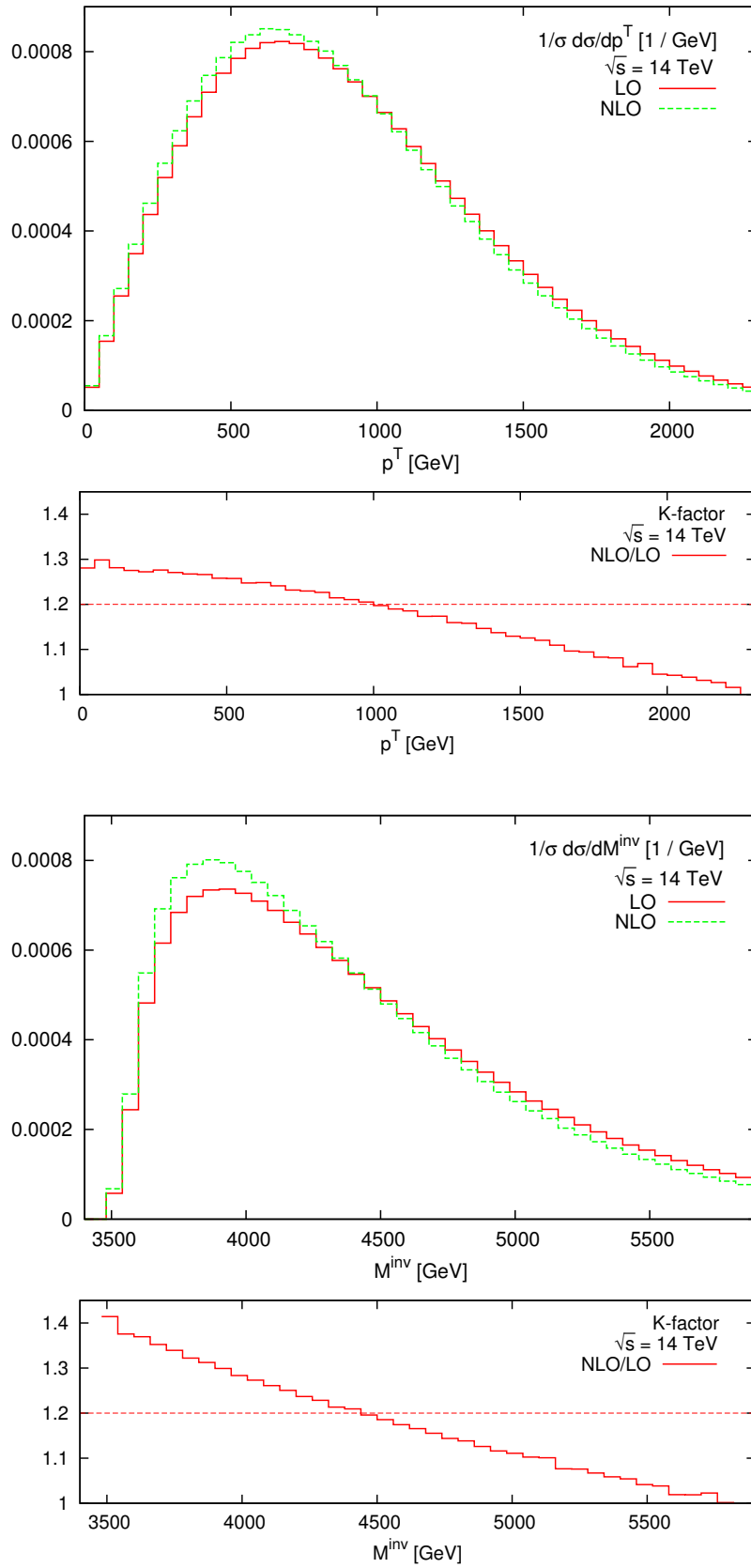


Figure 5.14: Normalized p_q^T (upper) and $M_{\bar{q}\bar{q}}^{\text{inv}}$ (lower) distributions and corresponding differential (full) and global (dashed) K -factors for a center-of-mass energy of 14 TeV.

Since the 8 TeV run at the LHC will be finished by the end of this year, it is interesting to have a look at distributions for a higher center-of-mass energy. For the same scenario as before at a center-of-mass energy of 14 TeV the total cross sections increase to

$$\sigma^{LO} = 14.66 \text{ fb} \quad \text{and} \quad \sigma^{NLO} = 17.64 \text{ fb} \quad (5.102)$$

resulting in a K -factor of

$$K = 1.20 . \quad (5.103)$$

The normalized p^T and invariant mass distributions, shown in Fig. 5.14, show larger effects due to the NLO corrections than their versions for 8 TeV. This fact is also reflected in the differential K -factors plotted underneath. The differential K -factor for the p^T distribution varies now in a range of 25 % and the one for the invariant mass distribution in a range of 35 %. Rescaling the invariant mass distribution by the global K -factor would thus over- and underestimate the tail and the threshold regions by almost 20%.

Certainly, the investigation at production level with unstable particles in the final state is only a first step towards a realistic analysis of the effects of NLO corrections on differential distributions. Nevertheless, they already give a first hint that for squark pair production at the LHC the leading order distributions cannot be simply multiplied by an overall K -factor to obtain correct NLO distributions and that fully differential distributions should be used for phenomenological studies.

5.7 Conclusion and Outlook

Facing the era of the LHC running and recording data, which can be used to search for supersymmetric extensions of the Standard Model, precise theoretical predictions are needed for the interpretation of these data. In order to improve predictions for the production of SUSY particles NLO SUSY QCD corrections need to be calculated and included. It is most useful to cast these NLO calculations into Monte-Carlo programs which can calculate cross sections as well as arbitrary distributions.

In this part of the thesis the NLO SUSY QCD corrections to squark pair production, the dominant channel for colored SUSY particles in the mass region currently tested at the LHC, have been presented. In order to deal with the IR divergencies arising in the virtual corrections and real emission matrix elements the Catani-Seymour subtraction formalism has been applied. The virtual contributions have been calculated using the software packages `FeynArts`, `FormCalc` and `LoopTools`. The UV divergencies have been canceled by renormalizing the masses and fields in the on-shell scheme and the strong coupling constant α_s in the $\overline{\text{MS}}$ scheme with decoupled heavy particles, i.e. taking into account only the five light quarks in the running of α_s . The real matrix elements have been obtained with the matrix element generator `Madgraph` and the Catani-Seymour subtraction dipoles and integrated dipoles,

including the finite collinear remainder, have been generated with the program `SuperAutoDipole`. All these building blocks of the calculation have been combined in a parton-level Monte-Carlo program.

All parts of the code have been checked carefully. Internal tests confirm the cancellation of the IR divergencies between the real emission matrix elements and the subtraction dipoles as well as between the virtual contributions and the integrated dipoles. The finite collinear remainder has been implemented as part of the 2-particle and as part of the 3-particle phase space allowing for a consistency check. Both implementations agree within the statistical errors. The latter implementation has been used for producing results as it is about a factor 1000 faster than the former. Apart from internal tests, all building blocks have been checked for a multitude of phase space points against an independent implementation of squark pair production in the `POWHEG BOX`, which has been carried out for a related project. All LO and NLO cross sections and distributions have been compared to results obtained with this independent code for various scenarios. Perfect agreement on all stages has been found.

Based on a previous calculation of NLO SUSY QCD corrections, where all squark masses have been assumed to be degenerate, the LO and NLO cross sections can be calculated with the publicly available program `Prospino2`. In this program apart from setting all squark masses to a common value in the NLO corrections, results for individual subchannels are returned by scaling the correctly calculated LO cross section with the K -factor of the total cross sections, thus assuming that it is constant in all subchannels. For scenarios with degenerate squark masses LO and NLO cross sections have been compared to results obtained with `Prospino2`. They agree within the small statistical errors. Since all subchannels have been treated independently in the calculation described in this thesis, the K -factor for each channel could be compared to the global K -factor. It has been found that these K -factors for relevant subchannels vary in a range of 20% and therefore subchannels should be treated independently since squarks of different chiralities can have different masses, decays and kinematic distributions.

The scale dependence of the NLO cross section is reduced substantially from $\pm 50\%$ to $\pm 15\%$ compared to the LO cross section for the scenario considered. The exemplary analysis of differential distributions revealed that the NLO corrections have bigger impact on the shape of the differential distributions than has been assumed so far, based on the distributions presented in [20] 16 years ago. Differential K -factors have been found to vary up to 35%, implying that scaling LO distributions with the global K -factor obtained from the total cross sections over- and underestimates certain regions of the distributions. Though based on unstable particles in the final state, this analysis illustrated that the full differential NLO corrections should be taken into account.

In order to further validate the phenomenological implications presented here, in the next step decays of the produced particles will be added for a more realistic analysis of the impact of NLO effects on the shape of distributions. The goal of a series of

related projects is to improve predictions for all SUSY decay cascades by including NLO corrections in production and decay stages. Furthermore parton shower effects on squark pair production at NLO are about to be studied [134], as a first candidate, since the virtual corrections calculated in this thesis have been implemented in the POWHEG BOX framework. In that sense, the calculation presented here is the basis for many more exciting studies and is a first step in paving the way towards a new powerful tool in the field of SUSY phenomenology.

Appendix A

Color Algebra Relations

$SU(3)$ denotes the group of 3×3 unitary matrices with determinant 1. Every matrix U of the group can be represented through the generators t^a ($a = 1, \dots, 8$). Since the matrix should be unitary, the generators have to be Hermitian. Since $\det U = 1$ the generators have to be traceless. The generators obey the algebra

$$[t^a, t^b] = i f_{abc} t^c, \quad (\text{A.1})$$

and are normalized as

$$\text{tr} [t^a t^b] = \frac{1}{2} \delta_{ab}. \quad (\text{A.2})$$

The f_{abc} are antisymmetric (under the interchange of any two indices) structure constants of the group. Furthermore an anticommutator relation holds

$$\{t^a, t^b\} = \frac{1}{3} \delta_{ab} \mathbf{1}_3 + d_{abc} t^c, \quad (\text{A.3})$$

where $\mathbf{1}_3$ is the 3×3 unity matrix and the d_{abc} are symmetric structure constants. The following relations can be derived from the definitions above and are useful for the calculation of the color linked Born amplitudes squared needed in the Catani-Seymour subtraction formalism.

$$f_{acd} f_{bcd} = 3 \delta_{ab} \quad (\text{A.4})$$

$$d_{acd} d_{bcd} = \frac{5}{3} \delta_{ab} \quad (\text{A.5})$$

$$d_{abc} f_{abd} = 0 \quad (\text{A.6})$$

$$t_{im}^a t_{mj}^a = \frac{4}{3} \delta_{ij} \quad (\text{A.7})$$

$$\text{tr} [t^a t^b t^c] = \frac{1}{4} (d_{abc} + i f_{abc}) \quad (\text{A.8})$$

$$(\text{tr} [t^a t^b t^c])^2 = \frac{1}{16} (d_{abc}^2 - f_{abc}^2) = -\frac{2}{3} \quad (\text{A.9})$$

$$\text{tr} [t^a t^b t^a t^b] = -\frac{2}{3} \quad (\text{A.10})$$

Appendix B

FCNC Vertex Counterterm

The squark-quark-neutralino part of the Lagrangian in the interaction basis [35], expressed in terms of the bare squark and quark fields, $\tilde{u}_i^{(0)}$ and $u_i^{(0)}$, and the bare quark mass matrix $\mathbf{m}_{ij}^{(0)}$, where $i, j = 1, 2, 3$ denote the generation indices and $l = 1, \dots, 4$ the neutralino mass eigenstates, is

$$\begin{aligned} \mathcal{L}_{\tilde{u}\tilde{u}\tilde{\chi}^0} = & -\bar{u}_i^{(0)} g e_{Ll}^{u_i} \tilde{u}_{iL}^{(0)} \mathcal{P}_R \tilde{\chi}_l^0 + \bar{u}_i^{(0)} \left(-\frac{g Z_{l4} \mathbf{m}_{ij}^{(0)}}{\sqrt{2} M_W \sin \beta} \right) \tilde{u}_{jR}^{(0)} \mathcal{P}_R \tilde{\chi}_l^0 \\ & -\bar{u}_i^{(0)} g e_{Rl}^{u_i} \tilde{u}_{iR}^{(0)} \mathcal{P}_L \tilde{\chi}_l^0 + \bar{u}_i^{(0)} \left(-\frac{g Z_{l4} \mathbf{m}_{ij}^{(0)}}{\sqrt{2} M_W \sin \beta} \right) \tilde{u}_{jL}^{(0)} \mathcal{P}_L \tilde{\chi}_l^0 + h.c. . \end{aligned} \quad (\text{B.1})$$

The couplings $e_{L,Rl}^{u_i}$ are defined as

$$\begin{aligned} e_{Ll}^{u_i} &= \sqrt{2} \left[\frac{Z_{l1}}{6} \tan \theta_W + \frac{1}{2} Z_{l2} \right], \\ e_{Rl}^{u_i} &= -\frac{2\sqrt{2}}{3} Z_{l1} \tan \theta_W, \end{aligned} \quad (\text{B.2})$$

with Z_{lm} being the elements of the 4×4 matrix which diagonalizes the neutralino mass matrix. Rotation to the mass eigenstates by means of Eqs. (4.2) and (4.10), exemplified for the right-chiral part of the coupling, yields

$$\begin{aligned} \mathcal{L}_{\tilde{u}\tilde{u}\tilde{\chi}^0}^R = & -\bar{u}_k^{m(0)} U_{ki}^{uL(0)} g e_{Ll}^{u_i} \tilde{W}_{is}^{(0)\dagger} \tilde{u}_s^{m(0)} \mathcal{P}_R \tilde{\chi}_l^0 \\ & + \bar{u}_k^{m(0)} U_{ki}^{uL(0)} \frac{-g Z_{l4} \mathbf{m}_{ij}^{(0)}}{\sqrt{2} M_W \sin \beta} \tilde{W}_{j+3s}^{(0)\dagger} \tilde{u}_s^{m(0)} \mathcal{P}_R \tilde{\chi}_l^0 + h.c. \\ & (i, j, k = 1, 2, 3, s = 1, \dots, 6). \end{aligned} \quad (\text{B.3})$$

Note, that $\tilde{W}_{is}^{(0)\dagger} \equiv \tilde{W}_{Lis}^{(0)\dagger}$, $\tilde{W}_{j+3s}^{(0)\dagger} \equiv \tilde{W}_{Rjs}^{(0)\dagger}$, *cf.* Eq. (4.11). Upon renormalization the bare quantities are replaced by [80]

$$\bar{u}^{m(0)} U^{u_L(0)} \rightarrow \bar{u}^m \left(1 + \frac{\delta Z^{L\dagger}}{2} \right) (1 + \delta u^{u_L}) U^{u_L} \quad (\text{B.4})$$

$$\tilde{W}_{L,R}^{(0)\dagger} \tilde{u}^{m(0)} \rightarrow \tilde{W}_{L,R}^\dagger (1 + \delta \tilde{w}^\dagger) \left(1 + \frac{\delta Z^{\tilde{u}}}{2} \right) \tilde{u}^m \quad (\text{B.5})$$

$$\mathbf{m}^{(0)} \rightarrow \mathbf{m} + \delta \mathbf{m}, \quad (\text{B.6})$$

where the indices have been suppressed. The field \tilde{u}^m denotes a six-component column vector. With the replacement $\tilde{W}_{L,R} = W_{L,R} U^{u_{L,R}}$, *cf.* Eq. (4.16), the Yukawa part of the coupling is transformed to

$$\begin{aligned} \frac{-gZ_{l4}}{\sqrt{2}M_W s_\beta} \bar{u}^m \left(1 + \frac{\delta Z^{L\dagger}}{2} \right) (1 + \delta u^{u_L}) U^{u_L} (\mathbf{m} + \delta \mathbf{m}) \cdot \\ U^{u_R\dagger} (1 + \delta u^{u_R\dagger}) W_R^\dagger (1 + \delta w_R^\dagger) \left(1 + \frac{\delta Z^{\tilde{u}}}{2} \right) \tilde{u}^m. \end{aligned} \quad (\text{B.7})$$

For the mass renormalization, the renormalization prescription is chosen such, that the bare mass matrices and hence $\delta \mathbf{m}$ are diagonal, *i.e.*

$$(1 + \delta u^{u_L}) U^{u_L} (\mathbf{m} + \delta \mathbf{m}) U^{u_R\dagger} (1 + \delta u^{u_R\dagger}) = (\mathbf{m}^D + \delta \mathbf{m}^D), \quad (\text{B.8})$$

where D denotes diagonal matrices. This is possible since the off-diagonal elements can be absorbed into the off-diagonal elements of the antihermitian part of the right-handed wave function renormalization matrices [151]. Exploiting the unitarity of the mixing matrices, the renormalized Lagrangian in the mass eigenstate basis is

$$\mathcal{L}_{\bar{u}\tilde{u}\tilde{\chi}^0} = \bar{u}_i^m (G_{isl}^R + \delta G_{isl}^R) \mathcal{P}_R \tilde{u}_s^m \tilde{\chi}_l^0 + \bar{u}_i^m (G_{isl}^L + \delta G_{isl}^L) \mathcal{P}_L \tilde{u}_s^m \tilde{\chi}_l^0 + h.c., \quad (\text{B.9})$$

with the couplings given by

$$G_{isl}^R = -ge_{Li}^{u_i} (W_L^\dagger)_{is} - \frac{gZ_{l4} m_{u_i} \delta_{ij}}{\sqrt{2}M_W \sin \beta} (W_R^\dagger)_{js} \quad (\text{B.10})$$

$$G_{isl}^L = -ge_{Rl}^{u_i} (W_R^\dagger)_{is} - \frac{gZ_{l4} m_{u_i} \delta_{ij}}{\sqrt{2}M_W \sin \beta} (W_L^\dagger)_{js} \quad (\text{B.11})$$

$$\begin{aligned} \delta G_{isl}^R = & -ge_{Li}^{u_i} \left[\frac{\delta Z_{ij}^{L\dagger}}{2} (W_L^\dagger)_{js} + (W_L^\dagger)_{it} \frac{\delta Z_{ts}^{\tilde{u}}}{2} + \delta u_{ij}^{u_L} (W_L^\dagger)_{js} + (W_L^\dagger)_{it} \delta \tilde{w}_{ts}^\dagger \right] \\ & - \frac{gZ_{l4}}{\sqrt{2}M_W \sin \beta} \left[\frac{\delta Z_{ij}^{L\dagger}}{2} m_{u_j} \delta_{jk} (W_R^\dagger)_{ks} + m_{u_i} \delta_{ij} (W_R^\dagger)_{jt} \frac{\delta Z_{ts}^{\tilde{u}}}{2} \right. \\ & \left. + m_{u_i} \delta_{ij} (W_R^\dagger)_{jt} \delta w_{R,ts}^\dagger + \delta m_{u_i} \delta_{ij} (W_R^\dagger)_{js} \right] \end{aligned} \quad (\text{B.12})$$

$$\begin{aligned}
\delta G_{isl}^L = & -g e_{Rl}^{u_i} \left[\frac{\delta Z_{ij}^{R\dagger}}{2} (W_R^\dagger)_{js} + (W_R^\dagger)_{it} \frac{\delta Z_{ts}^{\tilde{u}}}{2} + \delta u_{ij}^{u_R} (W_R^\dagger)_{js} + (W_R^\dagger)_{it} \delta \tilde{w}_{ts}^\dagger \right] \\
& - \frac{g Z_{l4}}{\sqrt{2} M_W \sin \beta} \left[\frac{\delta Z_{ij}^{R\dagger}}{2} m_{u_j} \delta_{jk} (W_L^\dagger)_{ks} + m_{u_i} \delta_{ij} (W_L^\dagger)_{jt} \frac{\delta Z_{ts}^{\tilde{u}}}{2} \right. \\
& \left. + m_{u_i} \delta_{ij} (W_L^\dagger)_{jt} \delta w_{R,ts}^\dagger + \delta m_{u_i} \delta_{ij} (W_L^\dagger)_{js} \right]. \quad (\text{B.13})
\end{aligned}$$

In the framework of MFV the W matrix is diagonal in flavour space at tree level at μ_{MFV} . At one-loop level flavour off-diagonal elements are induced through mixing matrix renormalization and the contributions from the off-diagonal field renormalization constants therein (see Eqs. (4.34) and (4.35)).

Appendix C

Catani Seymour Expressions

C.1 Singular Functions for Integrated Dipoles

The kernels \mathcal{V}_j and \mathcal{V}_a which enter the evaluation of the \mathbf{I} operator in the integrated dipoles depend on the flavour of parton j or a , respectively, and on the momenta and masses of both partons involved in the splitting. They can be decomposed into a sum of two contributions. The first one is singular in ϵ , i.e. in four dimensions, while the second one is finite in this respect:

$$\mathcal{V}_j(s_{jk}, m_j, m_k) = \mathcal{V}_j^{(S)}(s_{jk}, m_j, m_k) + \mathcal{V}_j^{(NS)}(s_{jk}, m_j, m_k). \quad (\text{C.1})$$

The singular part $\mathcal{V}^{(S)}$ is independent of flavour and spin of the parton and is therefore the same for quarks and squarks:

$$\mathcal{V}^{(S)}(s_{jk}, m_j, m_k) = \frac{1}{v_{jk}} \left(\frac{Q_{jk}^2}{s_{jk}} \right)^\epsilon \left[\frac{1}{\epsilon^2} \left(1 - \frac{1}{2}\rho_j^{-2\epsilon} - \frac{1}{2}\rho_k^{-2\epsilon} \right) - \frac{\pi^2}{12} (\Theta(m_j) + \Theta(m_k)) \right]. \quad (\text{C.2})$$

Here and in the following the abbreviation $Q_{jk}^2 \equiv s_{jk} + m_j^2 + m_k^2$ is introduced with $s_{jk} = 2p_j p_k$. The quantities ρ, ρ_j and ρ_k are obtained from

$$\rho = \sqrt{\frac{1 - v_{jk}}{1 + v_{jk}}} \quad (\text{C.3})$$

$$\rho_n(\mu_j, \mu_k) = \sqrt{\frac{1 - v_{jk} + 2\mu_n^2/(1 - \mu_j^2 - \mu_k^2)}{1 + v_{jk} + 2\mu_n^2/(1 - \mu_j^2 - \mu_k^2)}} \quad (n = j, k), \quad (\text{C.4})$$

with the substitution $\mu_n^2 \rightarrow m_n^2/Q_{jk}^2$ ($n = j, k$) and v_{jk} defined as

$$v_{jk} = \sqrt{1 - \frac{p_j^2 p_k^2}{(p_j p_k)^2}}. \quad (\text{C.5})$$

In practice the expanded expression is needed since the coefficients of the $1/\epsilon^2$ and $1/\epsilon$ terms are necessary. For brevity only the combinations relevant for the calculation of squark pair production are listed below. The singular part for partons j and k being massive is

$$\mathcal{V}^{(S)}(s_{jk}, m_j, m_k) = \frac{1}{v_{jk}} \left[\frac{1}{\epsilon} \ln \rho - \frac{1}{4} \ln^2 \rho_j^2 - \frac{1}{4} \ln^2 \rho_k^2 - \frac{\pi^2}{6} \right] + \frac{1}{v_{jk}} \ln \rho \ln \left(\frac{Q_{jk}^2}{s_{jk}} \right), \quad (\text{C.6})$$

while the singular part for parton j being massless reads

$$\mathcal{V}^{(S)}(s_{jk}, 0, m_k) = \frac{1}{2\epsilon^2} + \frac{1}{2\epsilon} \ln \frac{m_k^2}{s_{jk}} - \frac{1}{4} \ln^2 \frac{m_k^2}{s_{jk}} - \frac{\pi^2}{12} - \frac{1}{2} \ln \frac{m_k^2}{s_{jk}} \ln \frac{s_{jk}}{Q_{jk}^2} - \frac{1}{2} \ln \frac{m_k^2}{Q_{jk}^2} \ln \frac{s_{jk}}{Q_{jk}^2}. \quad (\text{C.7})$$

The non-singular terms $\mathcal{V}^{(\text{NS})}$ depend on the flavours, masses and spins of the partons. If j is a massless quark and k is a massive parton, then the corresponding non-singular part results in

$$\mathcal{V}_q^{(\text{NS})}(s_{jk}, 0, m_k) = \frac{\gamma_q}{\mathbf{T}_q^2} \left[\ln \frac{s_{jk}}{Q_{jk}^2} - 2 \ln \frac{Q_{jk} - m_k}{Q_{jk}} - \frac{2m_k}{Q_{jk} + m_k} \right] + \frac{\pi^2}{6} - \text{Li}_2 \left(\frac{s_{jk}}{Q_{jk}^2} \right), \quad (\text{C.8})$$

with the color charge operator \mathbf{T}_q already introduced in Eq. (3.19). The non-singular function $\mathcal{V}_j^{(\text{NS})}$ for j being a massive squark and k being a massive parton is

$$\mathcal{V}_{\tilde{q}}^{(\text{NS})}(s_{jk}, m_j, m_k) = \frac{\gamma_{\tilde{q}}}{\mathbf{T}_{\tilde{q}}^2} \ln \frac{s_{jk}}{Q_{jk}^2} - 2 \ln \frac{(Q_{jk} - m_k)^2 - m_j^2}{Q_{jk}^2} + \frac{4m_k(m_k - Q_{jk})}{s_{jk}} + \frac{\pi^2}{2} + \frac{1}{v_{jk}} \left[\ln \rho^2 \ln(1 + \rho^2) + 2 \text{Li}_2(\rho^2) - \text{Li}_2(1 - \rho_j^2) - \text{Li}_2(1 - \rho_k^2) - \frac{\pi^2}{6} \right], \quad (\text{C.9})$$

while for k being massless it simplifies to

$$\mathcal{V}_{\tilde{q}}^{(\text{NS})}(s_{jk}, m_j, 0) = \frac{\gamma_{\tilde{q}}}{\mathbf{T}_{\tilde{q}}^2} \ln \frac{s_{jk}}{Q_{jk}^2} + \frac{\pi^2}{6} - \text{Li}_2 \left(\frac{s_{jk}}{Q_{jk}^2} \right) - 2 \ln \frac{s_{jk}}{Q_{jk}^2}. \quad (\text{C.10})$$

Finally, the singular function Γ_j for the squark is

$$\Gamma_{\tilde{q}}(\mu, m_{\tilde{q}}) = \mathbf{T}_{\tilde{q}}^2 \left(\frac{1}{\epsilon} - \ln \frac{m_{\tilde{q}}^2}{\mu^2} - 2 \right) + \gamma_{\tilde{q}} \ln \frac{m_{\tilde{q}}^2}{\mu^2} = C_F \left[\frac{1}{\epsilon} + \ln \frac{m_{\tilde{q}}^2}{\mu^2} - 2 \right]. \quad (\text{C.11})$$

C.2 Finite Collinear Terms

The finite collinear terms which remain after all infrared divergencies have been canceled and reabsorbed into a redefinition of PDFs, contribute to the total cross section with two different initial state configurations. The first one stems from an initial state gluon splitting into a quark and antiquark. The corresponding partonic cross section can be written as follows

$$\begin{aligned} \sigma_{\text{coll}}^{gq} &= \int_0^1 dx \int d\Phi_m(x) (\mathbf{P}^{gq}(x, xp_a, p_b, k_1, k_2, \mu_F^2) + \mathbf{K}^{gq}(x)) \otimes d\sigma_{qq}^B(xp_a, p_b, k_1, k_2) \\ &+ \int_0^1 dx \int d\Phi_m(x) (\mathbf{P}^{gq}(x, p_a, xp_b, k_1, k_2, \mu_F^2) + \mathbf{K}^{gq}(x)) \otimes d\sigma_{qq}^B(p_a, xp_b, k_1, k_2) . \end{aligned} \quad (\text{C.12})$$

The longitudinal momentum fraction x enters the evaluation of the Born amplitude since one of the quarks in the initial state of this amplitude carries the momentum xp_a or xp_b while the original initial state parton, the gluon in this case, carries the momentum p_a . The insertion operators \mathbf{P}^{gq} and \mathbf{K}^{gq} involve color charge operators which act on the color space of the Born amplitude and give rise to the color linked Born amplitudes squared already mentioned in the discussion of the subtraction dipoles in Section 5.4 and of the integrated dipoles in Section 5.5. The contribution from the \mathbf{P} -operator in the first line of Eq. (C.12) is

$$\begin{aligned} \sigma_{\text{coll,P}}^{gq} &= \int_0^1 dx \int d\Phi_m(x) \mathbf{P}^{gq}(x, xp_a, p_b, k_1, k_2, \mu_F^2) \otimes d\sigma_{qq}^B(xp_a, p_b, k_1, k_2) \\ &= \int_0^1 dx \int d\Phi_m(x) \frac{\alpha_s}{2\pi} T_R [x^2 + (1-x)^2] \frac{1}{C_F} \cdot \\ &\quad \left[\ln \frac{\mu_F^2}{xs_{a1}} + \ln \frac{\mu_F^2}{xs_{a2}} + \ln \frac{\mu_F^2}{xs_{ab}} \right] \otimes |\mathcal{M}(xp_a, p_b, k_1, k_2)|^2 , \end{aligned} \quad (\text{C.13})$$

while the \mathbf{K} -operator yields

$$\begin{aligned} \sigma_{\text{coll,K}}^{gq} &= \int_0^1 dx \int d\Phi_m(x) \mathbf{K}^{gq}(x) \otimes d\sigma_{qq}^B(xp_a, p_b, k_1, k_2) \\ &= \int_0^1 dx \int d\Phi_m(x) \frac{\alpha_s}{2\pi} \left\{ T_R (x^2 + (1-x)^2) \ln \frac{1-x}{x} + 2 T_R x(1-x) \right. \\ &\quad \left. - \frac{T_R}{C_F} (x^2 + (1-x)^2) \left(\ln \frac{(1-x)s_{a1}}{(1-x)s_{a1} + m_1^2} + \ln \frac{(1-x)s_{a2}}{(1-x)s_{a2} + m_2^2} \right) \right. \\ &\quad \left. - \frac{T_R}{C_F} (x^2 + (1-x)^2) \ln(1-x) \right\} \otimes |\mathcal{M}(xp_a, p_b, k_1, k_2)|^2 . \end{aligned} \quad (\text{C.14})$$

The contributions of both operators to the second line of Eq. (C.12) are obtained through a transformation $xp_a \rightarrow p_a$ and $p_b \rightarrow xp_b$. In both contributions the constants $T_R = 1/2$ and $C_F = 4/3$ are color factors and the variables $s_{xy} = 2 \cdot p_x p_y$ stand for products of initial and final state momenta. Depending on its color structure

each term in Eqs. (C.13) and (C.14) has to be convoluted with the corresponding color linked Born amplitude squared. This fact is expressed by the symbolic notation $\otimes |\mathcal{M}(xp_a, p_b, k_1, k_2)|^2$.

The second initial state configuration stems from a quark splitting into a gluon and a quark. The corresponding partonic cross section $\sigma_{\text{coll}}^{qq}$ has the same pattern like $\sigma_{\text{coll}}^{gq}$ in Eq. (C.12). The \mathbf{P} -operator contributes in this case

$$\begin{aligned} \sigma_{\text{coll,P}}^{qq} &= \int_0^1 dx \int d\Phi_m(x) \mathbf{P}^{qq}(x, xp_a, p_b, k_1, k_2, \mu_F^2) \otimes d\sigma_{qq}^B(xp_a, p_b, k_1, k_2) \\ &= \frac{\alpha_s}{2\pi} \left(\frac{1+x^2}{1-x^2} \right)_+ \\ &\quad \left[\ln \frac{\mu_F^2}{xs_{a1}} + \ln \frac{\mu_F^2}{xs_{a2}} + \ln \frac{\mu_F^2}{xs_{ab}} \right] \otimes |\mathcal{M}(xp_a, p_b, k_1, k_2)|^2 . \end{aligned} \quad (\text{C.15})$$

The \mathbf{K} -operator yields

$$\begin{aligned} \sigma_{\text{coll,K}}^{qq} &= \int_0^1 dx \int d\Phi_m(x) \mathbf{K}^{qq}(x) \otimes d\sigma_{qq}^B(xp_a, p_b, k_1, k_2) \\ &= \frac{\alpha_s}{2\pi} \left\{ C_F \left(\frac{2}{1-x} \ln \frac{1-x}{x} \right)_+ - \delta(1-x) C_F (5 - \pi^2) \right. \\ &\quad - C_F (1+x) \ln \frac{1-x}{x} + C_F (1-x) \\ &\quad + \sum_{j=1,2} \left\{ -2 \left(\frac{\ln(1-x)}{1-x} \right)_+ - \left(\frac{2}{1-x} \right)_+ \ln(2-x) \right. \\ &\quad + \left. \left[\frac{2}{1-x} \left(1 + \ln \left(1-x + \frac{m_j^2}{s_{ja}} \right) \right) \right]_+ + 2 \delta(1-x) \right. \\ &\quad - \frac{3}{2} \delta(1-x) \left(\ln \frac{s_{ja} - 2m_j \sqrt{s_{ja} + m_j^2} + 2m_j^2}{s_{ja}} + \frac{2m_j}{\sqrt{s_{ja} + m_j^2} + m_j} \right) \\ &\quad \left. \left. 2 \ln \frac{2-x}{1-x} + (1+x) \ln \frac{(1-x)s_{ja}}{(1-x)s_{ja} + m_j^2} \right\} \right. \\ &\quad \left. - 2 \left(\frac{\ln(1-x)}{1-x} \right)_+ + \frac{\pi^2}{3} \delta(1-x) + (1+x) \ln(1-x) \right\} . \end{aligned} \quad (\text{C.16})$$

The $+$ -distribution appearing in both contributions for qq initial states is defined as

$$\begin{aligned} \int_0^1 dx g(x) f(x)_+ \Theta(x-z) &= \int_z^1 dx g(x) f(x)_+ \\ &= \int_z^1 dx (g(x) - g(1)) f(x) - \int_0^z dx g(1) f(x) . \end{aligned} \quad (\text{C.17})$$

This definition has to be applied to the four functions with $+$ -distributions in $\sigma_{\text{coll,P}}^{qq}$ and $\sigma_{\text{coll,K}}^{qq}$ and the results are listed separately in Section C.3 . Special care has to be

taken when evaluating the $+$ -distribution, which contains the kinematical variable $s_{ja} = 2p_a p_j$. While p_a is the original initial-state momentum of the incoming parton before the splitting, the final-state momentum $p_j = k_1$ or k_2 belongs to the x -boosted frame after the splitting: $x p_a + p_b = k_1 + k_2$. This fact is indicated by the label (x) in $s_{ja}^{(x)}$ in the following. Although appearing inside the $+$ -distribution, s_{ja} has to be treated as if being a function of x outside the distribution:

$$\begin{aligned}
& \int_0^1 dx \int d\Phi(x) \left[J(x, s_{ja}^{(x)}) \right]_+ |\mathcal{M}(\Phi(x))|^2 \Theta(x-z) \\
&= \int_0^1 dx \int d\Phi(x) \int_{-\infty}^{\infty} d\bar{s}_{ja} \delta(\bar{s}_{ja} - \bar{s}_{ja}^{(x)}) \left[J(x, s_{ja}^{(x)}) \right]_+ |\mathcal{M}(\Phi(x))|^2 \Theta(x-z) \\
&= \int_z^1 dx \left\{ \int d\Phi(x) J(x, s_{ja}^{(x)}) |\mathcal{M}(\Phi(x))|^2 \right. \\
&\quad \left. - \int d\Phi(1) J(x, s_{ja}^{(1)}) |\mathcal{M}(\Phi(1))|^2 \right\} \\
&\quad - \int_0^z dx \int d\Phi(1) J(x, s_{ja}^{(1)}) |\mathcal{M}(\Phi(1))|^2 .
\end{aligned} \tag{C.18}$$

Applying these prescriptions and folding the resulting partonic cross section with the PDFs according to Eq. (5.72) allows for expressing the finite collinear remainder in terms of a modified PDF parametrized as in Eq. (5.76). The coefficients $A_1(x, \tilde{x}_a)$, $A_2(x, \tilde{x}_a)$, $B(x, \tilde{x}_a)$, $C(x, \tilde{x}_a)$, $D_1(\tilde{x}_a)$ and $D_2(\tilde{x}_a)$ follow directly from the expressions for the \mathbf{P} - and \mathbf{K} -terms listed above after the substitution

$$\begin{aligned}
\tilde{x}_a &= x \cdot x_a \\
\int_0^1 dx_a \int_0^1 dx &= \int_0^x d\tilde{x}_a \int_0^1 \frac{dx}{x} \\
&= \int_0^1 d\tilde{x}_a \int_0^1 \frac{dx}{x} \Theta(x - \tilde{x}_a)
\end{aligned} \tag{C.19}$$

has been performed. This substitution is useful for the numerical evaluation of the finite remainder since the initial state momentum entering the Born matrix element $|\mathcal{M}(xp_a, p_b, k_1, k_2)|^2$ is changed to

$$xp_a = \frac{\tilde{x}_a}{x_a} p_a = \frac{\tilde{x}_a}{x_a} x_a P_{\text{Proton}} = \tilde{x}_a P_{\text{Proton}} . \tag{C.20}$$

This means, that the original 2-particle phase space can be used for the numerical evaluation of the Born amplitude.

In the following the coefficients of the modified PDFs are listed:

$$\begin{aligned}
A_1 &= \frac{2}{1-x} C_F \left(\ln \frac{\mu_F^2}{x s_{a1}} + \ln \frac{\mu_F^2}{x s_{a2}} + \ln \frac{\mu_F^2}{x s_{ab}} \right) \\
&+ C_F 2 \frac{\ln(1-x)}{1-x} \\
&- C_F 2 \left(\frac{\ln(1-x)}{1-x} - \frac{1}{1-x} \right) \\
&- C_F 2 \frac{\ln(1-x)}{1-x}
\end{aligned} \tag{C.21}$$

$$A_2 = \sum_{j=1,2} C_F \frac{2}{1-x} \tag{C.22}$$

$$\begin{aligned}
B &= -C_F(x+1) \left(\ln \frac{\mu_F^2}{x s_{a1}} + \ln \frac{\mu_F^2}{x s_{a2}} + \ln \frac{\mu_F^2}{x s_{ab}} \right) \\
&+ C_F \left(1-x - (1+x) \ln \frac{1-x}{x} - 2 \frac{\ln x}{x} \right) \\
&+ \sum_{j=1,2} C_F(1+x) \ln \frac{1-x}{1-x + m_j^2/s_{ja}^{(x)}} \\
&+ C_F(1+x) \ln(1-x)
\end{aligned} \tag{C.23}$$

$$\begin{aligned}
C &= T_R(x^2 + (1-x^2)) \left(\ln \frac{\mu_F^2}{x s_{a1}} + \ln \frac{\mu_F^2}{x s_{a2}} + \ln \frac{\mu_F^2}{x s_{ab}} \right) \\
&+ T_R(x^2 + (1-x^2)) \ln \frac{1-x}{x} + 2T_R x(1-x) \\
&- T_R(x^2 + (1-x^2)) \sum_{j=1,2} \ln \frac{(1-x)s_{ja}^{(x)}}{(1-x)s_{ja}^{(x)} + m_j^2} \\
&- T_R(x^2 + (1-x^2)) \ln(1-x)
\end{aligned} \tag{C.24}$$

$$\begin{aligned}
D_1 &= C_F \left(2 \ln(1-\tilde{x}_a) + \frac{3}{2} \right) \left(\ln \frac{\mu_F^2}{x s_{a1}} + \ln \frac{\mu_F^2}{x s_{a2}} + \ln \frac{\mu_F^2}{x s_{ab}} \right) \\
&+ C_F \left(\ln^2(1-\tilde{x}_a) - \frac{\pi^2}{3} - 5 + \pi^2 \right) \\
&- \sum_{j=1,2} C_F \left[-2 + \frac{3}{2} \left(\ln \frac{s_{ja}^{(1)} - 2m_j \sqrt{s_{ja}^{(1)} + m_j^2} + 2m_j^2}{s_{ja}^{(1)}} + \frac{2m_j}{\sqrt{s_{ja}^{(1)} + m_j^2} + m_j} \right) \right. \\
&\quad \left. + \ln^2(1-\tilde{x}_a) \right] \\
&- C_F \left(\ln^2(1-\tilde{x}_a) - \frac{\pi^2}{3} \right)
\end{aligned} \tag{C.25}$$

$$\begin{aligned}
D_2 &= - \sum_{j=1,2} 2 C_F \left\{ -\text{Li}_2 \left(\frac{s_{ja}^{(x)}}{m_j^2} \right) + \text{Li}_2 \left(\frac{s_{ja}^{(x)}(\tilde{x}_a - 1)}{m_j^2} \right) \right. \\
&\quad \left. - \ln(1-\tilde{x}_a)(1 + \ln(m_j^2/s_{ja}^{(x)})) \right\}
\end{aligned} \tag{C.26}$$

C.3 Solutions to Integrals with +-Distributions

In this section non-trivial integrals which arise in the calculation of the finite collinear remainder terms of the Catani-Seymour subtraction formalism are solved. These integrals involve the +-distribution which is resolved according to its definition in Eq. (C.18). Only integrals needed for the calculation of the squark pair production process are listed in the following.

The first integral needed emerges from Eq. (C.15) after convolution with the PDFs:

$$\begin{aligned}
& \int_0^1 \frac{dx}{x} f\left(\frac{z}{x}\right) \left(\frac{1+x^2}{1-x}\right)_+ \Theta(x-z) \\
&= \int_z^1 \frac{dx}{x} \left(f\left(\frac{z}{x}\right) - xf(z)\right) \frac{1+x^2}{1-x} - \int_0^z dx f(z) \frac{1+x^2}{1-x} \\
&= \int_z^1 \frac{dx}{x} \left(f\left(\frac{z}{x}\right) - xf(z)\right) \frac{2}{1-x} - \int_z^1 \frac{dx}{x} f\left(\frac{z}{x}\right) (1+x) . \\
&\quad + f(z) \left(\frac{3}{2} + 2 \ln(1-z)\right)
\end{aligned} \tag{C.27}$$

The second line of Eq. (C.16) gives rise to the following integral:

$$\begin{aligned}
& \int_0^1 \frac{dx}{x} f\left(\frac{z}{x}\right) \left(\frac{2}{1-x} \ln \frac{1-x}{x}\right)_+ \Theta(x-z) \\
&= \int_z^1 \frac{dx}{x} \left(f\left(\frac{z}{x}\right) - xf(z)\right) \frac{2 \ln(1-x)}{1-x} - \int_z^1 \frac{dx}{x} f\left(\frac{z}{x}\right) \frac{2 \ln x}{1-x} \\
&\quad + \int_0^1 dx f(z) \frac{2 \ln x}{1-x} - \int_0^z dx f(z) \frac{2 \ln(1-x)}{1-x} \\
&= \int_z^1 \frac{dx}{x} \left(f\left(\frac{z}{x}\right) - xf(z)\right) \frac{2 \ln(1-x)}{1-x} - \int_z^1 \frac{dx}{x} f\left(\frac{z}{x}\right) \frac{2 \ln x}{1-x} \\
&\quad + f(z) \left(\ln^2(1-z) - \frac{\pi^2}{3}\right) .
\end{aligned} \tag{C.28}$$

The next integral needed in Eq. (C.16) reads

$$\begin{aligned}
& \int_0^1 \frac{dx}{x} f\left(\frac{z}{x}\right) \left(\frac{\ln(1-x)}{1-x}\right)_+ \Theta(x-z) \\
&= \int_z^1 \frac{dx}{x} \left(f\left(\frac{z}{x}\right) - xf(z)\right) \frac{\ln(1-x)}{1-x} + f(z) \frac{1}{2} \ln^2(1-z) .
\end{aligned} \tag{C.29}$$

The integral in the last line of Eq. (C.16) gives

$$\begin{aligned}
& \int_0^1 \frac{dx}{x} f\left(\frac{z}{x}\right) \left(\frac{2}{1-x}\right)_+ \Theta(x-z) \\
&= \int_z^1 \frac{dx}{x} \left(f\left(\frac{z}{x}\right) - xf(z)\right) \frac{2}{1-x} + 2 \ln(1-z) .
\end{aligned} \tag{C.30}$$

The last integral needed for the calculation contains the kinematical variable s_{ja} so that Eq. (C.18) has to be applied:

$$\begin{aligned}
& \int_0^1 \frac{dx}{x} f\left(\frac{z}{x}\right) \left[\frac{2}{1-x} \ln \left(\frac{(1-x)s_{ja}^{(x)} + m_j^2}{s_{ja}^{(x)}} \right) \right]_+ \Theta(x-z) \quad (\text{C.31}) \\
&= \int_z^1 \frac{dx}{x} f\left(\frac{z}{x}\right) \frac{2}{1-x} \ln \ln \left((1-x) + \frac{m_j^2}{s_{ja}^{(x)}} \right) \\
&- \int_z^1 dx f(z) \frac{2}{1-x} \ln \ln \left((1-x) + \frac{m_j^2}{s_{ja}^{(1)}} \right) \\
&- \int_0^z dx f(z) \frac{2}{1-x} \ln \ln \left((1-x) + \frac{m_j^2}{s_{ja}^{(1)}} \right)
\end{aligned}$$

Here, the differently labeled kinematical variables denote

$$s_{ja}^{(x)} = 2 p_a p_j = 2 x_a P_{\text{Proton}} p_j = 2 \frac{z}{x} P_{\text{Proton}} p_j \quad (\text{C.32})$$

or

$$s_{ja}^{(1)} = 2 z P_{\text{Proton}} p_j , \quad (\text{C.33})$$

respectively.

Bibliography

- [1] J. Wess and B. Zumino, *Supergauge Transformations in Four-Dimensions*. Nucl.Phys. **B70** (1974) 39–50.
- [2] D. Volkov and V. Akulov, *Is the Neutrino a Goldstone Particle?* Phys.Lett. **B46** (1973) 109–110.
- [3] P. Fayet, *Spontaneously Broken Supersymmetric Theories of Weak, Electromagnetic and Strong Interactions*. Phys.Lett. **B69** (1977) 489.
- [4] P. Fayet, *Supersymmetry and Weak, Electromagnetic and Strong Interactions*. Phys.Lett. **B64** (1976) 159.
- [5] H. P. Nilles, *Supersymmetry, Supergravity and Particle Physics*. Phys.Rept. **110** (1984) 1–162.
- [6] H. E. Haber and G. L. Kane, *The Search for Supersymmetry: Probing Physics Beyond the Standard Model*. Phys.Rept. **117** (1985) 75–263.
- [7] M. Sohnius, *Introducing Supersymmetry*. Phys.Rept. **128** (1985) 39–204.
- [8] S. P. Martin, *A Supersymmetry primer*. arXiv:hep-ph/9709356.
- [9] **CMS** Collaboration, S. Chatrchyan *et al.*, *Observation of a new boson at a mass of 125 GeV with the CMS experiment at the LHC*. Phys.Lett. **B716** (2012) 30–61, arXiv:1207.7235 [hep-ex].
- [10] **ATLAS** Collaboration, G. Aad *et al.*, *Observation of a new particle in the search for the Standard Model Higgs boson with the ATLAS detector at the LHC*. Phys.Lett. **B716** (2012) 1–29, arXiv:1207.7214 [hep-ex].
- [11] F. Englert and R. Brout, *Broken Symmetry and the Mass of Gauge Vector Mesons*. Phys.Rev.Lett. **13** (1964) 321–323.
- [12] P. W. Higgs, *Broken Symmetries and the Masses of Gauge Bosons*. Phys.Rev.Lett. **13** (1964) 508–509.
- [13] P. W. Higgs, *Broken symmetries, massless particles and gauge fields*. Phys.Lett. **12** (1964) 132–133.

-
- [14] G. Guralnik, C. Hagen, and T. Kibble, *Global Conservation Laws and Massless Particles*. Phys.Rev.Lett. **13** (1964) 585–587.
- [15] P. W. Higgs, *Spontaneous Symmetry Breakdown without Massless Bosons*. Phys.Rev. **145** (1966) 1156–1163.
- [16] **ATLAS** Collaboration, *Search for squarks and gluinos with the ATLAS detector using final states with jets and missing transverse momentum at $\sqrt{s} = 8$ TeV*. ATLAS-CONF-2012-109 (2012) .
- [17] **ATLAS** Collaboration, G. Aad *et al.*, *Search for light scalar top quark pair production in final states with two leptons with the ATLAS detector in $\sqrt{s} = 7$ TeV proton-proton collisions*. arXiv:1208.4305 [hep-ex].
- [18] K.-i. Hikasa and M. Kobayashi, *Light Scalar Top at $e^+ e^-$ Colliders*. Phys.Rev. **D36** (1987) 724.
- [19] P. Falgari, C. Schwinn, and C. Wever, *NLL soft and Coulomb resummation for squark and gluino production at the LHC*. JHEP **1206** (2012) 052, arXiv:1202.2260 [hep-ph].
- [20] W. Beenakker, R. Hopker, M. Spira, and P. Zerwas, *Squark and gluino production at hadron colliders*. Nucl.Phys. **B492** (1997) 51–103, arXiv:hep-ph/9610490.
- [21] S. R. Coleman and J. Mandula, *All Possible Symmetries Of The S Matrix*. Phys.Rev. **159** (1967) 1251–1256.
- [22] Y. Golfand and E. Likhtman, *Extension of the Algebra of Poincare Group Generators and Violation of p Invariance*. JETP Lett. **13** (1971) 323–326.
- [23] R. Haag, J. T. Lopuszanski, and M. Sohnius, *All Possible Generators of Supersymmetries of the s Matrix*. Nucl.Phys. **B88** (1975) 257.
- [24] H. Baer and X. Tata, *Weak scale supersymmetry: From superfields to scattering events*. Cambridge University Press, 2006.
- [25] P. Fayet and J. Iliopoulos, *Spontaneously Broken Supergauge Symmetries and Goldstone Spinors*. Phys.Lett. **B51** (1974) 461–464.
- [26] L. O’Raifeartaigh, *Spontaneous Symmetry Breaking for Chiral Scalar Superfields*. Nucl.Phys. **B96** (1975) 331.
- [27] H. P. Nilles, *Dynamically Broken Supergravity and the Hierarchy Problem*. Phys.Lett. **B115** (1982) 193.
- [28] H. P. Nilles, *Supergravity Generates Hierarchies*. Nucl.Phys. **B217** (1983) 366.

- [29] A. H. Chamseddine, R. L. Arnowitt, and P. Nath, *Locally Supersymmetric Grand Unification*. Phys.Rev.Lett. **49** (1982) 970.
- [30] R. Barbieri, S. Ferrara, and C. A. Savoy, *Gauge Models with Spontaneously Broken Local Supersymmetry*. Phys.Lett. **B119** (1982) 343.
- [31] M. Dine and W. Fischler, *A Phenomenological Model of Particle Physics Based on Supersymmetry*. Phys.Lett. **B110** (1982) 227.
- [32] L. Alvarez-Gaume, M. Claudson, and M. B. Wise, *Low-Energy Supersymmetry*. Nucl.Phys. **B207** (1982) 96.
- [33] M. Dine and A. E. Nelson, *Dynamical supersymmetry breaking at low-energies*. Phys.Rev. **D48** (1993) 1277–1287, arXiv:hep-ph/9303230 [hep-ph].
- [34] L. Girardello and M. T. Grisaru, *Soft Breaking of Supersymmetry*. Nucl.Phys. **B194** (1982) 65.
- [35] M. Drees, R. Godbole, and P. Roy, *Theory and phenomenology of sparticles*. World Scientific, Singapore, 2004.
- [36] **D0** Collaboration, V. Abazov *et al.*, *Search for scalar top quarks in the acoplanar charm jets and missing transverse energy final state in $p\bar{p}$ collisions at $\sqrt{s} = 1.96$ -TeV*. Phys.Lett. **B665** (2008) 1–8, arXiv:0803.2263 [hep-ex].
- [37] **CDF** Collaboration, T. Aaltonen *et al.*, *Search for Scalar Top Quark Production in $p\bar{p}$ Collisions at $\sqrt{s} = 1.96$ TeV*. arXiv:1203.4171 [hep-ex].
- [38] A. Belitsky and A. Radyushkin, *Unraveling hadron structure with generalized parton distributions*. Phys.Rept. **418** (2005) 1–387, arXiv:hep-ph/0504030.
- [39] T. Lee and M. Nauenberg, *Degenerate Systems and Mass Singularities*. Phys.Rev. **133** (1964) B1549–B1562.
- [40] T. Kinoshita, *Mass singularities of Feynman amplitudes*. J.Math.Phys. **3** (1962) 650–677.
- [41] J. C. Collins, D. E. Soper, and G. F. Sterman, *Factorization of Hard Processes in QCD*. Adv.Ser.Direct.High Energy Phys. **5** (1988) 1–91, arXiv:hep-ph/0409313.
- [42] V. Gribov and L. Lipatov, *Deep inelastic $e p$ scattering in perturbation theory*. Sov.J.Nucl.Phys. **15** (1972) 438–450.
- [43] G. Altarelli and G. Parisi, *Asymptotic Freedom in Parton Language*. Nucl.Phys. **B126** (1977) 298.

- [44] Y. L. Dokshitzer, *Calculation of the Structure Functions for Deep Inelastic Scattering and $e^+ e^-$ Annihilation by Perturbation Theory in Quantum Chromodynamics*. Sov.Phys.JETP **46** (1977) 641–653.
- [45] G. 't Hooft, *Renormalization of Massless Yang-Mills Fields*. Nucl.Phys. **B33** (1971) 173–199.
- [46] G. 't Hooft, *Renormalizable Lagrangians for Massive Yang-Mills Fields*. Nucl.Phys. **B35** (1971) 167–188.
- [47] D. Ross and J. Taylor, *Renormalization of a Unified Theory Of Weak and Electromagnetic Interactions*. Nucl.Phys. **B51** (1973) 125–144.
- [48] A. Sirlin, *Radiative Corrections in the $SU(2)$ - $L \times U(1)$ Theory: A Simple Renormalization Framework*. Phys.Rev. **D22** (1980) 971–981.
- [49] A. Denner, *Techniques for calculation of electroweak radiative corrections at the one loop level and results for W physics at LEP-200*. Fortsch.Phys. **41** (1993) 307–420, [arXiv:0709.1075 \[hep-ph\]](#).
- [50] W. A. Bardeen, A. Buras, D. Duke, and T. Muta, *Deep Inelastic Scattering Beyond the Leading Order in Asymptotically Free Gauge Theories*. Phys.Rev. **D18** (1978) 3998.
- [51] G. 't Hooft and M. Veltman, *Regularization and Renormalization of Gauge Fields*. Nucl.Phys. **B44** (1972) 189–213.
- [52] S. Catani and M. Seymour, *NLO calculations in QCD: A General algorithm*. Nucl.Phys.Proc.Suppl. **51C** (1996) 233–242, [arXiv:hep-ph/9607318](#).
- [53] S. Catani, S. Dittmaier, M. H. Seymour, and Z. Trocsanyi, *The Dipole formalism for next-to-leading order QCD calculations with massive partons*. Nucl.Phys. **B627** (2002) 189–265, [arXiv:hep-ph/0201036](#).
- [54] A. Masiero and O. Vives, *New physics in CP violation experiments*. Ann.Rev.Nucl.Part.Sci. **51** (2001) 161–187, [arXiv:hep-ph/0104027](#).
- [55] Y. Grossman, Z. Ligeti, and Y. Nir, *Future prospects of B physics*. Prog.Theor.Phys. **122** (2009) 125–143, [arXiv:0904.4262 \[hep-ph\]](#).
- [56] G. Isidori, Y. Nir, and G. Perez, *Flavor Physics Constraints for Physics Beyond the Standard Model*. Ann.Rev.Nucl.Part.Sci. **60** (2010) 355, [arXiv:1002.0900 \[hep-ph\]](#).
- [57] R. S. Chivukula, H. Georgi, and L. Randall, *A Composite Technicolor Standard Model of Quarks*. Nucl.Phys. **B292** (1987) 93–108.
- [58] A. Buras, P. Gambino, M. Gorbahn, S. Jager, and L. Silvestrini, *Universal unitarity triangle and physics beyond the standard model*. Phys.Lett. **B500** (2001) 161–167, [arXiv:hep-ph/0007085](#).

- [59] G. D'Ambrosio, G. Giudice, G. Isidori, and A. Strumia, *Minimal flavor violation: An Effective field theory approach*. Nucl.Phys. **B645** (2002) 155–187, [arXiv:hep-ph/0207036](#).
- [60] C. Bobeth, M. Bona, A. J. Buras, T. Ewerth, M. Pierini, *et al.*, *Upper bounds on rare K and B decays from minimal flavor violation*. Nucl.Phys. **B726** (2005) 252–274, [arXiv:hep-ph/0505110](#).
- [61] P. Huet and A. E. Nelson, *Electroweak baryogenesis in supersymmetric models*. Phys.Rev. **D53** (1996) 4578–4597, [arXiv:hep-ph/9506477](#).
- [62] M. Carena, G. Nardini, M. Quiros, and C. Wagner, *The Baryogenesis Window in the MSSM*. Nucl.Phys. **B812** (2009) 243–263, [arXiv:0809.3760](#) [hep-ph].
- [63] Y. Li, S. Profumo, and M. Ramsey-Musolf, *Bino-driven Electroweak Baryogenesis with highly suppressed Electric Dipole Moments*. Phys.Lett. **B673** (2009) 95–100, [arXiv:0811.1987](#) [hep-ph].
- [64] A. Arbey, M. Battaglia, A. Djouadi, and F. Mahmoudi, *The Higgs sector of the phenomenological MSSM in the light of the Higgs boson discovery*. [arXiv:1207.1348](#) [hep-ph].
- [65] Z. Kang, T. Li, J. Li, and Y. Liu, *A Rediatively Light Stop Saves the Best Global Fit for Higgs Boson Mass and Decays*. [arXiv:1208.2673](#) [hep-ph].
- [66] M. R. Buckley and D. Hooper, *Are There Hints of Light Stops in Recent Higgs Search Results?* [arXiv:1207.1445](#) [hep-ph].
- [67] S. Bornhauser, M. Drees, S. Grab, and J. Kim, *Light Stop Searches at the LHC in Events with two b-Jets and Missing Energy*. Phys.Rev. **D83** (2011) 035008, [arXiv:1011.5508](#) [hep-ph].
- [68] M. Carena, A. Freitas, and C. Wagner, *Light Stop Searches at the LHC in Events with One Hard Photon or Jet and Missing Energy*. JHEP **0810** (2008) 109, [arXiv:0808.2298](#) [hep-ph].
- [69] M. Drees, M. Hanussek, and J. S. Kim, *Light Stop Searches at the LHC with Monojet Events*. [arXiv:1201.5714](#) [hep-ph].
- [70] G. Hiller and Y. Nir, *Measuring Flavor Mixing with Minimal Flavor Violation at the LHC*. JHEP **0803** (2008) 046, [arXiv:0802.0916](#) [hep-ph].
- [71] G. Hiller, J. S. Kim, and H. Sedello, *Collider Signatures of Minimal Flavor Mixing from Stop Decay Length Measurements*. Phys.Rev. **D80** (2009) 115016, [arXiv:0910.2124](#) [hep-ph].

- [72] M. Muhlleitner and E. Popena, *Light Stop Decay in the MSSM with Minimal Flavour Violation*. JHEP **1104** (2011) 095, arXiv:1102.5712 [hep-ph].
- [73] J. Donoghue, H. P. Nilles, and D. Wyler, *Flavor Changes in Locally Supersymmetric Theories*. Phys.Lett. **B128** (1983) 55.
- [74] **Particle Data Group** Collaboration, J. Beringer *et al.*, *Review of Particle Physics (RPP)*. Phys.Rev. **D86** (2012) 010001.
- [75] W. Siegel, *Supersymmetric Dimensional Regularization via Dimensional Reduction*. Phys.Lett. **B84** (1979) 193.
- [76] D. Capper, D. Jones, and P. van Nieuwenhuizen, *Regularization by Dimensional Reduction of Supersymmetric and Nonsupersymmetric Gauge Theories*. Nucl.Phys. **B167** (1980) 479.
- [77] W. Marciano and A. Sirlin, *On the Renormalization of the Charm Quartet Model*. Nucl.Phys. **B93** (1975) 303.
- [78] G. Degrassi, P. Gambino, and P. Slavich, *QCD corrections to radiative B decays in the MSSM with minimal flavor violation*. Phys.Lett. **B635** (2006) 335–342, arXiv:hep-ph/0601135.
- [79] A. Denner and T. Sack, *Renormalization of the Quark Mixing Matrix*. Nucl.Phys. **B347** (1990) 203–216.
- [80] Y. Yamada, *Gauge dependence of the on-shell renormalized mixing matrices*. Phys.Rev. **D64** (2001) 036008, arXiv:hep-ph/0103046.
- [81] P. Gambino, P. Grassi, and F. Madricardo, *Fermion mixing renormalization and gauge invariance*. Phys.Lett. **B454** (1999) 98–104, arXiv:hep-ph/9811470.
- [82] B. A. Kniehl, F. Madricardo, and M. Steinhauser, *Gauge independent W boson partial decay widths*. Phys.Rev. **D62** (2000) 073010, arXiv:hep-ph/0005060.
- [83] W. Porod, *SPheno, a program for calculating supersymmetric spectra, SUSY particle decays and SUSY particle production at e+ e- colliders*. Comput.Phys.Commun. **153** (2003) 275–315, arXiv:hep-ph/0301101.
- [84] W. Porod and F. Staub, *SPheno 3.1: Extensions including flavour, CP-phases and models beyond the MSSM*. Comput.Phys.Commun. **183** (2012) 2458–2469, arXiv:1104.1573 [hep-ph].
- [85] B. Allanach, *SOFTSUSY: a program for calculating supersymmetric spectra*. Comput.Phys.Commun. **143** (2002) 305–331, arXiv:hep-ph/0104145.

- [86] P. Z. Skands, B. Allanach, H. Baer, C. Balazs, G. Belanger, *et al.*, *SUSY Les Houches accord: Interfacing SUSY spectrum calculators, decay packages, and event generators*. JHEP **0407** (2004) 036, [arXiv:hep-ph/0311123](#).
- [87] B. Allanach, C. Balazs, G. Belanger, M. Bernhardt, F. Boudjema, *et al.*, *SUSY Les Houches Accord 2*. Comput.Phys.Commun. **180** (2009) 8–25, [arXiv:0801.0045 \[hep-ph\]](#).
- [88] M. Muhlleitner, A. Djouadi, and Y. Mambrini, *SDECAY: A Fortran code for the decays of the supersymmetric particles in the MSSM*. Comput.Phys.Commun. **168** (2005) 46–70, [arXiv:hep-ph/0311167](#).
- [89] A. Djouadi, M. Muhlleitner, and M. Spira, *Decays of supersymmetric particles: The Program SUSY-HIT (SUspect-SdecaY-Hdecay-InTerface)*. Acta Phys.Polon. **B38** (2007) 635–644, [arXiv:hep-ph/0609292](#).
- [90] C. Boehm, A. Djouadi, and Y. Mambrini, *Decays of the lightest top squark*. Phys.Rev. **D61** (2000) 095006, [arXiv:hep-ph/9907428](#).
- [91] E. Lunghi, W. Porod, and O. Vives, *Analysis of enhanced $\tan(\beta)$ corrections in MFV GUT scenarios*. Phys.Rev. **D74** (2006) 075003, [arXiv:hep-ph/0605177](#).
- [92] W. Porod and B. Allanach, *private communication*, 2011.
- [93] A. Barr, *Determining the spin of supersymmetric particles at the LHC using lepton charge asymmetry*. Phys.Lett. **B596** (2004) 205–212, [arXiv:hep-ph/0405052](#).
- [94] G. Hallenbeck, M. Perelstein, C. Spethmann, J. Thom, and J. Vaughan, *Model Discrimination with the CMS Detector: A Case Study*. Phys.Rev. **D79** (2009) 075024, [arXiv:0812.3135 \[hep-ph\]](#).
- [95] R. Horsky, M. Kramer, A. Muck, and P. M. Zerwas, *Squark Cascade Decays to Charginos/Neutralinos: Gluon Radiation*. Phys.Rev. **D78** (2008) 035004, [arXiv:0803.2603 \[hep-ph\]](#).
- [96] G. L. Kane and J. Leveille, *Experimental Constraints on Gluino Masses and Supersymmetric Theories*. Phys.Lett. **B112** (1982) 227.
- [97] P. Harrison and C. Llewellyn Smith, *Hadroproduction of Supersymmetric Particles*. Nucl.Phys. **B213** (1983) 223.
- [98] E. Reya and D. Roy, *Supersymmetric Particle Production at p anti- p Collider Energies*. Phys.Rev. **D32** (1985) 645.
- [99] S. Dawson, E. Eichten, and C. Quigg, *Search for Supersymmetric Particles in Hadron - Hadron Collisions*. Phys.Rev. **D31** (1985) 1581.

-
- [100] W. Beenakker, R. Hopker, M. Spira, and P. Zerwas, *Squark production at the Tevatron*. Phys.Rev.Lett. **74** (1995) 2905–2908, arXiv:hep-ph/9412272 [hep-ph].
- [101] W. Beenakker, R. Hopker, M. Spira, and P. Zerwas, *Gluino pair production at the Tevatron*. Z.Phys. **C69** (1995) 163–166, arXiv:hep-ph/9505416 [hep-ph].
- [102] W. Beenakker, M. Kramer, T. Plehn, M. Spira, and P. Zerwas, *Stop production at hadron colliders*. Nucl.Phys. **B515** (1998) 3–14, arXiv:hep-ph/9710451.
- [103] U. Langenfeld and S.-O. Moch, *Higher-order soft corrections to squark hadro-production*. Phys.Lett. **B675** (2009) 210–221, arXiv:0901.0802 [hep-ph].
- [104] A. Kulesza and L. Motyka, *Threshold resummation for squark-antisquark and gluino-pair production at the LHC*. Phys.Rev.Lett. **102** (2009) 111802, arXiv:0807.2405 [hep-ph].
- [105] A. Kulesza and L. Motyka, *Soft gluon resummation for the production of gluino-gluino and squark-antisquark pairs at the LHC*. Phys.Rev. **D80** (2009) 095004, arXiv:0905.4749 [hep-ph].
- [106] W. Beenakker, S. Brensing, M. Kramer, A. Kulesza, E. Laenen, *et al.*, *Soft-gluon resummation for squark and gluino hadroproduction*. JHEP **0912** (2009) 041, arXiv:0909.4418 [hep-ph].
- [107] W. Beenakker, S. Brensing, M. Kramer, A. Kulesza, E. Laenen, *et al.*, *Supersymmetric top and bottom squark production at hadron colliders*. JHEP **1008** (2010) 098, arXiv:1006.4771 [hep-ph].
- [108] W. Beenakker, S. Brensing, M. Kramer, A. Kulesza, E. Laenen, *et al.*, *NNLL resummation for squark-antisquark pair production at the LHC*. JHEP **1201** (2012) 076, arXiv:1110.2446 [hep-ph].
- [109] M. Beneke, P. Falgari, and C. Schwinn, *Threshold resummation for pair production of coloured heavy (*s*)particles at hadron colliders*. Nucl.Phys. **B842** (2011) 414–474, arXiv:1007.5414 [hep-ph].
- [110] M. R. Kauth, A. Kress, and J. H. Kuhn, *Gluino-Squark Production at the LHC: The Threshold*. JHEP **1112** (2011) 104, arXiv:1108.0542 [hep-ph].
- [111] M. R. Kauth, J. H. Kuhn, P. Marquard, and M. Steinhauser, *Gluino Pair Production at the LHC: The Threshold*. Nucl.Phys. **B857** (2012) 28–64, arXiv:1108.0361 [hep-ph].

- [112] S. Bornhauser, M. Drees, H. K. Dreiner, and J. S. Kim, *Electroweak contributions to squark pair production at the LHC*. Phys.Rev. **D76** (2007) 095020, [arXiv:0709.2544 \[hep-ph\]](#).
- [113] A. Arhrib, R. Benbrik, K. Cheung, and T.-C. Yuan, *Higgs boson enhancement effects on squark-pair production at the LHC*. JHEP **1002** (2010) 048, [arXiv:0911.1820 \[hep-ph\]](#).
- [114] W. Hollik, M. Kollar, and M. K. Trenkel, *Hadronic production of top-squark pairs with electroweak NLO contributions*. JHEP **0802** (2008) 018, [arXiv:0712.0287 \[hep-ph\]](#).
- [115] M. Beccaria, G. Macorini, L. Panizzi, F. Renard, and C. Verzegnassi, *Stop-antistop and sbottom-antisbottom production at LHC: A One-loop search for model parameters dependence*. Int.J.Mod.Phys. **A23** (2008) 4779–4810, [arXiv:0804.1252 \[hep-ph\]](#).
- [116] W. Hollik and E. Mirabella, *Squark anti-squark pair production at the LHC: The Electroweak contribution*. JHEP **0812** (2008) 087, [arXiv:0806.1433 \[hep-ph\]](#).
- [117] W. Hollik, E. Mirabella, and M. K. Trenkel, *Electroweak contributions to squark-gluino production at the LHC*. JHEP **0902** (2009) 002, [arXiv:0810.1044 \[hep-ph\]](#).
- [118] E. Mirabella, *NLO electroweak contributions to gluino pair production at hadron colliders*. JHEP **0912** (2009) 012, [arXiv:0908.3318 \[hep-ph\]](#).
- [119] J. Germer, W. Hollik, E. Mirabella, and M. K. Trenkel, *Hadronic production of squark-squark pairs: The electroweak contributions*. JHEP **1008** (2010) 023, [arXiv:1004.2621 \[hep-ph\]](#).
- [120] J. Germer, W. Hollik, and E. Mirabella, *Hadronic production of bottom-squark pairs with electroweak contributions*. JHEP **1105** (2011) 068, [arXiv:1103.1258 \[hep-ph\]](#).
- [121] W. Beenakker, R. Hopker, and M. Spira, *PROSPINO: A Program for the production of supersymmetric particles in next-to-leading order QCD*. [arXiv:hep-ph/9611232](#).
- [122] W. Hollik, J. M. Lindert, and D. Pagani, *NLO corrections to squark-squark production and decay at the LHC*. [arXiv:1207.1071 \[hep-ph\]](#).
- [123] G. A. Schuler, S. Sakakibara, and J. G. Korner, *USE OF FOUR-DIMENSIONAL SPIN METHODS IN THE CALCULATION OF RADIATIVE QCD CORRECTIONS*. Phys.Lett. **B194** (1987) 125.

- [124] R. Harlander, L. Mihaila, and M. Steinhauser, *Two-loop matching coefficients for the strong coupling in the MSSM*. Phys.Rev. **D72** (2005) 095009, [arXiv:0509048](#) [hep-ph].
- [125] R. Harlander, L. Mihaila, and M. Steinhauser, *Running of $\alpha(s)$ and $m(b)$ in the MSSM*. Phys.Rev. **D76** (2007) 055002, [arXiv:0706.2953](#) [hep-ph].
- [126] A. Bauer, L. Mihaila, and J. Salomon, *Matching coefficients for $\alpha(s)$ and $m(b)$ to $O(\alpha^2(s))$ in the MSSM*. JHEP **0902** (2009) 037, [arXiv:0810.5101](#) [hep-ph].
- [127] A. Kurz, M. Steinhauser, and N. Zerf, *Decoupling Constant for α_s and the Effective Gluon-Higgs Coupling to Three Loops in Supersymmetric QCD*. JHEP **1207** (2012) 138, [arXiv:1206.6675](#) [hep-ph].
- [128] T. Hahn, *Generating Feynman diagrams and amplitudes with FeynArts 3*. Comput.Phys.Commun. **140** (2001) 418–431, [arXiv:hep-ph/0012260](#).
- [129] T. Hahn and C. Schappacher, *The Implementation of the minimal supersymmetric standard model in FeynArts and FormCalc*. Comput.Phys.Commun. **143** (2002) 54–68, [arXiv:hep-ph/0105349](#).
- [130] T. Hahn and M. Perez-Victoria, *Automatized one loop calculations in four-dimensions and D-dimensions*. Comput.Phys.Commun. **118** (1999) 153–165, [arXiv:hep-ph/9807565](#).
- [131] T. Hahn, *A Mathematica interface for FormCalc-generated code*. Comput.Phys.Commun. **178** (2008) 217–221, [arXiv:hep-ph/0611273](#).
- [132] G. van Oldenborgh, *FF: A Package to evaluate one loop Feynman diagrams*. Comput.Phys.Commun. **66** (1991) 1–15.
- [133] S. Frixione, E. Laenen, P. Motylinski, B. R. Webber, and C. D. White, *Single-top hadroproduction in association with a W boson*. JHEP **0807** (2008) 029, [arXiv:0805.3067](#) [hep-ph].
- [134] R. Gavin, C. Hangst, M. Kramer, M. Muhlleitner, M. Pellen, *et al.*, *Matching Squark Pair Production at NLO with Parton Showers*. [arXiv:1305.4061](#) [hep-ph].
- [135] K. Hasegawa, S. Moch, and P. Uwer, *AutoDipole: Automated generation of dipole subtraction terms*. Comput.Phys.Commun. **181** (2010) 1802–1817, [arXiv:0911.4371](#) [hep-ph].
- [136] K. Hasegawa, *Super AutoDipole*. Eur.Phys.J. **C70** (2010) 285–293, [arXiv:1007.1585](#) [hep-ph].

- [137] J. Alwall, P. Demin, S. de Visscher, R. Frederix, M. Herquet, *et al.*, *MadGraph/MadEvent v4: The New Web Generation*. JHEP **0709** (2007) 028, [arXiv:0706.2334](#) [hep-ph].
- [138] T. Stelzer and W. Long, *Automatic generation of tree level helicity amplitudes*. Comput.Phys.Commun. **81** (1994) 357–371, [arXiv:hep-ph/9401258](#).
- [139] H. Murayama, I. Watanabe, and K. Hagiwara, *HELAS: HELicity Amplitude Subroutines for Feynman Diagram Evaluations* Tech. Rep. KEK-91-11, KEK, 1992.
- [140] G. P. Lepage, *VEGAS: An Adaptive Multidimensional Integration Program*.
- [141] K. Arnold, J. Bellm, G. Bozzi, F. Campanario, C. Englert, *et al.*, *Release Note – Vbfno-2.6.0*. [arXiv:1207.4975](#) [hep-ph].
- [142] K. Arnold, J. Bellm, G. Bozzi, M. Brieg, F. Campanario, *et al.*, *VBFNLO: A Parton Level Monte Carlo for Processes with Electroweak Bosons – Manual for Version 2.5.0*. [arXiv:1107.4038](#) [hep-ph].
- [143] K. Arnold, M. Bahr, G. Bozzi, F. Campanario, C. Englert, *et al.*, *VBFNLO: A Parton level Monte Carlo for processes with electroweak bosons*. Comput.Phys.Commun. **180** (2009) 1661–1670, [arXiv:0811.4559](#) [hep-ph].
- [144] J. Pumplin, D. Stump, J. Huston, H. Lai, P. M. Nadolsky, *et al.*, *New generation of parton distributions with uncertainties from global QCD analysis*. JHEP **0207** (2002) 012, [arXiv:hep-ph/0201195](#) [hep-ph].
- [145] H.-L. Lai, M. Guzzi, J. Huston, Z. Li, P. M. Nadolsky, *et al.*, *New parton distributions for collider physics*. Phys.Rev. **D82** (2010) 074024, [arXiv:1007.2241](#) [hep-ph].
- [146] K. Chetyrkin, J. H. Kuhn, and M. Steinhauser, *RunDec: A Mathematica package for running and decoupling of the strong coupling and quark masses*. Comput.Phys.Commun. **133** (2000) 43–65, [arXiv:0004189](#) [hep-ph].
- [147] R. Frederix, S. Frixione, F. Maltoni, and T. Stelzer, *Automation of next-to-leading order computations in QCD: The FKS subtraction*. JHEP **0910** (2009) 003, [arXiv:0908.4272](#) [hep-ph].
- [148] S. Alioli, P. Nason, C. Oleari, and E. Re, *A general framework for implementing NLO calculations in shower Monte Carlo programs: the POWHEG BOX*. JHEP **1006** (2010) 043, [arXiv:1002.2581](#) [hep-ph].
- [149] S. Frixione, Z. Kunszt, and A. Signer, *Three jet cross-sections to next-to-leading order*. Nucl.Phys. **B467** (1996) 399–442, [arXiv:hep-ph/9512328](#).

-
- [150] S. Frixione, *A General approach to jet cross-sections in QCD*. Nucl.Phys. **B507** (1997) 295–314, arXiv:hep-ph/9706545.
- [151] C. Balzereit, T. Mannel, and B. Plumper, *The Renormalization group evolution of the CKM matrix*. Eur.Phys.J. **C9** (1999) 197–211, arXiv:hep-ph/9810350.

Danksagung

Mein besonderer Dank geht an meine "Doktormutter" Prof. Dr. Margarete Mühlleitner, die mir eine Promotion in diesem interessanten Themengebiet ermöglicht hat. In zahlreichen Diskussionen und der engen Zusammenarbeit mit ihr durfte ich sehr viel dazulernen. Ich bin sehr dankbar für ihr ständiges Interesse an meiner Arbeit und die fortwährende Unterstützung.

Herrn Prof. Dr. Matthias Steinhauser danke ich herzlich für die Übernahme des Korreferats.

Im Laufe der Jahre am Institut für Theoretische Physik haben mich auch immer Diskussionen mit vielen Kollegen weitergebracht und so zum Gelingen dieser Arbeit beigetragen. Besonders erwähnen möchte ich in diesem Zusammenhang Ninh Le Duc, Bastian Feigl, Christian Hangst, Karol Kovařík, Sophy Palmer, Michael Rauch, Heidi Rzehak und Christian Schappacher. Herrn Prof. Dr. Ulrich Nierste danke ich für hilfreiche Kommentare beim Stop-Zerfall-Projekt. Dr. Michael Spira gebührt Dank für den intensiven Einsatz beim Vergleich mit Prospino und dafür, dass er sich stets etwas Zeit für meine Fragen genommen und mehrere Besuche ans PSI ermöglicht hat.

Für das Korrekturlesen der Arbeit möchte ich mich bei Bastian Feigl, Ramona Gröber, Christian Hangst, Karol Kovařík, Jan Sammet und Franziska Schissler bedanken.

Ein großer Teil meiner Arbeit wäre ohne eine reibungslos funktionierende Rechner-Infrastruktur nicht möglich gewesen. Für den damit verbundenen Arbeitsaufwand bedanke ich mich bei den Admins: Bastian Feigl, Christian Röhr und Simon Plätzer.

Ich habe das ITP immer als besonders angenehmen Ort zum Arbeiten empfunden. Dazu beigetragen haben nicht nur meine Bürokollegen Hamzeh Alavirad, Bastian Feigl und Christian Hangst, sondern auch alle anderen Diplomanden, Doktoranden und Postdocs, die stets für eine lockere Atmosphäre und wohltuende Kaffeepausen gesorgt haben. Vielen von ihnen danke ich auch für zahlreiche, vergnügliche Stunden außerhalb des Instituts, die oft genug eine willkommene Abwechslung waren.

Den Graduiertenkollegen "Hochenergiephysik und Teilchenastrophysik" sowie "Elementarteilchenphysik bei höchster Energie und höchster Präzision" gilt mein Dank für die finanzielle Unterstützung während der ganzen Zeit.

Ohne die Unterstützung und den Zuspruch vieler Freunde in Aachen und Karlsruhe wären die letzten Jahre nicht so schön gewesen, wie sie es waren. Besonderer Dank gilt hier Jan Sammet, der das gesamte Studium, vom ersten Tag an, mit mir bestritten hat.

Mein ganz herzlicher Dank geht an meine Eltern und meinen Bruder. Nicht nur ihre andauernde Unterstützung während meines gesamten Studiums sondern vor allem ihr Interesse und ihre Begeisterung für meine Arbeit sowie ihr Stolz auf mich, haben diese Arbeit erst möglich gemacht und mir durch schwierige Zeiten geholfen.

Zu guter Letzt möchte ich mich nochmal ausdrücklich bei Bastian für seine Liebe, seine Unterstützung, seinen Zuspruch, sein mit mir geteiltes Wissen, seine Geduld, und seine ganze Art, die mein Leben in den letzten Jahren unglaublich bereichert hat, bedanken.